Faculty of Science and Engineering

School of Electrical Engineering, Computing and Mathematical Sciences

Robust Multi-target Tracking

with Bootstrapped-GLMB Filter

Cong-Thanh Do

0000-0003-1748-2846

This thesis is presented for the Degree of

Doctor of Philosophy

of

Curtin University

June 2022

DECLARATION

To the best of my knowledge and belief, this thesis contains no material previously published by any other person, except where due acknowledgement has been made.

This thesis contains no material which has been accepted for the award of any other degree or diploma in any university.

Cong-Thanh Do

08 June 2022

ACKNOWLEDGEMENTS

First and foremost, I would like to express my special gratitude and admiration to my supervisors, Prof. Ba-Ngu Vo and Prof. Ba-Tuong Vo. Without their tremendous help, exceptional guidance, and consistent patience, I would not have continued to study at Curtin University for my doctoral degree, and this dissertation would never have been completed. It is an absolute pleasure to study under their supervision and to experience stress-relief from their amazing sense of humour. It is my privilege and fortune to be one of your students.

I would like to thank several sources of support. My PhD study was sponsored by a joint scholarship between the Ministry of Education and Training of Vietnam and the Curtin International Postgraduate Research Scholarship. Thanks to this scholarship, I was able to be a PhD candidate at Curtin University. Further, the financial support received from the School of Electrical Engineering and Computing at Curtin University has helped me study intensively without concern for financial problems. Moreover, I appreciate the dedicated administrative support from Professor Ian Howard, Mr Frankie Sia in the Mechanical Engineering Department, Ms Robyn, Ms Michelle, and other staff in the Electrical Engineering Department for their professional and friendly support and assistance. I will never forget my behind-the-scenes friend, who supported me financially without any doubt. Without her, I would be in trouble with my stipends while studying here.

I also thank my buddy at the University of Adelaide, Hoa Van Nguyen, who is the co-author of my first academic publication. I appreciate my buddy at Curtin University, Dat Nguyen, for his enthusiastic support, and assistance with coding, discussions, and jokey talks. Viet Nguyen, one of my best friends in Perth, has been a wonderful consultant when I faced dilemmas. He listened patiently while I shared my difficulties and sought his counsel. I have also expanded my knowledge of whiskey, cognac and wine from his expertise. I appreciate Diluka, Changbiom and Yuthika for sharing their happy stories about colourful life that made me laugh. Finally, I will never forget the joyful moments with our soccer team at Curtin University, which released my stress

and kept me physically strong.

My truly and heartfelt indebtedness comes to my gentle and indulgent spouse Huong Thi Thu Dao and my beloved children Chau Ngoc Bao Do and Anh Ngoc Bao Do, who always believe in me, and provide me with their endless love, inspiration and motivation. I extended my respectful appreciation to my parents, Chinh Dao and Dan Do, who nurture, raise and inspire me in every stage of my life. Without their endless love, I could not travel on this educational and career path. Finally, I am deeply indebted to my parents-in-law, who sent their beloved daughter to share every moment of life with me.

ABSTRACT

The challenges in multi-target tracking mainly stem from the random variations in the cardinality and states of targets during the tracking process. Further, the information on the model of newborn targets, their detection probabilities, and the statistics of the sensor's false alarms significantly complicate the tracking of multiple targets. In the literature, a great number of the proposed multi-target filtering algorithms simplify these challenges by assuming the information on the model parameters of newborn targets, the probability of target detections, and the clutter points provided by the sensor(s) known a priori. However, these assumptions do not hold in real-world applications, leading to incorrect and biased estimations of the filters. In addition, the adoption of a random vector to model a multi-target state is not sufficient, as the random vector has a known number with fixed order of elements.

Proposed by Mahler, the *Random Finite Sets* (RFS) is one of the main paradigms focusing on multi-target filtering. In the RFS approach, the multi-target tracking problem is accomodated in a top-down manner, with the multi-object dynamics (e.g., object motions, births, deaths and spawning) and measurement statistics all being considered. The set of multiple targets is considered as a random variable and its probability density is propagated through time using Bayes recursion. However, due to the complexity of the multi-target density, approximations or only some of its statistics (e.g., first moment and cardinality distribution) are propagated for tractability. Initially, filters constructed based on the RFS approach do not include target identities, then they are limited to applications that require the estimation of target trajectories.

Recently, an appealing technique has been proposed to overcome the aforementioned limitation of the (non-labelled) RFS-based filters by using *labelled RFSs*. Based on this technique, a first Bayes optimal multi-target tracker, the generalised labelled multi-Bernoulli (GLMB) filter, has been constructed with the capability of estimating trajectories of an unknown and time-varying number of targets. So far, this filter requires the performance of data association for both actual and measurement clutter targets, and it is relatively expensive. This dissertation addresses this limitation by

combining the technique of the non-labelled RFS filter with the GLMB implementation to accommodate unknown information on the clutter statistics, detection probability and the location of newborn targets with low computational cost. Moreover, a new technique for multi-sensor multi-target tracking to manage the uncertainty of clutter and detection based on the MS-GLMB filter is proposed.

The first key contribution of this dissertation is an algorithm for the single-sensor multi-target tracking problem based on the labelled RFS approach that performs without prior information on clutter rate and with low computational requirements. This can be useful since a mismatch in clutter parameters can result in poor performance of the tracker. The second contribution is providing an adaptive multi-target tracking algorithm based on the labelled RFS filter that removes the requirements for prior knowledge of the detection probability and clutter rate. Furthermore, this algorithm can initiate new tracks without prior knowledge of birth models. The third contribution is an efficient and robust algorithm that exploits the strengths of established filters to estimate target trajectories while learning the background parameters during operation.

LIST OF PUBLICATIONS

The following papers, based on work from this dissertation, have been published:

Journal articles

1. **C.-T. Do** and H. V. Nguyen. 'Tracking multiple targets from multistatic Doppler radar with unknown probability of detection', *Sensors*, vol. 19, no. 7, Art. no. 1672, Apr. 2019.

The author's contribution to this paper includes the theoretical development of the algorithm, implementation (MATLAB), evaluating, drafting, and finalising the paper. The co-authors contributed by providing insight into the development of implementation, discussion and proof-reading the paper.

2. **C.-T. Do**, T. T. D. Nguyen and W. Liu. 'Tracking multiple marine ships via multiple sensors with unknown backgrounds', *Sensors*, vol. 19, no. 22, Art. no. 5025, Sept. 2019.

The author's contribution to this paper includes the theoretical development of the algorithm, implementation (MATLAB), evaluating, drafting, and finalising the paper. The co-authors contributed by providing insight into the development of implementation, discussion and proof-reading the paper.

3. **C.-T. Do**, T. T. D. Nguyen, D. Moratuwage, C.Shim and Y. D. Chung. 'Multi-object tracking with an adaptive generalized labeled multi-Bernoulli filter', *Signal Processing*, Art. no. 108532, available online at https://doi.org/10.1016/j.sigpro.2022.108532.

The author's contribution to this paper includes the theoretical development of the algorithm, implementation (MATLAB), evaluating, drafting, and finalising the paper. The co-authors contributed by providing insight into the development of implementation, discussion and proof-reading the paper.

4. **C.-T. Do**, T. T. D. Nguyen and H. V. Nguyen. 'Robust multi-sensor generalized labeled multi-Bernoulli filter', *Signal Processing*, vol. 192, Art. no. 108368, Mar.

2022.

The author's contribution to this paper includes the theoretical development of the algorithm, implementation (MATLAB), evaluating, drafting, and finalising the paper. The co-authors contributed by providing insight into the development of implementation, discussion and proof-reading the paper.

Conference papers

1. **C.-T Do** and H. V. Nguyen, 'Multistatic Doppler-based marine ships tracking', *in Proc. of the Int. Conf. Control, Automation and Information Sciences*, Hangzhou, China, Oct. 2018.

The author's contribution to this paper includes the theoretical development of the algorithm, implementation (MATLAB), evaluating, drafting, and finalising the paper. The co-authors contributed by providing insight into the development of implementation, discussion and proof-reading the paper.

2. **C.-T. Do**, and T. T. D Nguyen. 'Multiple marine ships tracking from multistatic Doppler data with unknown clutter rate', *in Proc. of the 2019 Int. Conf. Control, Automation and Information Sciences*, Chengdu, China, Oct. 2019.

The author's contribution to this paper includes the theoretical development of the algorithm, implementation (MATLAB), evaluating, drafting, and finalising the paper. The co-authors contributed by providing insight into the development of implementation, discussion and proof-reading the paper.

CONTENTS

LIST OF FIGURES

LIST OF ABBREVIATIONS

CPHD	cardinalised probability hypothesis density
EKF	Extended Kalman Filter
GLMB	generalised labelled multi-Bernoulli
GNN	global nearest neighbour
i.i.d.	independent and identically distributed
GM-CPHD	Gaussian mixture - cardinalised probability hypothesis density
IC-GLMB	iterated corrector generalised labelled multi-Bernoulli
JIPDA	joint integrated probabilistic data association
JMS	jump Markov system
JPDA	joint probabilistic data association
KDE	kernel density estimation
LMB	labelled multi-Bernoulli
MAP	maximum a posteriori
MCMC	Markov chain Monte Carlo
MC	Monte Carlo
MHT	multiple hypothesis tracking
NN	nearest neighbour
OSPA	optimal sub-pattern assignment
$\text{OSPA}^{(2)}$	optimal sub-pattern assignment-on-optimal sub-pattern assignment
PDA	probabilistic data association
PHD	probability hypothesis density
RFS	random finite set
SMC	sequential Monte Carlo
SNR	signal-to-noise Ratio
TBD	track-before-detect
UKF	unscented Kalman filter
MS-GLMB	multi-sensor generalised labelled multi-Bernoulli
KF	Kalman filter
FISST	finite set statistics

LIST OF NOTATIONS

x	unlabelled target state
$\boldsymbol{x}$	labelled target state
X, Z, K, W	unlabelled random finite sets
$X^{(m)}$	unlabelled random finite set of targets of class m
$\boldsymbol{X}$	labelled random finite set.
$\boldsymbol{X}^{(m)}$	labelled random finite set of targets of class m in $\boldsymbol{X}$
$\mathcal{L}(\cdot)$	label set extraction function
$\Delta(\cdot)$	distinct label indicator function
$\delta_X(\cdot)$	generalised Kronecker delta function
$1_{\mathbb{X}}(\cdot)$	set inclusion function
$\langle \cdot, \cdot \rangle$	inner product of two functions
$[h(\cdot)]^X$	multi-target exponential
$\mathcal{N}(\cdot; m, P)$	Gaussian probability density function with mean m and covariance P
$\beta(\cdot; s, t)$	Beta distribution characterised by parameters s, t
μ_β	Beta distribution mean.
σ_β^2	Beta distribution covariance
$\|X\|$	cardinality of the set X
$\mathbb{E}(\cdot)$	expected value function
$\mathbb{R}$	space of real numbers
$\mathbb{R}^n$	space of n-dimensional real vectors.
$\mathbb{X}$	state space
$\mathbb{M}$	space of modes in a JMS
$\mathbb{L}$	label space
$\mathbb{L}^{(m)}$	label space for targets of class m
$\mathbb{B}$	label space for newly born targets
$\mathbb{B}^{(m)}$	label space for newly born targets of class m
$\mathbb{Z}$	measurement space
$\mathbb{C}$	discrete index space for components in a GLMB density

ℓ	target label
m	target class
$\kappa(\cdot)$	Poisson clutter intensity function
$\hat{\kappa}$	predicted clutter intensity
$\mathcal{F}_n(\cdot)$	set of n-element subsets
$\mathcal{F}(\cdot)$	set of subsets with any number of elements
$\phi(\cdot)$	state transition kernel
$f(\cdot\|\cdot)$	state transition density
$f^{(m)}(\cdot\|\cdot)$	state transition density for targets of class m
$h(\cdot)$	observation kernel
$g(\cdot\|\cdot)$	measurement likelihood function
$g^{(m)}(\cdot\|\cdot)$	measurement likelihood function for targets of class m
$\nu(\cdot)$	probability hypothesis density
$\vartheta(\cdot\|\cdot)$	Markovian mode switching probability in a JMS
ζ	kinematic state of an target
$p(\cdot)$	probability density function
$\pi(\cdot)$	unlabelled RFS density
$\boldsymbol{\pi}(\cdot)$	labelled RFS density.
$\rho(\cdot)$	cardinality probability density of an RFS
$p_D(\cdot)$	detection probability.
$p_D^{(m)}(\cdot)$	detection probability for targets of class m
$p_S(\cdot)$	survival probability
$p_S^{(m)}(\cdot)$	survival probability for targets of class m
I	random finite set of labels
$I^{(m)}$	random finite set of labels for targets of class m
θ	positive 1-1 mapping $\mathbb{L} \rightarrow Z$
$\theta^{(m)}$	positive 1-1 mapping $\mathbb{L}^{(m)} \rightarrow Z$
Θ	space of association maps
ξ	association map history
$\xi^{(m)}$	map ξ restricted to $\mathbb{L}_0^{(m)} \times ... \times \mathbb{L}_k^{(m)}$
Ξ	space of association map histories
k	time index
k_n	time index of n^{th} image frame

CHAPTER 1

INTRODUCTION

The modern estimation theory is a branch of statistics with a long history of development. One of the fundamental principles of this theory is the least-square method proposed in the early 19^{th} century by Carl Fredrich Gauss, one of the most influential mathematicians since antiquity [1, 2]. The terms *'estimation'* and *'filtering'* were introduced in the early 20^{th} century. Ronald Fisher, one of the most prominent statisticians, used the term *estimation* as a problem of *'estimating the value of one or more of the population parameters from a random sample of the population'* [3]. He is considered the father of the maximum likelihood method and Fisher information. More importantly, Fisher and his student, Calyampudi, introduced the Cramé-Rao bound, making it a fundamental tool for evaluating the quality of non-biased estimators. Later, Norbert Wiener and Andrey Kolmogorov proposed two independent works to estimate true signal values from noisy signals using Gauss's method in the frequency domain. While Kolmogorov focused on discrete-time signals [4] that contributed to the Russian Armed Forces defence strategy, Wiener worked with continuous time signals, and his work led to the Wiener filter [5] that was used in the anti-aircraft system of the United State Army.

In the mid-20th century, the trend of modelling systems in the time domain using the concept of state-space models was developed. In 1960, Rudolf Kalman proposed a method for estimating dynamic signals from noisy measurements called the Kalman filter (KF) [6]. The KF is an exact solution to the Bayes estimation and is one of the most extensively applied techniques for estimation and tracking due to its simplicity, optimality, and robustness [7]. Nevertheless, it is limited to the linear system models and Gaussian distributions. Efforts to extend this filter to handle the nonlinearity in the process and measurement models have created the extended KF (EKF) [8], and the cubature KF (UKF) [9]. In addition to the KF, the particle filter adopted the concept

of the sequential Monte Carlo (SMC) sampling to manage the nonlinear non-Gaussian model has been proposed in [10, 11].

Initially, these filters were developed to track a known and fixed number of targets, where the origin of the measurements is also known a priori. However, the number of targets and the individual states of these targets are actually unknown and randomly vary over time. The purpose of the multi-target tracking is to handle the challenges on estimating the number of targets and their trajectories from the noisy information collected by the sensor(s) in a coordinated manner [12–14]. Presently, there are three noteworthy paradigms focusing on the problem of multi-target tracking: the Joint Probabilistic Data Association (JPDA) Filter, Multiple Hypothesis Tracking (MHT) and Random Finite Set (RFS) [15]. The JPDA and the MHT approaches endeavour to alter single-target tracking algorithms to accommodate multiple targets using data association. Different from the two formers, the RFS paradigm provides a systematic and top-down formulation of multi-target estimation using a mathematical consistency based on the estimation theory backgrounds such as multi-target estimation error and Bayes optimality [14, 16]. Based on this formulation, the Bayesian recursion can be implemented to compute the multi-target density.

Using RFSs concept leads to developing a sequence of filtering methods for multi-targets tracking problem in both literature and practical applications such as the probability hypothesis density (PHD) [17] , cardinalized probability hypothesis density (CPHD) were proposed [18, 19], and the multi-Bernoulli filters [20, 21]. These filters and their extensions have been shown that they can well estimate the target states at each time step. However, they must apply heuristics for purpose estimate target states in a window of time [22, 23]. Recently, Vo and Vo proposed a theoretically rigorous and systematic study to estimate the trajectories of multiple targets based on the RFS approach [24] . The resultant filtering algorithm known as the generalized labelled multi-Bernoulli (GLMB) filter, can solve the problem of multi-target tracking in an exact-closed form. More important, the GLMB filter overcomes the drawback of the conventional RFS-based filters in the sense that it can simultaneously estimate the target states at each time step and the target trajectories in a window length [25]. Currently, the GLMB filter is considered the most scalable and effective algorithm since it is capable of tracking more than a million targets [26].

The GLMB filter has been adopted in many types of tracking problems, such as tracking with merged measurements [27], track-before-detect (TBD) [28, 29], extended targets [30], cell biology [31, 32], sensor scheduling [33], spawning targets [34, 35], distributed data fusion [36], field robotics [37, 38] and computer vision [39]. Furthermore, the method of using Gibbs sampling to improve the effective implementation of the GLMB filter has been proposed in [40]. In this work, the complexity of the GLMB filter is linear to the total number of measurements and quadratically in the number of hypothesised targets. Most recently, the GLMB filter has been extended to the multi-scan version [41], the multi-sensor (MS-GLMB) version [22], and the multi-sensor multi-scan version [42]. The GLMB filter is applied to several practical applications such as tracking the space debris [43, 44], crowd surveillance [39, 45], automation [46–48] and cell tracking [35, 49]. The goal of this dissertation is to adopt the advantages of the existing state-of-the-art RFS-based techniques to construct a simple but effective and robust algorithm that can adaptively learn the key parameters while filtering the real-world applications of tracking multi-target trajectories.

1.1 Motivation

The technique of using radio signals to detect targets, initiated in the first half of the last century, has been developed from a simple device to detect the aircraft to a set of very complicated systems. One of these systems is the radio detection and ranging, the RADAR, which is widely applied in not only civilian applications but also the modern warfare for prevention and interception strategies. This system is used to detect targets or obstacles. Furthermore, this system can estimate several parameters of the targets such as the velocity, range and bearing using its electromagnetic signals [50]. However, using radar tracking is subjected to clutter (caused by the environment) and various distortions (due to signal propagations); consequently, the accuracy of estimation and the probability of target detection are limited. The use of multi-static radar system (MRS) improves the tracking performance of the radar by using multiple pairs of transmitting and receiving antennas. These antennas are spatially distributed in the surveillance region [51] to maximise the accuracy of estimation and the probability of detection. The separate distribution in a large geographical area of the transmitters and receivers is the crucial characteristics of an MRS [52] since it allows a MRS system to observe targets from multiple directions. As targets can be detected at different

aspects, it leads to a notable increase in potential useful information, and remarkably expands the accurate recognition on detecting targets of the system [53]. Furthermore, using MRS is benefited from the increase of the resolution capability and resistances to the jamming and clutter [54]. In addition, the spatial distribution of radars prevents the whole radar system from physically being destroyed from attacks.

The complexity of the target tracking task increases with the antennae's degree of the radar system. First, for information fusion, the system needs radar stations and targets in lines of sight of each other, as well as requirements for synchronisation, phasing, the positioning of stations, and the transmission of reference signals and frequencies [54]. Second, in multi-target tracking, there are generic challenges, such as the unknown and randomly time-varying number of targets; uncertainties in detection, clutter and data association [15]; and nonlinearity and low observability of the Doppler measurement [55, 56]. The velocities and locations of moving targets must be observed continuously from their track history to heading for reliable detections. Doppler detectors (ones based on Doppler effect) using stationary radars can only detect moving targets because the reflected signals from stationary (or very slow-moving) targets are practically the same in the transmitted signals' frequencies. Therefore, tracking multiple targets using an MRS is a challenging problem, and it attracts many researchers from information fusion field. The purpose of multi-target tracking algorithms is to estimate the target state from observed data (measurements) such that the differences between the ground truth and the estimated multi-target state are as small as possible [23]. This dissertation is the first to handle the challenges in tracking multiple targets with unknown prior information regarding clutter rate, detection probability and birth model. Further, it is also the first to tackle the problem of tracking multiple marine ships via the Doppler radar system using a rigorous formulation based on labelled RFSs.

Multi-sensor architecture frequently occurs in multi-target tracking using radar system applications because it significantly improves machine perception. Depending on measurement functions, there are four types of sensor models: bearing, range, range-rate and position. The use of a bearing-only sensor model leads to the passive radar system, and combining the bearing model with either the range or range-rate models creates an active radar system. In addition, the model of position sensors is

usually applied to the drone-mounted camera [22].

This dissertation focuses on passive radar systems using bearing-only sensors. Bearing - only tracking is the problem of estimating multi-target trajectories with only the angle or direction of arrival measurements [57]. This problem has been widely studied in both defence and civilian applications, such as tracking missiles [58], underwater surveillance [59], autonomous navigation [60] via the deployment of airborne radars, sonars and other types of passive surveillance systems. However, due to the intrinsic nonlinearity and poor observability [61, 62], it is not always possible to construct a (proper) tractable filter with this type of measurement [63, 64]. Theoretically, the motion of the sensor platform must have at least one order higher than that of the target's motion to fully observe the kinematic state of the target [57, 65]. The strategy of integrating multiple sensors has been proposed in [66, 67] to increase observability. The multi-sensor framework reduces uncertainty in the system and increases the tracking algorithms' capability of to resolve the target state ambiguity. In addition to the technical challenges, the multi-target tracking solution is also subject to uncertainty induced by noise - corrupted measurements, false alarms, miss - detection and target appearances and disappearances. This dissertation proposes a new solution to the problem of multi-target tracking by adopting the benefits of the existing effective RFS trackers to track targets in unknown background information. While this solution can be applied to several types of multi-sensor settings, it has been applied to the bearing-only sensors in this dissertation.

1.2 Key contributions

- The first contribution of this dissertation is a robust algorithm for the single-sensor multi-target tracking problem based on the labelled RFS approach to track target trajectories with low computational cost. Currently, the existing RFS-based algorithms can handle real-world tracking problems where background models of clutter and detection profile are unknown. However, as the conventional RFS approach does not have the mechanism to address target tracks, RFS-based filters cannot estimate trajectories without using heuristic techniques. While a new branch of the RFS, the labelled RFS filter, uses target identities to track target trajectories in an unknown background environment, it is still computationally expensive. Therefore, a robust tracker presented in this dissertation is proposed

to overcome the aforementioned limitations of existing trackers. This tracker is constructed using two existing filters: the robust CPHD and the GLMB. Specifically, the robust CPHD is adopted to accommodate the mismatches in clutter rate and detection profile with low computational cost, and the GLMB filter, which can produce target trajectories, is used for the main filtering process. This contribution has published in the author's conference papers [68, 69] and journal articles [70, 71].The tracker is described in Chapter 3 and Chapter 4.

- The second contribution is a convenient plug-and-play multi-target tracker capable of adaptively learning the measurement clutter rate, probability of detection and target birth location online. Prior information such as the locations of newborn targets, the statistics of clutter measurements (also known as false alarms) generated by the sensor, and the target detection probability must be considered to realistically model the multi-target system. In general, this information is not practically available. Consequently, the trackers must be supplied with prior assumptions of these values, which usually leads to the inaccuracy of the tracking algorithms. Therefore, accurate inference of these parameters is important for achieving reliable tracking implementation in practice. The adaptive tracker proposed in Chapter 4 of this dissertation removes the needs of guessing the parameters for initiating trajectories, and it produces an efficient multi-target tracking algorithm sufficiently robust for many environments, including medium - clutter and low - clutter multi-target tracking applications. This contribution has published in the latest journal article of the author [72].
- The third contribution is a robust multi-sensor tracker that can learn and adapt with practical variations of the detection profile and clutter rate in the scenarios of tracking multiple targets based on the labelled RFS approach. In principle, using multiple sensors can improve the tracking performance because it significantly reduces uncertainty in target cardinality and their states. However, the major difficulty in multi-sensor tracking implementation is the NP-hard multi-dimensional ranked assignment problem. The robust multi-sensor algorithm in this dissertation is constructed based on the state-of-the-art MS-GLMB filter and robust CPHD filters to overcome difficulties in tracking scenarios with fluctuating backgrounds and a high number of sensors. Further, while the setting of the bearing-only sensors is introduced in Chapter 5 for the demonstration, this algo-

rithm can be applied to different types of sensors. This contribution has appeared in the author's journal article [73].

CHAPTER 2

BACKGROUND

This chapter aims to deliver a fundamental background on Bayesian estimation for the tracking of individual and multiple targets and to stimulate the adoption of labelled RFSs for estimation of multi-target trajectories. Specifically, Section 2.1 briefly summarises Bayesian state estimation, where random vectors are used to describe the dynamic and observation models. Section 2.2 introduces the fundamentals of RFSs to model the multi-target system. Section 2.3 presents the PHD and CPHD filters, which are the two first RFS - based filters, and their extensions to handle unknown clutter rate and detection profiles. Section 2.4 introduces labelled RFS and its applications in the multi-target system. Section 2.5 addresses the GLMB filter with separate prediction and update implementation. Finally, Section 2.6 and Section 2.7 present the MS-GLMB filter and the GLMB smoother, respectively.

2.1 Bayesian estimation

Assuming that a system is described by a state-space model in the discrete time domain, and a state of a single target at a given time k is entirely depicted by a state vector $x_k \in \mathbb{X} \subseteq \mathbb{R}^{p_x}$ where p_x is the dimension of the state. The evolution of the state vector $x_k \in \mathbb{R}^{n_x}$ to state $x_{k+1} \in \mathbb{R}^{n_x}$ at the next time step $k+1$ is described by the probability density of x_{k+1} conditioned on its state at previous time step x_k, that is, the so-called Markov transition density $f_{k+1|k}(x_{k+1}|x_k)$.

Given the true state vector x_k, a measurement process can generate a noisy measurement vector $z_k \in \mathbb{Z} \in \mathbb{R}^{n_z}$. The relationship between z_k and x_k is described by the measurement likelihood function $g_k(z_k|x_k)$. This function is the probability density of receiving a measurement z_k given a true target state x_k. From this assumption, knowledge of the target state x_k given a sequence of all measurements from the first time step

to time k is given by the filtering density $p_k(x_k|z_{1:k})$, where $z_{1:k} = (z_1, \ldots, z_k)$.

At the next time step $k+1$, the Bayes recursion updates the filtering density by fusing the data in the current filtering density $p_k(x_k|z_{1:k})$ with data collected in a newly generated measurement z_{k+1}. This updated filtering density is denoted by $p_{k+1}(x_{k+1}|z_{1:k+1})$. For compactness, the subscript k for the current time step is dropped, the subscript $k+1$ for the next time step is replaced with '+', and the dependence of the state on the past measurement is also dropped, i.e., $p_k(x_k|z_{1:k}) \triangleq p(x)$. Specifically, this updated filtering density can be calculated from the Markov transition density $f_+(x_+|x)$, previous density $p(x)$, and the measurement likelihood function $g_+(z_+|x_+)$ using the Chapman-Kolmogorov equation Eq. (2.1) and Bayes' rule Eq. (2.2) as follows.

$$p_+(x_+) = \int p(x) f_+(x_+|x)\, dx, \tag{2.1}$$

$$p_+(x_+|z_+) = \frac{g_+(z_+|x_+) p_+(x_+)}{\int g_+(z_+|x_+) p_+(x_+)\, dx_+}. \tag{2.2}$$

The above Bayes recursion propagates the probability density of the target state to the next time instance in two steps. First, the prediction step forward predicts the current density using the Chapman-Kolmogorov equation Eq. (2.1). Next, the predicted density is updated via Bayes rule Eq. (2.2). However, the Bayes filter does not always admit an analytical solution; hence, approximations must be used.

2.2 RFSs

Using a random vector is insufficient to model a multi-target state. In a random vector, the number of elements is specified and the order of elements is fixed. However, in a multi-target system, the target states and the target cardinality are unknown and vary randomly over time. This feature means that it is inadequate to model the multi-target system where the target states and the target cardinality are unknown and vary randomly over time.

In [14], the concept of RFSs has been developed as a principled technique for accommodating the problems of multi-target state estimation and data fusion in a consistent, systematic, and rigorous manner. An RFS is defined as a random variable that receives finite sets as its value. In an RFS, the cardinality (i.e., the number of elements) is random, and the states of elements are unknown, and the elements themselves are

disorganised [24].

In the RFS paradigm, the set integral of a function $f : \mathcal{F}(\mathbb{X}) \mapsto \mathbb{R}$ (where $\mathcal{F}(\mathbb{X})$ denoting a class of finite subsets of $\mathbb{X}$, and $\mathbb{R}$ being the real line) is specified by [14] as follows:

$$\int f(X)\,\delta X = \sum_{n=0}^{\infty} \frac{1}{n!} \int f(\{x_1,\ldots,x_n\})\, d(x_1,\ldots,x_n)\,. \tag{2.3}$$

The standard inner product of two functions $h(x)$ and $q(x)$ is defined as:

$$\langle h,q \rangle \triangleq \int h(x) q(x)\, dx. \tag{2.4}$$

The multi-target exponential is defined as:

$$[g]^X \triangleq \prod_{x \in X} g(x)\,, \tag{2.5}$$

where g is a real-valued function raised to a set X (i.e., the arguments of g are elements belong to X which can be scalars, vectors, or sets) and $[g]^{\varnothing} = 1$.

The generalised Kronecker delta function whole arbitrary arguments can be scalars, vectors, or sets, etc., it is denoted by:

$$\delta_Y(X) = \begin{cases} 1, & \text{if } X = Y \\ 0, & \text{if } X \neq Y \end{cases}. \tag{2.6}$$

The indicator function of the set Y is denoted as:

$$1_Y(X) = \begin{cases} 1, & \text{if } X \subseteq Y \\ 0, & \text{otherwise} \end{cases}. \tag{2.7}$$

When the set X has only one element x, that is, $X = \{x\}$, we can write $1_Y(x)$ for $1_Y(\{x\})$. The number of elements in a given finite set X is called the cardinality of the set X and is denoted by $|X|$.

Given an RFS with probability density π [74], its intensity, or its first-order statistical moment, is defined as a function $\nu : X \to [0,\infty)$ whose integral $\int_Y \nu(x)\, dx$ on any

region $Y \in \mathbb{X}$ is the expected number of targets in Y [17],

$$\int_Y \nu(x)\,dx = \int \pi(X)\,|X \cap Y|\delta X \tag{2.8}$$

The cardinality distribution for this RFS is given as [16]:

$$\rho(n) = \int_{|X|=n} \pi(X)\delta X \tag{2.9}$$

2.2.1 Standard multi-target dynamic model

In multi-target tracking, the number of targets and the states of those targets are randomly time-varying. The standard multi-target dynamics can be modelled using RFSs to capture the appearance and disappearance of targets, and the evolution of the individual target states. Assuming that, at the current time step, N targets (i.e., N single target states $x_1, \ldots, x_N$) appear in the surveillance area, and the values of each target state are taken from the state space $\mathbb{X}$. In the RFS formulation, the set of these targets is called the multi-target state and is denoted by X. Each target state $x \in X$ can exist with survival probability $p_{S,+}(x)$ and evolve to a new target state x_+ at the next time step with the transition probability density $f_+(x_+|x)$, or being terminated with probability $1 - p_{S,+}(x)$ (see Figure 2.1). Consequently, given a single-target state $x \in X$, its behaviour at the next time step is modelled by a Bernoulli RFS $F_+(x)$ with $r = p_{S,+}(x)$ and $p(\cdot) = f_+(x_+|x)$ [75].

Assuming targets are conditionally independent, then the RFS of the surviving targets from the current time step to the next time step is a multi-Bernoulli and described by [75],

$$S_+(X) = \bigcup_{x \in X} F_+(x)\,. \tag{2.10}$$

Noting that a multi-Bernoulli RFS is completely characterised by the set $\left\{\left(r^{(i)}, p^{(i)}\right)\right\}_{i=1}^{M}$, where i is the index of the transitioned i^{th} target, M is a constant number of indepen-

dent Bernoulli RFSs. The density of $S_+(X)$ is denoted by $\pi_{S,+}(\cdot|X)$ with [14]

$$\pi_{S,+}(x_1,\ldots,x_n)=\begin{cases}\prod_{i=1}^{M}\left(1-r^{(i)}\right) & \text{if } n=0\\ \prod_{i=1}^{M}\left(1-r^{(i)}\right)\sum_{1\le j_1\ne,\ldots,\ne j_n\le M}\prod_{i=1}^{n}\frac{r^{(j_i)}p^{(j_i)}(x_i)}{1-r^{(j_i)}}, & \text{if } 1\le n\le M\\ 0 & \text{if } n>M\end{cases} \tag{2.11}$$

Since the new targets can present randomly in the surveillance region, they should be represented in the dynamic model. Denote B_+ be the set of newborn targets, then B_+ can be modelled as either a Poisson RFS, an independently and identically distributed (i.i.d) cluster RFS or a multi-Bernoulli RFS. Therefore, there are survived and newborn targets at the next time step. The complete RFS of these targets is:

$$X_+ = S_+(X)\cup B_+. \tag{2.12}$$

Denote $\pi_{B,+}(\cdot)$ the probability density of the set of newborn targets, then the multi-target transition density $f_+(X_+|X)$ can be written as a finite set statistics (FISST) convolution as follows [75]:

$$f_+(X_+|X) = \sum_{Y_+\subseteq X_+}\pi_{S,+}(Y_+|X)\cdot\pi_{B,+}(X_+-Y_+). \tag{2.13}$$

Noting that the evolution of the multi-target state with time is described in both Eq. (2.12) and Eq. (2.13). Further, the elemental models of target motion, new target appearance and disappearance are incorporated in these two equations.

2.2.2 Standard multi-target measurement model

At the current time step, a sensor can detect a single-target state $x\in X$ with a probability of detection $p_D(x)$ or it can miss-detect this state with probability $1-p_D(x)$. Consequently, a noisy measurement z with measurement likelihood $g(z|x)$ is generated if x is detected; otherwise an empty set $\varnothing$ is generated if the state x is miss-detected. Hence, each target producing a measurement can be modelled by a Bernoulli RFS $D(x)$ specified by parameters $(r,p(\cdot))$ where $r=p_D(x)$ and $p(\cdot)=g(\cdot|x)$. Suppose that each target cannot generate more than one measurement, and each measurement is conditionally independent of the others. The set of all detections is a multi-Bernoulli RFS denoted by $D(X)$ whose probability density $\pi_D(\cdot|X)$ can be described by a multi-

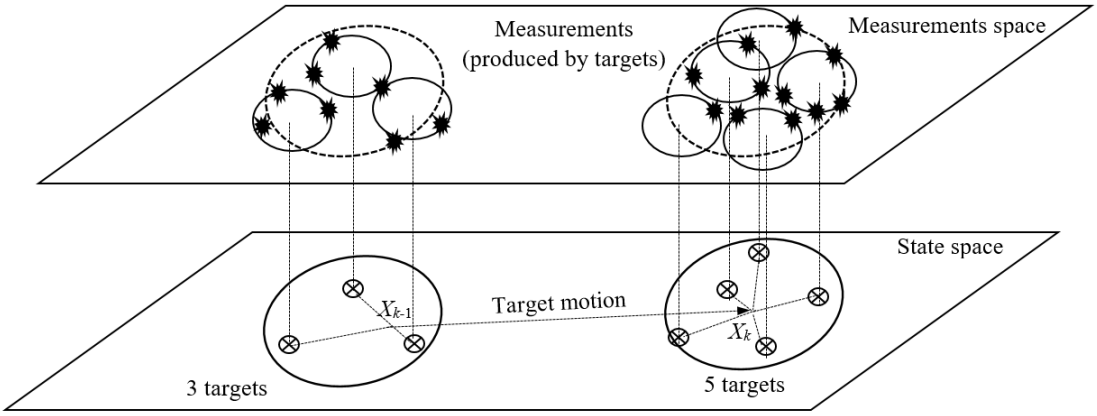

Figure 2.1: Illustration of the multi-target state evolution in state space. Three targets at the previous time step and five targets at the next time step. At each time step, each target can generate a random number of measurements [75].

Bernoulli RFS given in Eq. (2.11) with set of parameters $\{(p_D(x), g(\cdot|x))\}_{x\in X}$.

Since measurements can be generated not only from actual targets but also from false alarms, or clutter, the construction of the measurement model should cover all information from those sources. As clutter-generated measurements usually follow either the Poisson or i.i.d. cluster processes, the set of these measurements is modelled by a corresponding RFS K with probability density $\pi_K(\cdot)$. Consequently, at the current time step, the set of measurements Z is the superposition of all measurements generated from the actual targets and clutter-generated targets,

$$Z = D(X) \cup K. \tag{2.14}$$

Hence, the multi-target likelihood can be given by a finite set statistics convolution [24]

$$g(Z|X) = \sum_{W\subseteq Z} \pi_K(Z - W)\pi_D(W|X), \tag{2.15}$$

where the discrepancy between sets Z and W is denoted by $Z - W$.

2.2.3 Multi-target Bayes filter

The multi-target Bayes filter (in the context of the RFS approach) aims to estimate a finite set X of single target states $\{x_1, x_2, \ldots, x_n\} \subset \mathbb{X}$ at each time step. Let $\pi(X)$ be the multi-target probability density at the current time step, the multi-target Bayes filter uses the Chapman-Kolmogorov equation to compute the predicted multi-target

density at the next time step, as follows [24]:

$$\pi_+(X_+) = \int \pi(X) f_+(X_+|X)\,\delta X, \tag{2.16}$$

where $f_+(X_+|X)$ is the multi-target transition density. Then, the predicted multi-target state X_+ is partially observed, and the likelihood of a set of measurements Z_+ given observations on multi-target state X_+ is presented by $g(Z_+|X_+)$. At the next time step, the multi-target filtering density is computed using Bayes rule:

$$\pi_+(X_+|Z_+) = \frac{g_+(Z_+|X_+)\pi_+(X_+)}{\int g_+(Z_+|X)\pi_+(X)\delta X}. \tag{2.17}$$

The multi-target Bayes filter recursively propagates the multi-target filtering density in time using Eq. (2.16) and Eq. (2.17). However, since these two equations have combinations of multi-target densities and integrations in nature, the multi-target Bayes recursion is numerically intractable in most applications [75]. Hence, approximations are required to derive tractable filtering algorithms.

2.3 PHD and CPHD filters

2.3.1 PHD filter

The function of multi-target tracking algorithms is to refine the states of targets from noisy measurements such that the errors between the cultivated estimates of the multi-target state and the ground truth are as small as possible [23]. Based on the RFS approach, Mahler [17] proposed an algorithm that attains a tractability for tracking multiple targets. In this algorithm, only the intensity function, or the PHD, is propagated using an approximation of the Bayes recursion. This function is called the first moment of the multi-target density and is defined on the single-target state space. The unique property of the PHD function has been presented in Eq. (2.8). Furthermore, the PHD filter permits explicit modeling of miss-detections, Poisson clutter processes, target birth and death, and spawning of new targets from their parents [14]. The PHD filter has the potential benefit of low complexity in computation with order $\mathcal{O}(mn)$ which is linear in the number of both targets n, and measurements m in the current set Z [14].

Let $\nu(x)$ and $\nu_{B,+}(x_+)$ respectively present the filtering PHD at the current time step and the PHD of spontaneous newborn targets at the next time step. The predicted PHD at the next time step is computed by:

$$\nu_+(x_+) = \nu_{B,+}(x_+) + \int p_{S,+}(x_+) f_+(x_+|x) \nu(x) dx. \tag{2.18}$$

Similarly, at the next time step, a sensor generates a set of measurements Z_+. The set Z_+ contains the measurements generated from true targets and the clutter-generated measurements with assumed clutter intensity κ_+. The new PHD at next time step is then computed as follows:

$$\nu_+(x_+|Z_+) = \nu_+(x_+)(1 - p_{D,+}(x_+)) + \sum_{z \in Z_+} \frac{\nu_+(x_+) p_{D,+}(x_+) g_+(z|x_+)}{\kappa_+(z) + \int p_{D,+}(x) g_+(z|x) \nu_+(x) dx} \tag{2.19}$$

Currently, there are two techniques for the performance of the PHD filter: the sequential Monte Carlo (SMC) [74, 76, 77] and Gaussian mixtures (GM) [78]. The analyses of convergence properties of these two techniques are given in [79, 80] and [81], respectively. In [82], the GM PHD filter is extended with the use of jump Markov models to handle the manoeuvring targets those change between multiple linear Gaussian models. Recently, the PHD filter has been applied to the problem of tracking multiple targets with multi-detection systems [83], with mobile limited field-of-view sensor [84] and extended to multi-sensor multi-target tracking [85, 86] and smoothing [87, 88].

While the PHD filter has several potential advantages as mentioned in [14, Chap.16], it also has disadvantages. Since the PHD filter propagates the intensity of the multi-target state recursively in time, its state estimates are highly variable with the appearance of clutter and, especially, miss-detection [14, Chap.16]. Further, it cannot produce an accurate estimate number of targets in a highly dynamic multi-target scene [14, Chap.16]. Moreover, since only the intensity of the multi-target state is propagated rather than the full multi-target state density, a substantial amount of information is lost in the PHD recursion. Consequently, the PHD filter has certain limitations in practice.

2.3.2 CPHD filter

A further investigation based on the PHD filter has been performed in [19]. The CPHD filter has overcome the limitations of the PHD filter while retaining its benefits. This filter recursively propagates the multi-target intensity (i.e., first moment of multi-target density) and the number of targets' distribution (i.e., the cardinality distribution) in time to estimate the target states at each time step. Similar to other RFS-based filters, it is presumed in the CPHD filter that a target can only generate one measurement at most. The accuracy in tracking and localization of targets using the CPHD filter is more advanced than the PHD filter. Specifically, The CPHD filter permits the maximum a posteriori estimator to estimate the total number of targets rather than the less-accurate expected a posteriori estimator in the PHD filter [14]. Further, the CPHD filter accept that the clutter process can be i.i.d cluster RFS [14], and the prior and predicted multi-target RFSs are also i.i.d cluster processes [18]. However, by introducing the cardinality distribution in its recursion, the CPHD filter is more computationally demanding than the PHD filter. Specifically, the computational complexity in the CPHD filter is order $\mathcal{O}\left(m^3 n\right)$ compared to order $\mathcal{O}\left(mn\right)$ in the PHD filter [14].

Let ρ be the cardinality distribution of the existing targets at the current time step, and $\rho_{B,+}$ be the cardinality distribution of the spontaneous newborn targets at the next time step. The prediction step of the CPHD filter at the next time step including predicted PHD and cardinality distribution is described by

$$\nu_+\left(x_+\right) = \nu_{B,+}\left(x_+\right) + \int \nu\left(x\right) p_{S,+}\left(x\right) f_+\left(x_+|x\right) dx \tag{2.20}$$

$$\rho_+\left(n\right) = \sum_{j=0}^{n} \Pi_+\left[\nu,\rho\right]\left(j\right) \rho_{B,+}\left(n-j\right) \tag{2.21}$$

where

$$\Pi_+\left[\nu,\rho\right]\left(j\right) = \sum_{l=j}^{\infty} \frac{C_j^i \rho\left(l\right) \left\langle p_{S,+},\nu\right\rangle^j \left\langle 1-p_{S,+},\nu\right\rangle^{l-j}}{\left\langle 1,\nu\right\rangle^l} \tag{2.22}$$

and $C_j^l = \frac{l!}{j!(l-j)!}$ is the binomial coefficient. $\langle\cdot,\cdot\rangle$ represents the inner product of two functions or sequences those take real numbers as their values. Specifically, $\langle\xi,\chi\rangle = \int \xi\left(\alpha\right)\chi\left(\alpha\right) d\alpha$ if ξ and χ are real-valued functions, or $\langle\xi,\chi\rangle = \sum_{j=0}^{\infty} \xi\left(j\right)\chi\left(j\right)$ if ξ and χ are real-valued sequences.

The new PHD and cardinality distribution are computed by

$$\nu_+(x_+|Z_+) = \frac{\langle \Upsilon_+^1[\nu_+; Z_+], \rho_+ \rangle}{\langle \Upsilon_+^0[\nu_+; Z_+], \rho_+ \rangle} [\nu_+(x_+)(1 - p_{D,+}(x_+))] + \sum_{z \in Z_+} [\psi_{z,+}(x_+)\nu_+(x_+)] \frac{\langle \Upsilon_+^1[\nu_+; Z_+ - \{z\}], \rho_+ \rangle}{\langle \Upsilon_+^0[\nu_+; Z_+], \rho_+ \rangle} \tag{2.23}$$

$$\rho_+(n|Z_+) = \frac{\Upsilon_+^0[\nu_+; Z_+](n)\rho_+(n)}{\langle \Upsilon_+^0[\nu_+; Z_+], \rho_+ \rangle} \tag{2.24}$$

where

$$\Upsilon_+^u[\nu, Z](n) = \sum_{j=0}^{\min(|Z|,n)} (|Z| - j)! \frac{\langle 1 - p_{D,+}, \nu \rangle^{n-(j+u)}}{\langle 1, \nu \rangle^n} \left[P_{j+u}^n \rho_{K,+}(|Z| - j) e_j(\Xi_+(\nu, Z)) \right], \tag{2.25}$$

$$\psi_{z,+}(x_+) = \frac{\langle 1, \kappa_+ \rangle}{\kappa_+(z)} p_{D,+}(x_+) g_+(z|x_+), \tag{2.26}$$

$$\Xi_+(\nu, Z) = \{\langle \nu, \psi_{z,+} \rangle : z \in Z\}, \tag{2.27}$$

$$e_k(Z) = \sum_{S \subseteq Z, |S| = k} \left(\prod_{\xi \in S} \xi \right) \text{ with } e_0(Z) = 1 \tag{2.28}$$

with $P_{j+u}^n = \frac{n!}{(n-j-u)!}$ be the permutation coefficient, $u = 0, 1$, and $\rho_{K,+}(\cdot)$ be the cardinality distribution of clutter at the next time step. $e_k(\cdot)$ is the elementary symmetric function [89] of order k defined for a given measurement set Z, and $|S|$ is the number of elements (i.e., the cardinality), of the set S.

Implementations of the CPHD filter can use either SMC approximations or GMs, as in [18, 90, 91], with KF for linear Gaussian models and extended KF, cubature KF for nonlinear Gaussian models. The CPHD filter with the jump Markov system dynamics was presented in [92] to handle the manoeuvring targets. The CPHD filter can also accommodate spawning targets [93, 94] and extended targets [30, 95].

Although the CPHD filter is still applied in several applications because of its advantage of low computational complexity, its implementation assumes that the state-dependent detection probability and clutter rate are known in prior and time constants. These assumptions limit the ability of the CPHD filter in practical applications where these two parameters are unknown and time-varying. To overcome the limitations of the CPHD filter, the robust CPHD filter has been proposed to estimate clutter statistics

and the detection probabilities of targets.

2.3.3 Robust CPHD filters

In multi-target tracking, there are two notable uncertainty sources: clutter statistics and detection probability [96]. Clutter statistics or false alarms are the measurements that are not generated from any actual target, and detection probability models the capability that targets can be detected by sensor. The information on these parameters highly affects the accuracy and effectiveness of the tracker, hence it is crucial in Bayesian multi-target estimation. Since these two parameters are typically both unknown and unpredictably vary over time, incorrect information of either clutter or detection models results in the degradation or biased implementation of filtering methodologies. Practically, they must be estimated from trainning data or tuned manually [96].

In [96], the CPHD filter is extended to jointly estimate the clutter rate and detection probability online (the robust CPHD). In this technique, the clutter statistics are considered as an RFS of *'clutter generators'* or *'false targets'*, and incorporated with the non-homogeneous and unknown detection profile into single target state. This section summarises the technique generalised from the CPHD filter to handle unknown detection profiles and unknown clutter models.

Each kinematic part of state x is superseded by a new state $x_a = (x, a)$ where a is an augmented variable representing the probability of detecting x, and taking value on space of detection probability $\mathbb{X}^{(\Delta)} = [0, 1]$.

For consistency in notations, the functions or variables on the spaces of true targets, clutter generators and unknown detection probability, are described using the superscripts $^{(1)}$,$^{(0)}$and $^{(\Delta)}$, respectively. In addition, the functions or variables on the hybrid and augmented state space is denoted using superscript $^{(h)}$.

The augmented multi-target state is then described as follows:

$$X_a = (x_{a,1}, \ldots, x_{a,n}) = \{(x_1, a_1), \ldots, (x_n, a_n)\} \tag{2.29}$$

Similarly, the state of the augmented clutter-generated target is described by $c_c = [x_c, b]$

with $x_c \in \mathbb{X}^{(0)}$ as the generator target state and $b \in \mathbb{X}^{(\Delta)}$. The augmented clutter-generated multi-target state is:

$$X_c = (c_{c,1}, \ldots, c_{c,m}) = \{(x_{c,1}, b_1), \ldots, (x_{c,m}, b_m)\} \tag{2.30}$$

Assuming that the clutter-generated targets and real targets are statistically independent, the multi-target state is then a combination of these two types of (augmented) targets. Therefore, the augmented hybrid space $\mathbb{X}^{(h)}$ that includes the multi-target state is given as follows [96]:

$$\mathbb{X}^{(h)} = \left[\mathbb{X}^{(1)} \times \mathbb{X}^{(\Delta)}\right] \uplus \left[\mathbb{X}^{(0)} \times \mathbb{X}^{(\Delta)}\right] \tag{2.31}$$

where $'\uplus'$ is the disjoint union, and $'\times'$ is the Cartersian product.

Since the multi-target state and multi-target measurements now become the hybrid ones, the integral Eq. (2.3) is rewritten as follows [96]:

$$\int_{\mathbb{X}^{(h)}} f^{(h)}\left(x^{(h)}\right) dx^{(h)} = \int_{\mathbb{X}^{(\Delta)}} \int_{\mathbb{X}^{(1)}} f^{(h)}(x, a)\, dx da + \int_{\mathbb{X}^{(\Delta)}} \int_{\mathbb{X}^{(0)}} f^{(h)}(x_c, b)\, dx_c db \tag{2.32}$$

The joint probabilities of detection are denoted as follows:

$$p_D^{(h)}\left(x^{(h)}\right) = p_{D,a}(x_a) \triangleq a \text{ if } x^{(h)} = (x, a) \in \mathbb{X}^{(1)} \times \mathbb{X}^{(\Delta)} \tag{2.33}$$

$$p_D^{(h)}\left(x^{(h)}\right) = p_{D,c_c} \triangleq b \text{ if } x^{(h)} = (x_c, b) \mathbb{X}^{(0)} \times \mathbb{X}^{(\Delta)}. \tag{2.34}$$

The measurement likelihood is:

$$g(z|x_a) = g_a(z|x, a) \triangleq g(z|x) \tag{2.35}$$

$$g(z|c_c) = g_c(z|x_c, b) \triangleq g(z|x_c) \tag{2.36}$$

The robust CPHD filter recursively propagates the posterior PHD and posterior cardinality distribution in time as the same as that of the conventional CPHD filter. In a robust CPHD filter, the target state is defined as a hybrid and augmented state. Further, due to the statistical independence assumption between clutter and true targets, the PHD on the hybrid state space can be decomposed into the PHD of the actual

target state and that of the clutter-generated target state. The estimated mean value of the clutter rate is calculated from the posterior mean number of clutter-generated targets and the clutter target detection probability. Since the target state encompasses the unknown detection probability, this augmented unknown parameter it is calculated within the CPHD recursion (with augmented state space).

The robust CPHD can be implemented using the Beta - Gaussian mixture to describe the PHD of the actual newborn targets RFS and the Beta mixture for the clutter generator target birth RFS [96]. This implementation results in a solution which is closed-form of the CPHD recursion in handling a jointly unknown clutter rate and detection probability. As the number of mixture terms exponentially increases with time, pruning and merging of these mixture terms must be carried out to prevent this number from unbounded growth. A predetermined threshold is set for pruning to remove mixture components with lower weights. The Hellinger distance between the two Beta - Gaussian components is adopted in the performance of the component merging. The truncation of cardinality distribution is also employed to ensure tractable proagation.

2.4 Labelled RFSs

While the terms multi-target tracking and multi-target filtering can be used interchangeably, they have a subtle difference [97]. Both multi-target tracking and multi-target filtering estimate target states and target cardinality, however, multi-target tracking also estimates the target identities, allowing trajectory estimation [97]. Unlabelled RFS-based filters are suitable for the filtering problem since they propagate the kinematic parts of target states without their labels (i.e., their identities). Unlabelled RFS-based tractable multi-target filtering algorithm (for instance, the PHD and CPHD) have been developed for estimating target states, but not target trajectories, at each time step.

The idea of track labelling has been mentioned in [14, 98] to track target trajectories. This idea has been developed further in a theoretically rigorous and systematic manner in [24, 99]. This 'labelled RFS' method has been proposed to estimate multi-target trajectories via labelling individual target states. A labelled RFS is indeed an RFS where each element is assigned a distinct label as its identity [24, 97]. The kinematic state of single target and its identity then can be jointly modelled using this framework. Further, the labelled RFS framework also provides analytic solutions to the multi-target

inference and estimation problem [24].

The labelled RFS has several advantages compared to the unlabelled RFS concept in theoretical and real-world multi-target tracking applications. Specifically, labelled RFS filters can handle object identity implicitly within their models and can naturally estimate the target trajectories; the unlabelled counterparts cannot perform this task without using heuristics [25]. Moreover, while the unlabelled RFSs cannot provide estimates of information on target ancestries, labelled RFSs conceptually provide a mechanism to trace targets' ancestors by incorporating identity ancestry information into the modelling and estimation of spawning targets [34]. In addition, while the RFS-based filters without using target identity such as the PHD, CPHD, and the cardinality balanced multi-Bernoulli are subjected to the *'spooky effect'* (i.e., the effect of shifting the PHD mass of the miss-detected target onto the detected target without consideration on their physical separation), the RFS filters using target identity (the labelled RFS filters) are not [16, 100].

Each target state has a distinct label ℓ to distinguish the time-evolving tracks from different target states. Each distinct label $\ell = (s, \alpha) \in \mathbb{L}$ at time k comprises two components: time of birth, $s \leq k$, and a distinctive index α to distinguish targets born at the same time as illustrated in Figure 2.2. Let $\mathbb{B}_k$ be the space of the labels assigned to targets born at time k, then the space of the labels for all targets is the disjoint union $\mathbb{L}_k = \mathbb{L}_{k-1} \uplus \mathbb{B}_k$. Consequently, each labelled target state $\boldsymbol{x}$ at time k is simply an kinematic part of state which is unlabelled $x \in \mathbb{X}$ augmented with a distinct label $\ell \in \mathbb{L}_k$, $\boldsymbol{x} = (x, \ell) \in \mathbb{X} \times \mathbb{L}_k$.

A labelled multi-target state at time k is then a labelled RFS $\boldsymbol{X} \subset \mathbb{X} \times \mathbb{L}$ consisting of all elements with their distinct labels.

$$\boldsymbol{X} = \{(x_1, \ell_1), \ldots, (x_n, \ell_n)\} \tag{2.37}$$

A sequence of labelled states with the identical label at sequential times creates the trajectory of a unique target [41]. The set integral Eq. (2.3) is rewritten for a function

$\boldsymbol{f}(\boldsymbol{X})$ of a labelled RFS $\boldsymbol{X}$ as follows [24, 97]

$$\int \boldsymbol{f}(\boldsymbol{X})\delta\boldsymbol{X} = \sum_{n=0}^{\infty} \frac{1}{n!} \sum_{(\ell_1,\ldots,\ell_n)\in\mathbb{L}^n} \int_{\mathbb{X}^n} \boldsymbol{f}(\{(x_1,\ell_1),\ldots,(x_n,\ell_n)\}) d(x_1,\ldots,x_n) . \quad (2.38)$$

To extract labels from the set $\boldsymbol{X}$ in Eq. (2.37), the label extraction function $\mathcal{L}(\boldsymbol{X})$ is defined as follows

$$\mathcal{L}(\boldsymbol{X}) \triangleq \{\mathcal{L}(\boldsymbol{x}) : \boldsymbol{x} \in \boldsymbol{X}\} \quad (2.39)$$

where $\mathcal{L} : \mathbb{X} \times \mathbb{L}_k \to \mathbb{L}_k$ is the projection that maps from a labelled RFS to the labels and satisfies $\mathcal{L}(x,\ell) = \ell$. The distinct label indicator is denoted as,

$$\Delta(\boldsymbol{X}) = \delta_{|\boldsymbol{X}|}(|\mathcal{L}(\boldsymbol{X})|) , \quad (2.40)$$

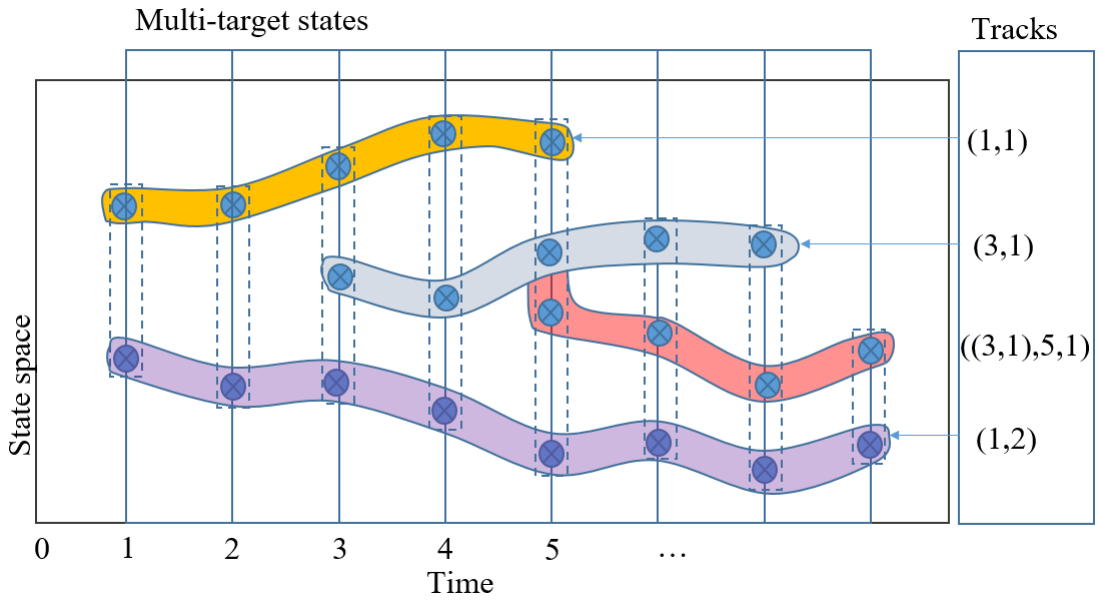

Figure 2.2: An illustration of label assignment for tracks of births and spawnings. Two tracks born at time 1 and a track born at time 3 are labelled as (1,1), (1,2), and (3,1) while a track spawned from track (3,1) at time 5 is assigned the label ((3,1)5,1) [34, 97].

Definition 1. A labelled RFS with state space $\mathbb{X}$ and a discrete label space $\mathbb{L}$ is an RFS on $\mathbb{X} \times \mathbb{L}$, such that each realisation $\boldsymbol{X}$ has distinct labels, that is, a realisation $\boldsymbol{X}$ of a labelled RFS always satisfies $\Delta(\boldsymbol{X}) = 1$.

In the following paragraphs, two specific classes of labelled RFSs, the labelled

multi-Bernoulli (LMB) and the GLMB [24] are defined.

Definition 2. [24, 101] An LMB RFS is a labelled RFS with state space $\mathbb{X}$ and discrete label space $\mathbb{L}$, which is distributed according to the following the density

$$\pi(\boldsymbol{X}) = \Delta(\boldsymbol{X})\omega(\mathcal{L}(\boldsymbol{X}))[p(\cdot)]^{\boldsymbol{X}} \tag{2.41}$$

where

$$\omega(L) = \prod_{\ell\in\mathbb{L}} \frac{1_L(\ell) r^{(\ell)}}{1-r^{(\ell)}} \prod_{\ell\in\mathbb{L}} \left(1-r^{(\ell)}\right) \tag{2.42}$$

$$p(x,\ell) = p^{(\ell)}(x) \tag{2.43}$$

where $r^{(\ell)}$ is the existence probability of the target and $p^{(\ell)}(\cdot)$ is the probability density corresponding to label $\ell \in \mathbb{L}$.

Definition 3. [24] A GLMB RFS is a labelled RFS with state space $\mathbb{X}$ and discrete label space $\mathbb{L}$, which is distributed according to

$$\boldsymbol{\pi}(\boldsymbol{X}) = \Delta(\boldsymbol{X}) \sum_{c\in\mathbb{C}} \left[p^{(c)}\right]^{\boldsymbol{X}} \omega^{(c)}(\mathcal{L}(\boldsymbol{X})) \tag{2.44}$$

where $\mathbb{C}$ is a set of arbitrary discrete indexes, and $\omega^{(c)}(L)$ and $p^{(c)}$ satisfy:

$$\sum_{L\subseteq\mathbb{L}} \sum_{c\subseteq\mathbb{C}} \omega^{(c)}(L) = 1, \tag{2.45}$$

$$\int_{x\in\mathbb{X}} p^{(c)}(x,\ell)dx = 1. \tag{2.46}$$

Eq. (2.44) shows that, a GLMB can be clarified as a mixture of multi-target exponentials. Each mixture component is a product of a weight $\omega^{(c)}(\mathcal{L}(\boldsymbol{X}))$ with a multi-target exponential $\left[p^{(c)}\right]^{\boldsymbol{X}}$, where $p^{(c)}$ is a probability density of each target.

The cardinality distribution and the intensity function (the PHD) of a GLMB RFS are computed as follows (see Proof. in [24]).

$$\rho(n) = \sum_{L\in\mathcal{F}_n(\mathbb{L})} \sum_{c\in\mathbb{C}} \omega^{(c)}(L) \tag{2.47}$$

$$\upsilon(x) = \sum_{c\in\mathbb{C}} \sum_{\ell\in\mathbb{L}} p^{(c)}(x,\ell) \sum_{L\in\mathbb{L}} 1_L(\ell)\, \omega^{(c)}(L). \tag{2.48}$$

Remark 4. It can be observed from Definition 2 and Definition 3 that when the GLMB RFS consists of a single component, it is an LMB RFS. It means the LMB is a singular version of the GLMB.

The δ−GLMB given in the following definition is a stronger form of the GLMB filter for more efficient implementation of the multi-target GLMB tracker.

Definition 5. [24] A δ−GLMB RFS with state space $\mathbb{X}$ and label space $\mathbb{L}$ is a special case of the GLMB RFS with

$$\begin{aligned} \mathbb{C} &= \mathcal{F}(\mathbb{L}) \times \Xi \\ \omega^{(c)}(L) &= \omega^{(I\xi)}(L) = \omega^{(I\xi)} \delta_I(L) \\ p^{(c)} &= p^{(I\xi)} = p^{(\xi)} \end{aligned}$$

in which Ξ is a discrete space. A δ−GLMB RFS is distributed according to,

$$\boldsymbol{\pi}(\boldsymbol{X}) = \Delta(\boldsymbol{X}) \sum_{(I,\xi) \in \mathcal{F}(\mathbb{L}) \times \Xi} \omega^{(I\xi)} \delta_I(\mathcal{L}(\boldsymbol{X})) \left[p^{(\xi)} \right]^{\boldsymbol{X}}, \tag{2.49}$$

where each $I \in \mathcal{F}(\mathbb{L})$ is a set of labels of tracks, each $\xi \in \Xi$ denotes an association map history up to current time, each $p^{(\xi)}(\cdot, \ell)$ represents a probability density of the kinematic part of state of track ℓ for the association map history ξ. The hypothesis that the set I has an association map history ξ is denoted by the pair (I,ξ). Each weight $\omega^{(I\xi)}$ is non-negative representing the probability of hypothesis (I,ξ) with

$$\sum_{I,\xi} \omega^{(I\xi)} = 1.$$

The cardinality distribution of a δ−GLMB is defined as:

$$\Pr(|\boldsymbol{X}| = n) = \sum_{I,\xi} \omega^{(I\xi)} \delta_n[|I|].$$

The track with label $\ell \in \mathbb{L}$ has its existence probability $r(\ell)$ and probability density

$p(x,\ell)$ given as follows:

$$r(\ell) = \sum_{I\xi} 1_I(\ell)\omega^{(I\xi)},$$
$$p(x,\ell) = \frac{1}{r(\ell)} \sum_{I\xi} p^{(\xi)}(x,\ell) 1_I(\ell)\omega^{(I\xi)}.$$

2.4.1 Standard labelled multi-target dynamic model

Given a labelled state $\boldsymbol{x} = (x,\ell)$ at the current time stepm this state can exist and evolve to a new state $\boldsymbol{x}_+ = (x_+,\ell_+)$ at the next time step with survival probability $p_S(x,\ell)$ and transition probability density $f_{S,+}(x_+|x,\ell)\,\delta_\ell(\ell_+)$. However, the state $\boldsymbol{x}$ can ceases with probability $q_S(x,\ell) = 1 - p_S(x,\ell)$. It should be noted that a labelled state changes its kinematic part in the transition only, but its label is preserved.

Following [24, 97], the multi-target transition density for the surviving target set $\boldsymbol{X}_S$ is given by

$$\boldsymbol{f}_{S,+}(\boldsymbol{X}_{S,+}|\boldsymbol{X}) = \Delta(\boldsymbol{X}_{S,+})\,\Delta(\boldsymbol{X}) 1_{\mathcal{L}(\boldsymbol{X})}(\mathcal{L}(\boldsymbol{X}_{S,+}))[\Phi_{S,+}(\boldsymbol{X}_{S,+};\cdot)] \tag{2.50}$$

where

$$\boldsymbol{\Phi}_{S,+}(\boldsymbol{X}_{S,+}|x,\ell) = (1 - p_S(x,\ell))\left(1 - 1_{\mathcal{L}(\boldsymbol{X}_{S,+})}(\ell)\right) + \sum_{(x_+,\ell_+)\in\boldsymbol{X}_{S,+}} \delta_\ell(\ell_+)\, p_S(x,\ell)\, f_{S,+}(x_+|x,\ell) \tag{2.51}$$

Similarly, at the next time step, for each $\ell_+ \in \mathbb{B}_+$, a new target with state (x_+,ℓ_+) can be born with probability $p_{B,+}(\ell_+)$ and density $f_{B,+}(x_+,\ell_+)$ or unborn with probability $q_{B,+}(\ell_+) = 1 - p_{B,+}(\ell_+)$ the set $\boldsymbol{B}$ of new targets born at the next time step is distributed according to

$$\boldsymbol{f}_{B,+}(\boldsymbol{B}) = \Delta(\boldsymbol{B})\omega_{B,+}(\mathcal{L}(\boldsymbol{B}))[p_{B,+}]^{\boldsymbol{B}}. \tag{2.52}$$

In Eq. (2.52), set $\boldsymbol{B}$ is modelled as an LMB RFS. Hence, the birth weight $\omega_{B,+}(\cdot)$ and the single target birth density $p_{B,+}(\cdot,\ell)$ are given as in Eq. (2.42) and Eq. (2.43), respectively. Note that the label space $\mathbb{B}$ of newborn targets and label space $\mathbb{L}$ of the survival targets are disjointed (i.e., $\mathbb{L} \cap \mathbb{B} = \varnothing$).

The labelled multi-target state $\boldsymbol{X}_+$ is the disjoint union of survivals and new births

as follows:

$$\boldsymbol{X}_{+} = \boldsymbol{X}_{S,+} \uplus \boldsymbol{X}_{B,+}. \tag{2.53}$$

Assuming surviving targets and new births are independent, then the multi-target transition density is described by [24]:

$$\boldsymbol{f}_{+}(\boldsymbol{X}_{+}|\boldsymbol{X}) = \boldsymbol{f}_{S,+}(\boldsymbol{X}_{S,+} \cap (\mathbb{X} \times \mathbb{L})|\boldsymbol{X})\boldsymbol{f}_{B,+}(\boldsymbol{X}_{B,+} - (\mathbb{X} \times \mathbb{L})) \tag{2.54}$$

2.4.2 Standard labelled multi-target measurement model

Assuming that, each detection from sensor(s) is not dependent of other detections and clutter, and conditional on $\boldsymbol{X}$, the single-sensor multi-target likelihood is presented by [24, 97]:

$$g(Z|\boldsymbol{X}) \propto \sum_{\theta \in \Theta} 1_{\Theta(\mathcal{L}(\boldsymbol{X}))}(\theta)[\psi_Z(x,\ell;\theta)]^{\boldsymbol{X}} \tag{2.55}$$

where Θ is the space of positive 1 - 1 mapping $\theta : \mathbb{L} \to \{0,1,\ldots,|Z|\}$, such that $[\theta(j) = \theta(i) > 0] \Rightarrow j = i$ (meaning that each measurement is assigned to a maximum of one target), and $\Theta(I)$ is the subset of Θ with domain I. The function $\psi_Z(x,\ell;\theta)$ is given by [24]

$$\psi_Z(x,\ell;\theta) = \begin{cases} \frac{p_D(x,\ell)g(z_{\theta(\ell)}|x,\ell)}{\kappa(z_{\theta(\ell)})}, & \text{if } \theta(\ell) > 0 \\ 1 - p_D(x,\ \ell) & \text{if } \theta(\ell) = 0. \end{cases} \tag{2.56}$$

where $\kappa(\cdot)$ is the clutter intensity.

2.5 GLMB filter

The central idea of the labelled RFSs concept is that each kinematic part of the target state is augmented with a unique label (a distinct identity) so that the unique trajectory of each target can be identified. The GLMB filter has been developed in [24, 97] using the labelled RFSs concept to model the multi-target state to address the problem of tracking target trajectories. Since the GLMB filter can guarantee propagating target tracks with unique labels, it is a true multi-target Bayes filter [25]. The GLMB has been proved in [24] that it is an exact closed-form solution to the multi-object Bayesian estimation. Furthermore, it brings on a first computationally tractable exact solution that has proved to be Bayes-optimal by generalising the concept of the RFSs to that of the labelled RFSs [16]. Consequently, the GLMB filter has proved to have Bayes

optimal track management [25].

The GLMB filter has also been used to solve several practical application problems in multi-target tracking. Moreover, the benefits of this filter are demonstrated in several applications in other fields of study, for instance, computer vision [39, 102], cell biology [31, 32, 35, 49, 103], simultaneous localisation and mapping (SLAM) [37, 38], and for the control and collaboration of multiple drones [46, 104]. Further, extensions of the GLMB filter have been used to handle track-before-detect (TBD) [28, 29], spawning objects [31, 34, 35], merged measurements [27, 105, 106], extended objects [30, 107, 108] centralised multi-sensor tracking [22], distributed tracking [36, 109, 110]. , and multi-object state smoothing [41]. The GLMB filter has been studied with sensor control problems for single-sensor [111] and multiple sensors [112–115]. The GLMB filtering has also been applied with several methods to manage the problem of multiple sensors, such as the fusion methods for cooperation of sensors [116, 117], the GCI method for multi-target data fusion [109, 118], the Cauchy-Schwarz divegence for passive sensor management [119, 120], an unified method for multi-sensor management [121], and correlations between two labelled multi-target systems [122]. Particularly, the effectiveness of the GLMB filter has clearly demonstrated in the application of simultaneously tracking over a million $2D$ targets per scan on-the-fly in a significant clutterred environment using off-the-shelf computing equipment[26]. Therefore, the GLMB filter is reckoned the most efficacious multi-object tracker currently available [23].

There are two implementations of the GLMB filter: the separate prediction update process and the joint prediction update process, as given in [24, 40]. The preliminary work of the author on the GLMB filter using a separate prediction update process has been reported [68]. This section represents the separate prediction update implementation of the GLMB filter and summarises the main points of the joint prediction update process. The details of the GLMB filter with joint-stage are given in the next chapter.

2.5.1 Separate prediction update GLMB filter

GLMB prediction

Given the multi-target filtering density is a δ–GLMB with the form of Eq. (2.49) at the current time step, then the predicted multi-target density at the next time step is also a δ–GLMB, and can be computed under the standard multi-target dynamic model

Eq. (2.53) as follows [24, Proposition 10]:

$$\pi_+(\boldsymbol{X}_+) = \Delta(\boldsymbol{X}_+) \sum_{(I_+,\xi)\in\mathcal{F}(\mathbb{L}_+)\times\Xi} \omega_+^{(I_+,\xi)} \delta_{I_+}(\mathcal{L}(\boldsymbol{X}_+)) \left[p_+^{(\xi)}\right]^{\boldsymbol{X}_+} \tag{2.57}$$

where

$$\omega_+^{(I_+,\xi)} = \omega_S^{(\xi)}(I_+\cap\mathbb{L})\omega_B(I_+\cap\mathbb{B}), \tag{2.58}$$

$$p_+^{(\xi)}(x,\ell) = 1_{\mathbb{L}}(\ell)p_S^{(\xi)}(x,\ell) + (1-1_{\mathbb{L}}(\ell))p_B(x,\ell), \tag{2.59}$$

$$p_S^{(\xi)}(x,\ell) = \frac{\left\langle p_S(\cdot,\ell)f(x|\cdot,\ell), p^{(\xi)}(\cdot,\ell)\right\rangle}{\bar{p}_S^{(\xi)}(\ell)}, \tag{2.60}$$

$$\bar{p}_S^{(c)}(\ell) = \int \left\langle p_S(\cdot,\ell)f(x|\cdot,\ell), p^{(\xi)}(\cdot,\ell)\right\rangle dx, \tag{2.61}$$

$$\omega_S^{(\xi)}(L) = \left[\bar{p}_S^{(\xi)}\right]^L \sum_{I\subseteq\mathbb{L}} 1_I(L)\omega^{(I,\xi)}\left[q_S^{(\xi)}\right]^{I-L}, \tag{2.62}$$

$$q_S^{(\xi)}(\ell) = \left\langle q_S(\cdot,\ell), p^{(\xi)}(\cdot,\ell)\right\rangle \tag{2.63}$$

In principle, the number of predicted components in the GLMB filtering density is large since it involves all combinations of target survivals, newborn targets, deaths. For the efficient implementation of the prediction, approximations must be adopted to increase diminish the computational requirements by cutting the low-weight components. To generate the best hypotheses with the highest weights for each parent hypothesis (I,ξ), the K–shortest path algorithm has been applied in [24]. This algorithm allows finding the K number of paths between two nodes in a weighted graph with minimum costs [123].

Generally, the surviving target weights are larger than that of the newborn targets; components with the newborn target would be dropped [97]. When the number of predicted components is insuficient, the hypothesis with newborn targets maynot be retained; consequently, the filter may not detect newborn targets [97]. In the GLMB filter implementation, the group of newborn targets and the surviving targets are considered independently; then, the best hypotheses for each group can be generated by solving the two K–shortest path problems separately for these two groups. The overall best predicted hypotheses are created by combining these two groups of hypotheses. This method of implementation is intuitive and highly parallelisable and can compute the best terms of predictions.

GLMB update

Given that the predicted multi-target density is a δ–GLMB filtering density with the form of Eq. (2.49) at the curent time step and a given set of measurement Z, then the updated multi-target density is also a δ–GLMB, and is calculated as follows [24, Proposition 11]:

$$\pi(\boldsymbol{X}|Z) = \Delta(\boldsymbol{X}) \sum_{(I,\xi)\in\mathcal{F}(\mathbb{L})\times\Xi} \sum_{\theta\in\Theta} \omega^{(I,\xi,\theta)}(Z)\delta_I(\mathcal{L}(\boldsymbol{X}))\left[p^{(\xi,\theta)}(\cdot|Z)\right]^{\boldsymbol{X}} \tag{2.64}$$

where

$$\omega^{(I,\xi,\theta)}(Z) = \frac{\delta_{\theta^{-1}(\{0:|Z|\})}(I)\omega^{(I,\xi)}\left[\bar{p}_Z^{(\xi,\theta)}\right]^I}{\sum_{(I,\xi)\in\mathcal{F}(\mathbb{L})\times\Xi} \sum_{\theta\in\Theta} \delta_{\theta^{-1}(\{0:|Z|\})}(I)\omega_k^{(I,\xi)}\left[\bar{p}_Z^{(\xi,\theta)}\right]^I}, \tag{2.65}$$

$$p^{(\xi,\theta)}(x,\ell|Z) = \frac{p^{(\xi)}(x,\ell)\,\psi_Z(x,\ell;\theta)}{\bar{p}_Z^{(\xi,\theta)}(\ell)} \tag{2.66}$$

$$\bar{p}_Z^{(\xi,\theta)}(\ell) = \left\langle p^{(\xi)}(\cdot,\ell), \psi_Z(\cdot,\ell;\theta)\right\rangle. \tag{2.67}$$

The association map function $\theta : \mathbb{L} \to \{0,1,\ldots,|Z|\}$ belongs to the association map space Θ, such that $\theta(i) = \theta(j) > 0$ implies $i = j$. This condition implies that each track can only generate at most one measurement at each time step. $\psi_Z(x,\ell;\theta)$ is given in Eq. (2.56).

Theoretically, entire possible associations of measurements to targets must be involved in the update stage of the GLMB filter. However, these associations embrace the generating and updated components. Hence, the number of associations is too large and increases because of the increases in the number of targets and measurements. Measurement gating and pruning need to be used to reduce the calculational expense in the update state and to delete the negligible components and keep the necessary posterior GLMB components using a specific threshold.

A technique called Murty's ranked assignment algorithm has been proposed in [24] to implement the truncation with the benefit of not having to propagating all the components in the recursion. This technique [124] is an extension of the Hungarian method [125] used to solve the optimal assignment problem for the best assignments. Using

Murty's algorithm in tracking requires a cost matrix with the costs of each object-to-measurement mapping. An other advantage of the Murty's algorithm is that it can obtain a given number of the best components (i.e., the components with highest weights) of the multi-target filtering density without comprehensively generating all probable mappings. However, the complexity of the GLMB filter implementation depends on the complexity of Murty's algorithm, which is quartic in the number of measurements [24].

2.5.2 Joint prediction update GLMB filter

The standard GLMB filter with two-stage implementation described in Section 2.5.1 requires performing truncations of the GLMB densities in prediction and update stages independently; it is intuitively and structurally inefficient. Specifically, resolving a ranked assignment problem for individual term of the predicted GLMB to perform truncation in the update step results in wasted computations. Since the summation of the predicted GLMB is truncated separately from the update stage, a meaningful proportion of the predicted terms can generate updated terms that have minor weights [40]. Further, as Murty's ranked assignment algorithm applied to remove insignificant components in the update stage has a complexity (at best) of quartic of the number of measurements, large computational resources are wasted. The implementation of this algorithm in [40] has been proposed using a joint prediction update step to mitigate computational wastage. The details of this filter are given in Section 3.2.1.

2.6 MS GLMB filter

The Bayesian approach is not only applied to solve the multi-target tracking problem using single sensor; it is also extended to handle the tracking problem using multiple sensors. The final objective in the Bayesian approach is to construct the multi-target posterior probability density given the entire of the noisy measurements reported by the sensors. As this posterior probability density involves entirely available statistical information, it is a complete solution to the multi-target problem using multiple sensors [126, Chap. 15].

In the RFS framework, among several recently proposed multi-sensor multi-target filters [14, 16], the centralised MS GLMB filter [22] is considered state-of-the-art. While the Bayes recursive filters used in multi-sensor multi-target tracking usually consist of

two stages (prediction and update), the MS GLMB filter applies the joint prediction update for its implementation. This results in a faster and more efficient implementation with quadratic complexity in the number of hypothesised targets but linearity in the total number of observed data from all sensors. This section briefly summarises the main points of this MS GLMB filter.

2.6.1 Multi-sensor multi-target observation model

In the problem of tracking multiple targets using multiple sensors, the likelihood function in Eq. (2.55) is extended to the multiple sensors case. This concept of this extension has been introduced in [22]. It is based on the assumption that, V sensors labelled from 1 to V are used in the surveillance area, and all sensors are independent. Particularly, each single target state $\boldsymbol{x}$ can be detected by a sensor $v^{th} \in \{1{:}V\}$ with probability of detection $p_D^{(v)}(\boldsymbol{x})$ and generates a measurement $z_j^{(v)} \in Z^{(v)}$ with likelihood $g_D^{(v)}\left(z^{(v)}|\boldsymbol{x}\right)$, where $Z^{(v)} = z_{1:|Z^{(v)}|}^{(v)} \in \mathbb{Z}$ be the set of measurements. However, this single-target state can also be miss-detected with probability $1 - p_D^{(v)}(\boldsymbol{x})$ and generate an empty value of measurement. Moreover, the sensor can generate measurements from false alarms, which are different from actual targets, then the set $Z^{(v)}$may consist of these measurements. The set of measurements originated from false alarms can be modelled by a Poisson RFS with intensity $\kappa^{(v)}$. The standard multi-target likelihood function for sensor v is described as follows [24, 97]

$$g^{(v)}\left(Z^{(v)}|\boldsymbol{X}\right) \propto \sum_{\theta^{(v)}\in\Theta^{(v)}} 1_{\Theta^{(v)}(\mathcal{L}(\boldsymbol{X}))}\left(\theta^{(v)}\right)\left[\psi_{Z^{(v)}}^{(v,\theta^{(v)}\circ\mathcal{L}(\cdot))}(\cdot)\right]^{\boldsymbol{X}}, \tag{2.68}$$

where: the association maps $\theta^{(v)} : \mathbb{L} \to \left\{0{:}\left|Z^{(v)}\right|\right\}$ is positive 1 - 1 (i.e., maps satisfy the condition that a distinct agurment is mapped to a distinct positive value);$\theta^{(v)}\circ\mathcal{L}(\boldsymbol{x}) = \theta^{(v)}(\mathcal{L}(\boldsymbol{x}))$; $\Theta^{(v)}$ is the set of $\theta^{(v)}$; given a domain I, the subset of $\Theta^{(v)}$ is defined as $\Theta^{(v)}(I)$; and:

$$\psi_{\left\{z_{1:M^{(v)}}\right\}}^{(v,j)}(\boldsymbol{x}) = \begin{cases} \frac{p_D^{(v)}(\boldsymbol{x})g^{(v)}(z_j|(x\ell))}{\kappa^{(v)}(z_j)} & \text{if } j = 1 : M^{(v)} \\ 1 - p_D^{(v)}(\boldsymbol{x}) & \text{if } j = 0. \end{cases} \tag{2.69}$$

The map $\theta^{(v)}$ prescribes that a target with label ℓ generates an observation $z_{\theta(\ell)} \in Z^{(v)}$, with miss-detected targets allocated to 0. The positive 1 - 1 characteristic give the meaning of the $\theta^{(v)}$ that it is $1-1$ on the set of detected labels (i.e., $\left\{\ell : \theta^{(v)}(\ell) > 0\right\}$), and ensures each target generate at most one measurement in $Z^{(v)}$. For the conve-

nience of representation, the notations in Eq. (2.55) is re-applied in this section with the superscript $^{(v)}$ added to imply the index of the sensor. Assuming that all sensors are independent from each other conditionally, [1], the abbreviations used in multi-target tracking using multiple sensors are given as follows:

$$Z \triangleq \left(Z^{(1)}, \ldots, Z^{(V)}\right), \tag{2.70}$$

$$\Theta \triangleq \Theta^{(1)} \times \cdots \times \Theta^{(V)}, \tag{2.71}$$

$$\Theta(I) \triangleq \Theta^{(1)}(I) \times \cdots \times \Theta^{(V)}(I), \tag{2.72}$$

$$\theta \triangleq \left(\theta^{(1)}, \ldots, \theta^{(V)}\right), \tag{2.73}$$

$$1_{\Theta(I)}(\theta) \triangleq \prod_{v=1}^{V} 1_{\Theta^{(v)}(I)}\left(\theta^{(v)}\right), \tag{2.74}$$

$$\psi_Z^{(j^{(1)},\ldots,j^{(V)})}(x,\ell) \triangleq \prod_{v=1}^{V} \psi_{Z^{(v)}}^{(v,j^{(v)})}(x,\ell), \tag{2.75}$$

the multi-sensor multi-target likelihood now can be simplified as follows:

$$g(Z|\boldsymbol{X}) = \prod_{v=1}^{V} g^{(v)}\left(Z^{(v)}|\boldsymbol{X}\right) \propto \sum_{\theta \in \Theta} 1_{\Theta(\mathcal{L}(\boldsymbol{X}))}(\theta)\left[\psi_Z^{(\theta \circ \mathcal{L}(\cdot))}(\cdot)\right]^{\boldsymbol{X}}. \tag{2.76}$$

Note that, the extended association map θ with multiple sensors is also positive $1-1$ if all other terms $\theta^{(i)}, (i = 1, \ldots, V)$, are positive $1-1$, and $\theta^{(v)} \circ \mathcal{L}(\boldsymbol{x}) = \theta^{(v)}(\mathcal{L}(\boldsymbol{x}))$.

The truncation technique must be used to truncate the low-weight components at every single step to prevent the exponential increase in the number of terms in the GLMB filtering density. By preserving the highest weighted components, the component truncation minimises the L_1 approximation error [97] and can be formulated as a multi-dimensional assignment problem [127] which is NP-hard in the implementation of the MS GLMB. A two-sensor GLMB filter implementation using Murty's algorithm was introduced in [128]. This solution has a computational complexity of $\mathcal{O}\left(\left(m^{(1)}m^{(2)}\right)^4\right)$.

An algorithm exploiting the Gibbs sampler in [40] for truncating the GLMB sum using joint prediction update GLMB filter in the MS GLMB filtering density was proposed in [22]. This method is more efficient than Murty's algorithm since its complex-

[1] More precisely, given the (multi-target) state, the uncertainty (which is caused by measurement noise, misdetections and false alarms) from individual sensor is self-dependent, meaning that the sensors donot intervene or impact on each other when receiving the measurements or detections.

ity is linear in the total number of observations and quadratic in the number of hypothesised targets. Hence, this implementation is particularly advantageous in a jam-packed clutterred environment where a high number of measurements is presented [25]. Further developments using Gibbs sampling, based on minimally Markovian stationary distribution to truncate insignificant components of the GLMB, was introduced in [22]. In this development, the stationary distribution has been used as the *'importance function'* for sampling components, as its support involves one of the optimal sampling functions [22]. Most importantly, this algorithm results in an online multi-sensor multi-target tracking with a computational complexity of $\mathcal{O}\left(TP^2\prod_{s=1}^{V}m^{(s)}\right)$, where P is the number of hypothesised tracks and T is the number of sampled solutions from the Gibbs sampler [22], making it a very applicable and scalable solution in practice.

2.7 GLMB smoother

The GLMB has been further extended to the multi-scan version, which eliminates track fragmentation an important drawback in multi-target tracking filters and significantly improves tracking performance with the smoothing-while-filtering algorithm [41]. The state-of-the-art GLMB smoother involves the (labelled) posterior density instead of the filtering density to estimate the multi-target state; therefore, it results in a significantly better estimation of multi-target trajectories than the conventional Bayes filters. Moreover, this smoother can be efficiently implemented based on Gibbs sampling and overcomes the N-P hard multi-dimensional assignment problem. While the traditional multi-scan algorithms can handle up to 10 scans, the technique described in [41] can handle 100 scans. The details of the GLMB smoother have been reported in [41].

The recursive multi-scan GLMB filter initiates newborn trajectories, updates surviving trajectories, ceases vanishing trajectories, and retains trajectories that disappeared previously. New trajectory initiations and the update of survival trajectories in the multi-scan GLMB recursion are identical to those of the recursion of the GLMB filter without marginalisation of bygone labels and kinematic target states [41]. Since the computation of smoothing GLMB posterior with more than two scans is NP-hard problem, one of the proposed solutions for this problem is Gibbs sampling. The details of this technique when applied to multi-scan GLMB recursion are described in [41].

While the GLMB smoother has several advantages, it has a high memory requirement and complexity. Currently, the GLMB smoother is adopted to the problems of single-sensor multi-target tracking with prior knowledge of background information. This allows further investigations of the GLMB smoother in accommodating unknown background information and in multi-sensor multi-target tracking scenarios.

CHAPTER 3

MULTI-TARGET TRACKING WITH AN UNKNOWN CLUTTER RATE

This thesis aims to solve the multi-target tracking problem with unknown clutter, unknown detection probability and unknown birth model. Since this problem is generally complicated, the simpler problem of unknown clutter rate is first addressed in this chapter to improve the readability and serve as a building block for more complex problem with several unknown parameters.

This chapter presents a Bootstrapped-GLMB filter based on the techniques of the λ-CPHD filter [96] and the conventional GLMB filter [24] to estimate multi-target trajectories without prior information on clutter rate. Specifically, the λ-CPHD is implemented to estimate the unknown clutter rate. The resultant estimate is then bootstrapped into the GLMB filter to track target trajectories. Provided that the fluctuation of this unknown parameter varies slower than the rate of measurement data update, the Bootstrapped-GLMB filter can adaptively learn the background parameter while filtering. The outcomes of this chapter have been published in the author's conference paper [69].

3.1 Introduction

In multi-target tracking, clutter statistics or false alarms are accounted the remarkable source of uncertainty that highly influences the effectiveness of a tracker [96]. Clutter is the set of false measurements that are not generated from actual targets. As the clutter statistics randomly vary with time, the clutter intensity is an unknown information. Therefore, the assumption on a prior known knowledge of the clutter intensity does not hold in practical applications. Any mismatch in clutter parameter leads to the poor implementation of the tracker. Pratically, this parameter must be estimated from

training data or tuned manually [96].

In the literature, there are several proposed filters built on the premise of the RFS approach to implement multi-target tracking with unknown information on the clutter rate [96, 129]. In [130], the author proposed using the algorithm of [96] to estimate the clutter rate, then bootstrapped the resulting value into the CPHD filter [18]. In [129], a multi-Bernoulli filter has been employed to estimate these unknown parameters using the same idea with the robust CPHD filter. However, these filters cannot produce target tracks. Conversely, the GLMB filter can handle unknown clutter rates by considering clutter false targets which are different from the actual targets [131]. However, since data association needs to be implemented on these two types of targets, the computational expense is significant. Other methods based on GLMB filter that do require the clutter rate to be known include the TBD approach [28, 29] and a bootstrapping method with a robust multi-Bernoulli filter [132]. This chapter contributes an efficient tracker that can produce target trajectories and accommodate the unknown clutter rate on-the-fly.

The method in this chapter is to utilise the advances of the existing filters to track target trajectories efficiently without knowing the clutter statistics. Specifically, this method exploits the advantage of the λ–CPHD given in [96] to accommodate the randomness of clutter rate and the benefit of the GLMB filter [24] in tracking target trajectories. The structure of this filter is demonstrated in Figure 3.1. Specifically, by running the λ–CPHD independently to estimate the clutter rate only before bootstrapping into the conventional GLMB filter, the resultant filter can track target trajectories with low computational cost.

Section 3.2 presents the concept of using the bootstrapping method to handle the unknown information on clutter rate. Specifically, the combination of the prediction and update stages for the main filtering process of the GLMB filter is presented in Section 3.2.1. Section 3.2.2 represents the basis of the proposed bootstrapping method for accommodating the unknown clutter rate. The quantitative studies outlined in Section 3.3 examine the accuracy and effectiveness of the proposed bootstrapping method for the theoretically linear dynamic model and the practically nonlinear dynamic model when applied to the tracking of multiple marine vessels. Last but not least, Section 3.4

concludes this chapter.

3.2 Bootstrapped filter with an unknown clutter rate

This section provides the details of the Bootstrapped-GLMB filter that is capable of tracking multi-target trajectories with no prior knowledge of clutter rate. Particularly, as shown in Figure 3.1, the λ–CPHD filter is adopted to estimate the value of the clutter rate then this estimated value is bootstrapped into the GLMB filter. The standard GLMB filter is used as the main process of generating target trajectories. Such a combination is benefited from the low complexity of the CPHD filtering implementation in estimating clutter rate online and the capability of tracking target trajectories using labelled RFS formulation of the GLMB filter.

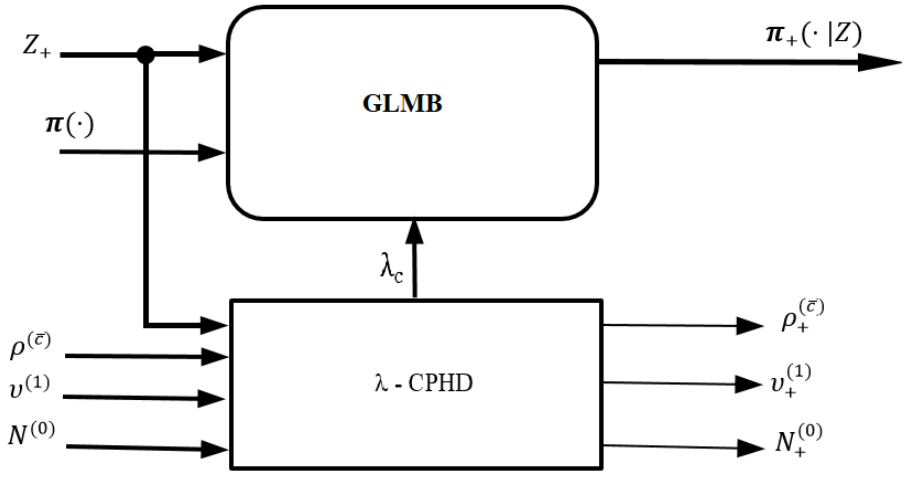

Figure 3.1: The overall diagram for Bootstrapped-GLMB estimator with an unknown clutter rate

3.2.1 GLMB filtering formulation

Given the standard model Eq. (2.53) of the multi-target dynamic system, and the multi-target filtering density is a GLMB density as given in Eq. (2.49) at the current time step, i.e.,

$$\boldsymbol{\pi}(\boldsymbol{X}) = \Delta(\boldsymbol{X}) \sum_{(I,\xi)\in\mathcal{F}(\mathbb{L})\times\Xi} \omega^{(I,\xi)} \delta_I(\mathcal{L}(\boldsymbol{X})) \left[p^{(\xi)}\right]^{\boldsymbol{X}} \tag{3.1}$$

The joint prediction update GLMB filter is constructed by combining the separate prediction and update stages presented in Section 2.5.1 into a single stage. Hence, the

resulting measurement-updated GLMB density is described by [40]

$$\boldsymbol{\pi}_{+}\left(\boldsymbol{X}_{+}|Z_{+}\right) \propto \Delta\left(\boldsymbol{X}_{+}\right) \sum_{I,\xi,I_{+},\theta_{+}} \omega^{(I,\xi)} \omega_{Z_{+}}^{(I,\xi,I_{+},\theta_{+})} \delta_{I_{+}}\left[\mathcal{L}\left(\boldsymbol{X}_{+}\right)\right]\left[p_{Z_{+}}^{(\xi,\theta_{+})}\right]^{\boldsymbol{X}_{+}}, \tag{3.2}$$

where $\xi \in \Xi, I \in \mathcal{F}\left(\mathbb{L}\right), I_{+} \in \mathcal{F}\left(\mathbb{L}_{+}\right), \theta_{+} \in \Theta_{+}\left(I_{+}\right)$ is a positive 1 - 1 association map $\theta_{+}: I_{+} \rightarrow \{0:|Z_{+}|\}$ with Z_{+} as set of observed measurements at the next time step, and

$$\omega_{Z_{+}}^{(I,\xi,I_{+},\theta_{+})} = 1_{\Theta_{+}(I_{+})}\left(\theta_{+}\right)\left[1-\bar{p}_{S}^{(\xi)}\right]^{I-I_{+}}\left[\bar{p}_{S}^{(\xi)}\right]^{I\cap I_{+}}\left[1-r_{B,+}\right]^{\mathbb{B}_{+}-I_{+}} r_{B}^{\mathbb{B}_{+}\cap I_{+}}\left[\bar{\psi}_{Z_{+}}^{(\xi,\theta_{+})}\right]^{I_{+}} \tag{3.3}$$

$$\bar{p}_{S}^{(\xi)}\left(\ell\right) = \left\langle p^{(\xi)}\left(\cdot,\ell\right), p_{S}\left(\cdot,\ell\right)\right\rangle \tag{3.4}$$

$$\bar{\psi}_{Z_{+}}^{(\xi,\theta_{+})}\left(\ell_{+}\right) = \left\langle \bar{p}_{+}^{(\xi)}\left(\cdot,\ell_{+}\right), \psi_{Z_{+}}^{(\theta_{+}(\ell_{+}))}\left(\cdot,\ell_{+}\right)\right\rangle \tag{3.5}$$

$$\bar{p}_{+}^{(\xi)}\left(x_{+},\ell_{+}\right) = 1_{\mathbb{L}}\left(\ell_{+}\right)\frac{\left\langle p_{S}\left(\cdot,\ell_{+}\right) f_{+}\left(x_{+}|\cdot,\ell_{+}\right), p^{(\xi)}\left(\cdot,\ell_{+}\right)\right\rangle}{\bar{p}_{S}^{(\xi)}\left(\ell_{+}\right)} + 1_{\mathbb{B}_{+}}\left(\ell_{+}\right) p_{B,+}\left(x_{+},\ell_{+}\right) \tag{3.6}$$

$$p_{Z_{+}}^{(\xi,\theta_{+})}\left(x_{+},\ell_{+}\right) = \frac{\bar{p}_{+}^{(\xi)}\left(x_{+},\ell_{+}\right)\psi_{Z_{+}}^{(\theta_{+}(\ell_{+}))}\left(x_{+},\ell_{+}\right)}{\bar{\psi}_{Z_{+}}^{(\xi,\theta_{+})}\left(\ell_{+}\right)} \tag{3.7}$$

The multi-target filtering density in Eq. (3.2) involves all possible combinations of newborn, disappeared, and surviving targets together with associations of new measurements to hypothesised labels [40]. To propagate Eq. (3.2), for each hypothesis (I,ξ) in the filtering density, a set of pairs $(I_{+},\theta_{+}) \in \mathcal{F}\left(\mathbb{L}_{+}\right) \times \Theta_{+}\left(I_{+}\right)$ with significant weights $\omega_{+,Z}^{(I,\xi,I_{+},\theta_{+})}$ needs to be generated without exhaustively searching the space $\mathcal{F}\left(\mathbb{L}_{+}\right) \times \Theta_{+}\left(I_{+}\right)$. A Gibbs sampler, a special case of the Metropolis Hasting Markov Chain Monte Carlo (MCMC), proposed in [40] is adopted to perform this task. This sampler is capable of computationally efficiently breaking down a complex high-dimensional problem into simple, low-dimensional problems. Particularly, in the GLMB filter, the Gibbs sampler selects significant components (thoses with the highest weights) of the GLMB filtering density only; this significantly reduces the computational cost.

Given the GLMB filtering density in Eq. (3.2), the estimated multi-target state or trajectories can be extracted [24, 31]. Note that the standard GLMB filter formulation uses the assumption on a known and fixed average intensity of clutter. In this work, this parameter is unknown and time-varying, it is estimated and bootstrapped into

the standard GLMB filter from an independently run λ-CPHD filter as introduced in Section 3.2.2. Both the GLMB and λ–CPHD filters in this section are implemented using Gaussian mixtures.

For the convenience of representation, in the following, the Gaussian distribution is denoted by $\mathcal{N}(x; m, P)$, where m and P are, respectively, the mean and covariance of variable x. The unlabelled target state is distributed according to Gaussian distribution, (i.e., $p(x, \ell) = \mathcal{N}(x, m, P)$). The evolution of the unlabelled target state follows a Gaussian transition density, that is:

$$f_+(x_+|x, \ell_+) = \mathcal{N}(x_+, F_+x, Q_+) \tag{3.8}$$

where F_+ is the matrix of state transition, and Q_+ is the covariance of process noise. The measurement likelihood of generating a noisy measurement z from a detected target is given by:

$$g_+(z|x_+, \ell_+) = \mathcal{N}(z; H_+x_+, R_+). \tag{3.9}$$

where H_+ is the measurement matrix, and R_+ is the covariance of measurement noise.

The models Eq. (3.8) and Eq. (3.9) are then substituted into Eq. (3.5),Eq. (3.6), and Eq. (3.7) to compute the GLMB filtering density. Note that, in the performance of the joint prediction update GLMB estimator, the birth process follows a labelled Poisson RFS with intensity $\nu_{B,+} = \sum_{i=1}^{n} \omega_{B,+}\mathcal{N}(z; m_{B,+}, P_{B,+})$ [24] where $m_{B,+}$ is the mean of Gaussian birth density of the birth component, and $P_{B,+}$ is the birth density covariance of the birth component. The detection probability is state-independent and assumed to be known and fixed. The clutter is distributed according to Poisson RFS with intensity $\kappa_+(z) = \lambda_c\mathcal{U}(\mathbb{Z})$ with λ_c be the clutter rate and $\mathcal{U}(\mathbb{Z})$ be a uniform density on the space $\mathbb{Z}$ of measurements.

3.2.2 Clutter rate estimation

The basic idea in the λ–CPHD filter is to consider clutter as 'clutter-generated targets' or 'false targets' that are different from actual targets, then model them using an RFS. That is, clutter targets involve new appearances, disappearances and survivals, as well as detections, misses and measurements. The set of clutter targets also exhibits a similar dynamic process as an actual target set. Since the sensor measurements involve

the information on actual targets and clutter-generated targets, the multi-targets state is a finite set of these two types of targets estimated using data given in the sequence of measurement sets. A CPHD filter extended from the ordinary CPHD recursion to accomodate the unknown information on clutter rate has been given in [96]. This filter can implement in an exact closed-form solution to the Bayesian recursion using Gaussian mixture techniques.

Using the assumption on the known detection profile, the recursion for estimating the hybrid target state yields information on the target cardinality, individual actual target states, and the unknown clutter rate. In this section, the method for estimating the clutter rate using the CPHD recursion is represented. In this CPHD recursion, the intensity functions of the actual and clutter-generated targets are separately propagated jointly alongside with the cardinality distribution of all targets.

Since there are actual and clutter-generated targets in the multi-target state space, some definitions are given to facilitate the discussion on handling the unknown clutter rate using the λ–CPHD filter. These definitions are then used to recursively compute the intensity and cardinality distribution in the λ–CPHD recursion. Denote $\mathbb{X}^{(0)}$ be the state space for clutter-generated targets; then the hybrid state space is the disjoint union of two state spaces:

$$\mathbb{X}^{(\bar{c})} = \mathbb{X}^{(1)} \uplus \mathbb{X}^{(0)}. \tag{3.10}$$

Suppose that, the actual targets and the clutter-generated targets are statistically independent, the hybrid multi-target state denoted by $X^{(\bar{c})} \in \mathcal{F}\left(\mathbb{X}^{(\bar{c})}\right)$ involves these two types of targets. Noting that these target states are the unions of corresponding surviving and new-born target states as described in Eq. (2.12). The evolution of the hybrid multi-target state at the next time step is denoted by $X_{+}^{(\bar{c})} \in \mathcal{F}\left(\mathbb{X}^{(\bar{c})}\right)$.

Similarly, clutter-generated targets are assumed to have the same spatial measurement distribution, detection and generation probabilities. Furthermore, each clutter-generated target can generate at most one measurement at each time step [96].

Let $\nu_k^{(\bar{c})}(\cdot)$ denote the posterior intensity of a hybrid multi-target state at the current

time step; then, it can be decomposable as follows:

$$\nu^{(\bar{c})}\left(x^{(\bar{c})}\right) = \begin{cases} \nu^{(1)}(x), & x^{(\bar{c})} = x \\ \nu^{(0)}(x_c), & x^{(\bar{c})} = x_c \end{cases} \tag{3.11}$$

where $\nu^{(1)}(\cdot)$ and $\nu^{(0)}(\cdot)$ are the posterior intensities for actual and clutter targets, respectively. Since the posterior intensity $\nu^{(0)}(\cdot)$ is completely characterised by the posterior mean number of clutter targets $N^{(0)}$, it is sufficient to recursively propagate $\nu^{(1)}(\cdot)$, $N^{(0)}$, and the posterior cardinality distribution of the hybrid target state $\rho^{(\bar{c})}(\cdot)$ in the CPHD filter to handle the clutter-generated targets instead of propagating .

The λ–CPHD filter can be implemented to estimate the clutter rate using Gaussian mixtures or SMC methods. This section represents the implementation of the λ–CPHD filter using the Gaussian mixture techniques described in [96]. The cardinality distribution of clutter is assumed to be binomial. The λ–CPHD filter can be implemented with the following assumptions.

• The probability distribution of each actual target state is Gaussian, (i.e., $p(x) = \mathcal{N}(x, m, P)$), and the state follows the linear Gaussian transition and measurement models as follows:

$$f_+^{(1)}(x_+|x) = \mathcal{N}(x_+, F_+x, Q_+) \tag{3.12}$$

$$g_+(z|x_+) = \mathcal{N}(z; H_+x_+, R_+). \tag{3.13}$$

where F_+, Q_+ and H_+, R_+ have been defined under Eq. (3.8) and Eq. (3.9), respectively.

• The survival probability $p_{S,+}^{(1)}(\cdot)$ and the detection probability $p_{D,+}^{(1)}(\cdot)$ are state independent.

• The PHD of the actual newborn target RFS is a Gaussian mixture, described by:

$$\nu_{B,+}^{(1)}(x_+) = \sum_{i=1}^{J\nu_{B,+}} \omega_{\nu_B,+}^{(i)} \mathcal{N}\left(x_+; m_{\nu_B,+}^{(i)}, P_{\nu_B,+}^{(i)}\right) \tag{3.14}$$

where $J_{\nu_B,+}$ is the maximum number of Gaussian components corresponding to newborn targets, $\omega_{\nu_B,+}^{(i)}$ is the weight of the i^{th} component corresponding to i^{th} newborn target, and $m_{\nu_B,+}^{(i)}$ and $P_{\nu_B,+}^{(i)}$ are the mean and covariance of the newborn target x.

Prediction : [96, Proposition 5] Given the posterior mean number of clutter generator $N^{(0)}$, posterior cardinality distribution $\rho^{(\bar{c})}$ and the predicted intensity $\nu^{(1)}$ at the current time step in the form of a Gaussian mixture:

$$\nu^{(1)}(x) = \sum_{i=1}^{J} \omega^{(i)} \mathcal{N}\left(x; m^{(i)}, P^{(i)}\right) \tag{3.15}$$

then the prediction of intensity at the next time step is also a Gaussian mixture and

$$\nu_{+}^{(1)}(x_{+}) = \nu_{B,+}^{(1)}(x_{+}) + p_{S,+}^{(1)} \sum_{j=1}^{J} \omega^{(j)} \mathcal{N}\left(x_{+}; m_{S,+}^{(j)}, P_{S,+}^{(j)}\right) \tag{3.16}$$

$$N_{+}^{(0)} = N_{B,+}^{(0)} + p_{S,+}^{(0)} N^{(0)} \tag{3.17}$$

$$\rho_{+}^{(\bar{c})}\left(n^{(\bar{c})}\right) = \sum_{j=0}^{n^{(\bar{c})}} \rho_{B,+}^{(\bar{c})}\left(n^{(\bar{c})} - j\right) \sum_{l=j}^{\infty} C_j^l \rho^{(\bar{c})}(l) (1-\phi)^{l-j} \phi^j, \tag{3.18}$$

where

$$\phi = \left(\frac{p_{S,+}^{(1)} \sum_{i=1}^{J} \omega^{(i)} + p_{S,+}^{(0)} N^{(0)}}{p_{S,+}^{(1)} \sum_{i=1}^{J} \omega^{(i)} + N^{(0)}} \right) \tag{3.19}$$

and $\nu_{+}^{(1)}(x_{+})$ is given in Eq. (3.14),

$$m_{S,+}^{(j)} = F m^{(j)}, \tag{3.20}$$

$$P_{S,+}^{(j)} = Q + F P^{(j)} F^T. \tag{3.21}$$

Update : [96, Proposition 6] Given $\nu_{+}^{(1)}(x_{+})$ is a Gaussian mixture given by:

$$\nu_{+}^{(1)}(x_{+}) = \sum_{i=1}^{J_{+}} \omega_{+}^{(i)} \mathcal{N}\left(x_{+}; m_{+}^{(i)}, P_{+}^{(i)}\right) \tag{3.22}$$

and given the measurement set Z_{+}, the updated values of the intensity, mean number of clutter-generated targets and hybrid cardinality distribution are given as follows

$$\nu_+^{(1)}(x_+|Z_+) = \nu_+^{(1)}(x_+)\frac{q_{D,+}^{(1)}(x_+)\frac{\left\langle \Upsilon_+^{(1)}\left[\nu_+^{(\bar{c})};Z_+\right],\rho_+^{(\bar{c})}\right\rangle}{\left\langle \Upsilon_+^{(0)}\left[\nu_+^{(\bar{c})};Z_+\right],\rho_+^{(\bar{c})}\right\rangle}}{\sum_{i=1}^{J_+}\omega_+^{(i)}+N_+^{(0)}} + \sum_{z\epsilon Z_+}\sum_{j=1}^{J_+}\omega_{D,+}^{(j)}(z)\mathcal{N}\left(x_+,m_+^{(j)}(z),P_{+|Z_+}^{(j)}\right), \tag{3.23}$$

$$N_{+|Z_+}^{(0)} = \frac{q_{D,+}^{(0)}(x_+)\frac{\left\langle \Upsilon_+^{(1)}\left[\nu_+^{(\bar{c})};Z_+\right],\rho_+^{(\bar{c})}\right\rangle}{\left\langle \Upsilon_+^{(0)}\left[\nu_+^{(\bar{c})};Z_+\right],\rho_+^{(\bar{c})}\right\rangle}N_+^{(0)}}{\sum_{i=1}^{J_+}\omega_+^{(i)}+N_+^{(0)}} + \sum_{z\epsilon Z_+}\frac{p_{D,+}^{(0)}(x_+)g_+^{(0)}(z)}{p_{D,+}^{(0)}N_+^{(0)}g_+^{(0)}(z)+p_{D,+}^{(1)}\sum_{i=1}^{J_+}\omega_+^{(i)}q_+^{(j)}(z)}N_+^{(0)} \tag{3.24}$$

$$\rho_{+|Z_+}^{(\bar{c})}\left(n^{(\bar{c})}\right) = \begin{cases} 0 & n^{(\bar{c})} < |Z_+| \\ \frac{\rho_+^{(\bar{c})}(n^{(\bar{c})})\Upsilon_+^{(0)}\left[\nu_+^{(\bar{c})};Z_+\right](n^{(\bar{c})})}{\left\langle \rho_+^{(\bar{c})},\Upsilon_+^{(0)}\right\rangle} & n^{(\bar{c})} \geq |Z_+|, \end{cases} \tag{3.25}$$

where

$$\Upsilon_+^{(u)}\left[\nu_+^{(\bar{c})};Z_+\right]\left(n^{(\bar{c})}\right) = \begin{cases} 0 & n^{(\bar{c})} < |Z_+|+u \\ P_{|Z_+|+u}\Phi^{n^{(\bar{c})}-(|Z_+|+u)} & n^{(\bar{c})} \geq |Z_+|+u \end{cases} \tag{3.26}$$

$$\Phi_+ = 1 - \frac{p_{D,+}^{(1)}\sum_{i=1}^{J_+}\omega_+^{(i)}+p_{D,+}^{(0)}N_+^{(0)}}{\sum_{i=1}^{J_+}\omega_+^{(i)}+N_+^{(0)}}, \tag{3.27}$$

$$\omega_{D+}^{(j)}(z) = \frac{p_{D,+}^{(1)}\omega_+^{(j)}q_+(z)}{p_{D,+}^{(0)}N_+^{(0)}g_+^{(0)}(z)+p_{D,+}^{(1)}\sum_{i=1}^{J_+}\omega_+^{(i)}q_+^{(j)}(z)}, \tag{3.28}$$

$$q_+^{(j)}(z) = \mathcal{N}\left(z;H_+m_+^{(j)},H_+P_+^{(j)}H_+^T+R_+\right), \tag{3.29}$$

$$m_+^{(j)}(z) = m_+^{(j)}+K_+^{(j)}\left(z-H_+m_+^{(j)}\right), \tag{3.30}$$

$$P_{+|Z_+}^{(j)} = \left[I-K_+^{(j)}H_+\right]P_+^{(j)}, \tag{3.31}$$

$$K_+^{(j)} = P_+^{(j)}H_+^T\left[H_+P_+^{(j)}H_+^T+R_+\right]^{-1}. \tag{3.32}$$

The estimated mean number of actual targets and estimated mean clutter rate are given

by

$$\hat{N}_{+}^{(1)} = \sum_{j=1}^{J_{+}} \omega_{+}^{(j)}. \tag{3.33}$$

$$\hat{\lambda}_{c+} = N_{+}^{(0)} p_{D,+}^{(0)}. \tag{3.34}$$

While performing CPHD filtering for an unknown clutter rate, the total number of mixture components exponentially increases with time; then, the pruning and merging of these mixture components must be implemented. Further, the truncation of posterior cardinality at a sufficiently high number of components enables a tractable propagation [96]. The truncation implementation is, therefore, employed. These procedures are similar to those of the conventional CPHD and PHD filters [18, 78].

3.3 Numerical study

The implementation of the Bootstrapped-GLMB filter is compared to the other three filters: the λ−CPHD filter [96], the ideal GLMB filter [24], and the robust GLMB filter [131] to validate its accuracy and effectiveness. These comparisons are conducted with theoretical linear and nonlinear dynamic models in an unknown clutter rates environment.

The adjective $'ideal'$ is used with the meaning that the filter runs with known and fixed parameters of clutter rate and probability of detection. The "Robust-GLMB filter" is defined for the filter given in [131] with a known detection rate and an assumed unknown clutter rate. Further, clutter statistics in both the ideal-GLMB and Robust-GLMB are assumed to follow a Poisson RFS with uniform spatial density.

For comparison of the Bootstrapped-GLMB filter with the other three filters mentioned, the optimal sub-pattern assignment (OSPA) [133] and the OSPA$^{(2)}$ [26] are applied. Specifically, the OSPA metric is used to calculate the distance (error) between the true set of targets and the estimated set of targets at each time step of the filtering process. The OSPA error consists of two components: the localisation and cardinality errors.

The OSPA distance $\bar{d}_{p}^{(c_o)}$ between two finite sets $X = \{x_1, \ldots, x_m\}$ and $Y = \{y_1, \ldots, y_n\} \in$

$\mathcal{F}(\mathbb{X}), (m \leq n)$ is defined as follows

$$\bar{d}_p^{(c_o)}(X,Y) \triangleq \left(\frac{1}{n}\left(\min_{\pi\in\prod_n}\sum_{i=1}^{m} d^{(c_o)}\left(x_i, y_{\pi(i)}\right)^p + c_o^p(n-m)\right)\right)^{\frac{1}{p}} \tag{3.35}$$

where order parameter $p \geq 1$ and cut-off parameter $c_o > 0$ determine the sensitivity to outliers and the weighting for errors due to cardinality and localisation, respectively [133]. $d^{(c_o)}(x,y) \triangleq min(c_o, \|x-y\|), \forall x, y \in \mathbb{X}$, and $\prod_n$ denote the set of permutation on $\{1,2,\ldots,n\}, n \in \mathbb{N}$.

The OSPA$^{(2)}$ metric is constructed from the OSPA metric to capture errors between two sets of tracks over a certain period of time. From the OSPA metric, given two tracks $f, g \in \mathbb{U}$ where $\mathbb{U}$ is the space of tracks, a base distance is defined as a time-averaged OSPA distance over a window of length l_w as follows [26]

$$\tilde{d}^{(c_o)}(f,g) \triangleq \frac{1}{l_w}\sum_{t=1}^{l_w} d^{(c_o)}\left(\{f(t)\}, \{g(t)\}\right) \tag{3.36}$$

Given two sets of tracks $X = \left\{f^{(1)}, f^{(2)}, \ldots, f^{(m)}\right\}$, $Y = \left\{g^{(1)}, g^{(2)}, \ldots, g^{(n)}\right\}$, where $X, Y \in \mathcal{F}(\mathbb{U})$ and $\mathcal{F}(\mathbb{U})$ is the space of all finite subsets of $\mathbb{U}$, the OSPA$^{(2)}$ metric is given as follows [26]

$$\tilde{d}_p^{(c_o)}(X,Y) \triangleq \left(\frac{1}{n}\left(\min_{\pi\in\prod_n}\sum_{i=1}^{m} \tilde{d}^{(c_o)}\left(f^{(i)}, g^{(\pi(i))}\right)^p + c_o^p(n-m)\right)\right)^{\frac{1}{p}} \tag{3.37}$$

The OSPA metric captures the differences between the set of actual targets and that of the estimated targets among all four filters. The OSPA$^{(2)}$ metric is used in three GLMB filters to capture the difference between the true and estimated sets of target tracks over a certain time window. Since the CPHD filter estimates a set of target states at each scan only, the The OSPA$^{(2)}$ metric cannot be applied to this filter. In this section, both OSPA and OSPA$^{(2)}$ have the norm order of $p = 1$ and cut-off of $c_o = 100m$ for linear and nonlinear scenarios. The window length for the OSPA$^{(2)}$ metric is set at $l_w = 10$ time steps .

3.3.1 Linear dynamic model

For the experiment with linear dynamic model, the tracking scenario involved 12 targets that follow a linear Gaussian model and move with constant velocities. The ground truths of the start and end positions of each target track are demonstrated in Figure 3.2. Each kinematic part of target state is described by a $4D$ vector with components be the target's position and velocity defined in planar coordinates, i.e, $x_k = [p_x, p_y, \dot{p}_x, \dot{p}_y]^T$, where T is the transpose operator. The information on the position of a target at each time step is captured in the noisy measurement vector $z_k = [z_x, z_y]^T$. The linear Gaussian transition density and measurement model for a single target are given as follows:

$$f_+(x_+|x) = \mathcal{N}(x_+; Fx, Q) \tag{3.38}$$

$$h(z|x_+) = \mathcal{N}(z; H_+x_+, R_+) \tag{3.39}$$

where $F = \begin{bmatrix} I_2 & tI_2 \\ 0_2 & I_2 \end{bmatrix}; Q = \sigma_\nu^2 \begin{bmatrix} \frac{t^4}{4}I_2 & \frac{t^3}{2}I_2 \\ \frac{t^3}{2}I_2 & t^2I_2 \end{bmatrix}; H = \begin{bmatrix} I_2 & 0_2 \end{bmatrix}$, $R = \sigma_\varepsilon^2 I_2$. I_n, 0_n, and t denote the $n \times n$ identity and zero matrices, and sampling time, respectively. The standard deviations of the process noise and measurement noise are set at $\sigma_\nu = 5m/s^2$ and $\sigma_\varepsilon = 10m$.

An area of $[-1000, 1000]m \times [-1000, 1000]m$ is chosen as the surveillance of interest, that is, the volume of the surveillance area is $V = 4 \times 10^6 \left(m^2\right)$. The total time steps set at $K = 100$ are simulated with $t = 1s$.

New births for actual targets are assumed to be distributed with labelled Poisson RFS distribution with intensity $\nu_B^{(1)}(x) = \sum_{i=1}^4 \omega_B \mathcal{N}\left(x; m_B^{(i)}, P_B\right)$ where $\omega_B = [0.04, 0.02]$, $m_B^{(1)} = [0, 0, 0, 0]^T$, $m_B^{(2)} = [400, -600, 0, 0]^T$, $m_B^{(3)} = [-800, -200, 0, 0]^T$, $m_B^{(4)} = [-200, 800, 0, 0]^T$ and $P_B = \text{diag}([10, 10, 10, 10]^T)^2$. The survival probability is fixed at $p_S = 0.99$.

In this linear tracking scenario, the detection probability for sensor measurements is $p_D^{(1)} = 0.98$. For all three filters, clutter returns are generated to a binomial cardinality with $N^{(0)} = 100, p_D^{(0)} = 0.7$, and clutter probability density $1/V$ is uniform spatial over the surveillance region. The mean value of the clutter rate is then 70 points per scan, and the average clutter intensity is $\gamma_c^{(0)} = N^{(0)} p_D^{(0)}/V = 1.75 \times 10^{-5} \left(m^{-2}\right)$. Note that

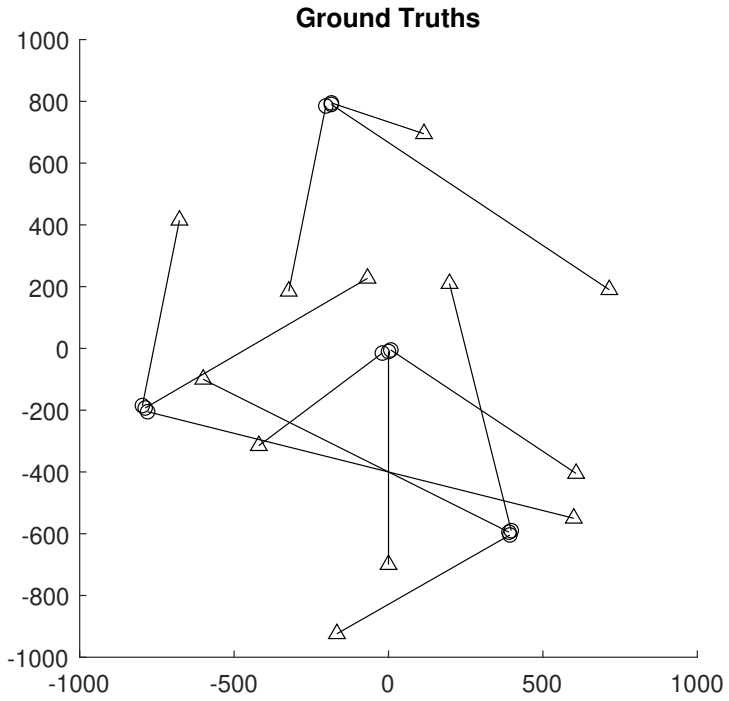

Figure 3.2: Ground truths of the linear tracking scenario

this value is unknown to the filter. The clutter-generated targets are modelled to the filter with the mean rate of newborn $N_B^{(0)} = 30$, while the deaths are given by the survival probability of $p_S^{(0)} = 0.9$, and returns are given by detection probability $p_D^{(0)} = 0.4$. The density of clutter returns $g_+^{(0)}(z)$ is assumed to be uniform in the space of measurements. For the initialisation of the filter, the initial value of intensity for actual targets is set at zero; then, the number of actual targets is zero. The initial clutter rate is given by subtracting of the total received measurement at the first time scan from the average newborn targets and the rate of detections for actual targets.

Note that, the ideal-GLMB filter uses mean clutter rate of $\lambda_c = 70$ returns at each scan, the average intensity $\gamma_c = 1.75 \times 10^{-5} \left(m^{-2}\right)$, and the detection probability $p_D = 0.98$ as known and fixed parameters for its implementation.

Pruning and merging thresholds for Gaussian components at each scan are 10^{-5} and $4m$, respectively. The highest number of Gaussian terms is set at $J_{max} = 100$, and the joint clutter-actual target cardinality distribution is $N_{max} = 300$ terms.

The evaluation of the implementation of the four filters using the OSPA metric

over 100 Monte Carlo (MC) runs is shown in Figure 3.3. While all filters estimate the target state at each time step in the clutter environment well, the implementation of the Bootstrapped-GLMB filter is slightly better than the robust-GLMB filter and the λ−CPHD filter. Since the ideal-GLMB is assumed to run with the correct clutter rate, it has the lowest OSPA errors among all four filters.

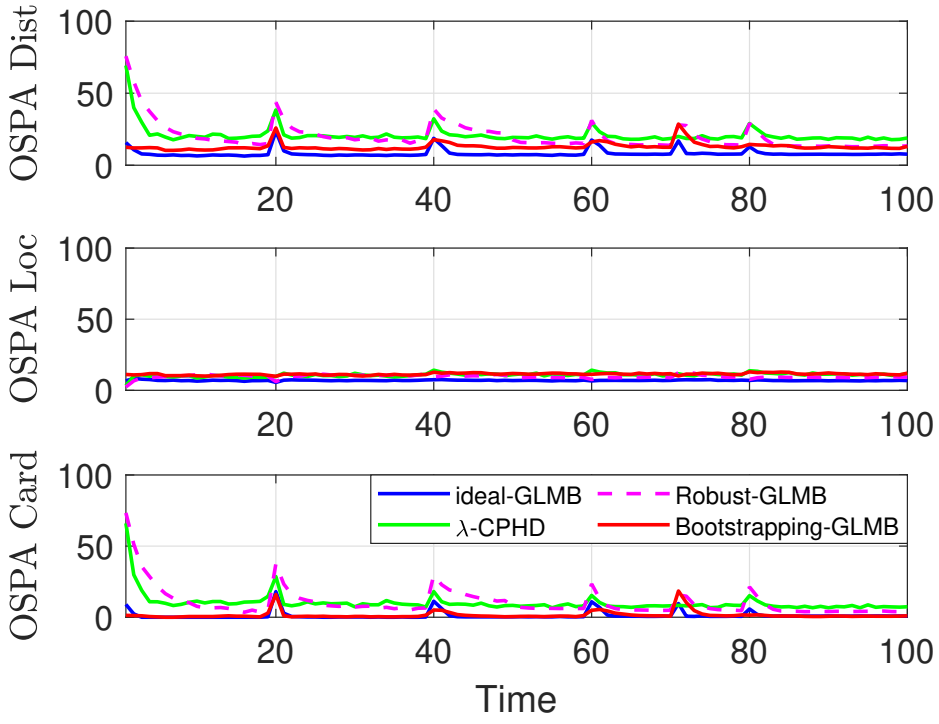

Figure 3.3: Linear tracking scenario: Mean OSPA errors for the four filters.

The comparison of trajectory estimates among three GLMB filters using the OSPA$^{(2)}$ metric is shown in Figure 3.4. In terms of the miss distance, using OSPA$^{(2)}$ on the estimated target positions, the best performance is still the ideal-GLMB filter; however, there is a small difference between the implementation of the Bootstrapped-GLMB and that of the Robust-GLMB filter. This result is reasonable since the ideal-GLMB is provided with the correct clutter rate, and the other two GLMB filters must estimate this parameter in their implementation. The same number of maximum hypotheses were used for our Bootstrapped-GLMB and the Robust-GLMB filters. However, since the Robust-GLMB filter requires more hypotheses to sufficiently capture the data associations of the actual and clutter targets, the number of hypotheses is exhausted. Hence, it does not perform as well as our method, which only needs to perform data association

for actual targets. The cardinality estimations are demonstrated in Figure 3.5. It can be observed that the proposed Bootstrapped- GLMB filter tends to overestimate the number of targets when new-born targets appear. This phenomenon might be due to the high number of clutter measurements and the proposed filter underestimates the clutter rate. However, this underestimation is unnoticeable and the filter converges to the correct number of targets rapidly.

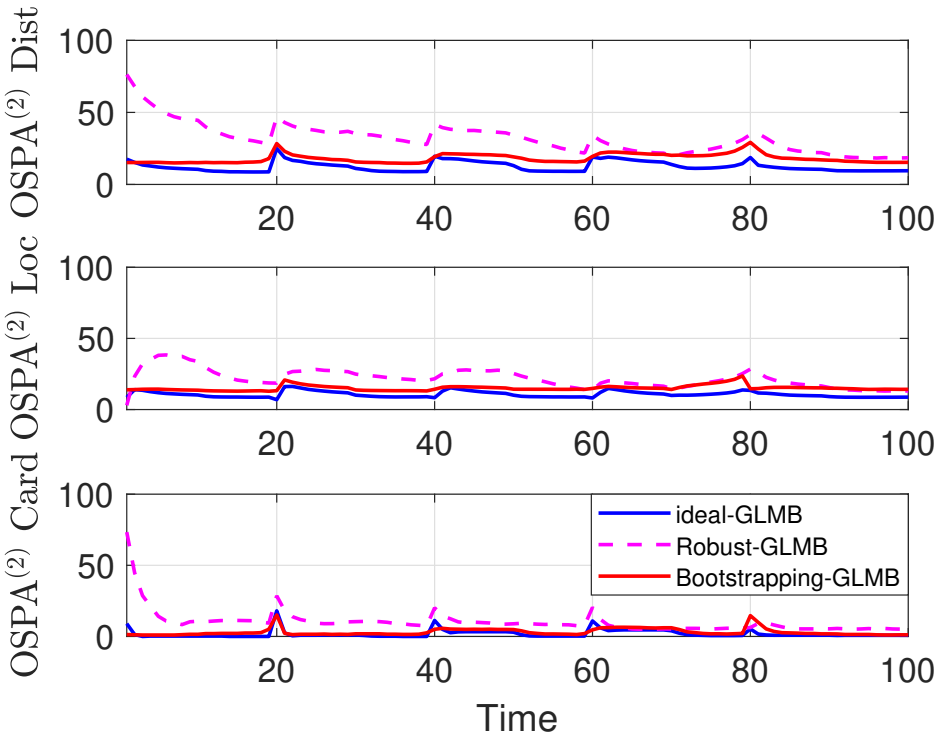

Figure 3.4: Linear tracking scenario: Mean OSPA$^{(2)}$ errors for three GLMB-based filters.

3.3.2 Nonlinear dynamic model

This subsection describes how the four filters are implemented in the nonlinear dynamic model to track 10 marine ships using Doppler measurements with an unknown clutter rate. Each ship is assumed to move with a constant turn motion model. The Doppler measurement system involves two spatially distributed receivers and a cooperative transmitter. The ground truths, start and end positions of the target trajectories, as well as the positions of the sensing equipment, are shown in Figure 3.6. Each ship is presented by a $5D$ state vector x in the surveillance area $x = \left[\mu, \dot{\mu}, \lambda, \dot{\lambda}, \alpha\right]^T$, where: μ and λ are longitudinal and latitudinal positions of the target, respectively, with $\dot{\mu}$ and $\dot{\lambda}$ being their corresponding velocities and α is the course (or turn rate) of the tar-

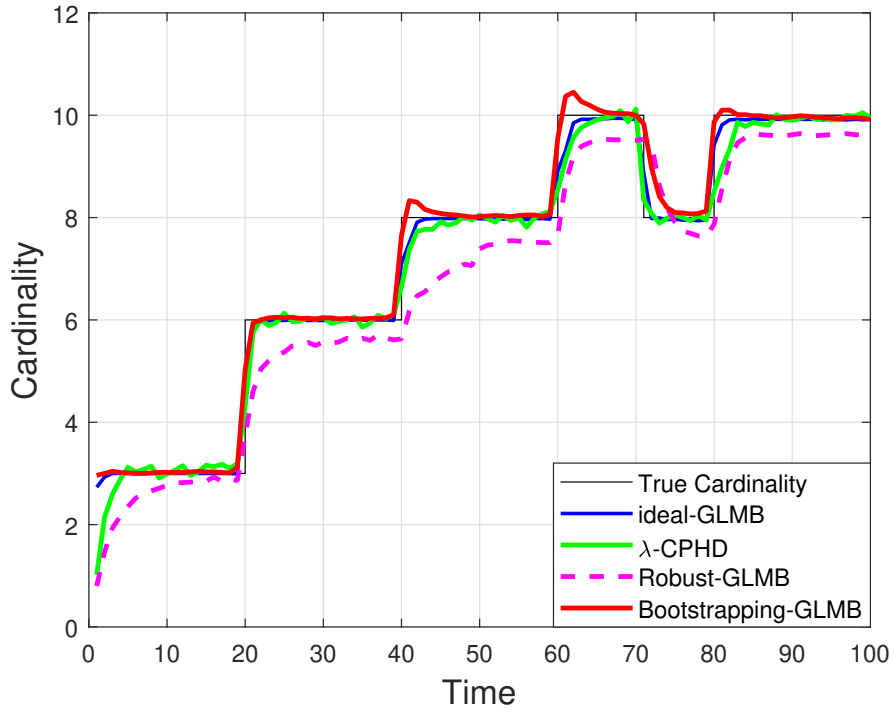

Figure 3.5: Linear tracking scenario: Mean estimated cardinality for the four filters.

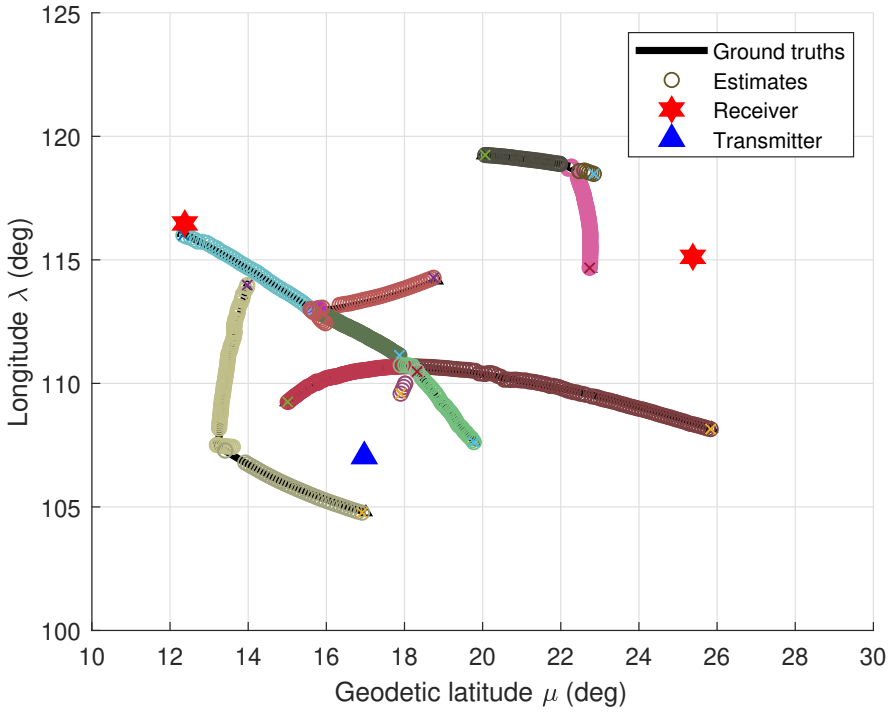

Figure 3.6: The groundtruths of the marine ships tracking scenario ($\circ$: initial track position; Δ : end track position).

get. Note that the longitudinal and latitudinal measurements are in degrees (°) and the distance, speed and time are given in nautical miles (M), knots (kn), and hours (h), respectively. The transition model for a single target is a Gaussian:

$$f_+(x_+|x) = \mathcal{N}(x_+; F(x,\alpha)\,x, Q) \tag{3.40}$$

where[1]

$$F(x,\alpha) = \begin{bmatrix} 1 & \frac{\sin(\alpha t)}{\alpha} & 0 & \frac{(\cos(\alpha t)-1)}{\alpha} & 0 \\ 0 & \cos(\alpha t) & 0 & -\sin(\alpha t) & 0 \\ 0 & -\frac{(\cos(\alpha t)-1)}{\alpha} & 1 & -\frac{\sin(\alpha t)}{\alpha} & 0 \\ 0 & \sin(\alpha t) & 0 & \cos(\alpha t) & 0 \\ 0 & 0 & 0 & 0 & 1 \end{bmatrix}; Q = \begin{bmatrix} \sigma_\alpha^2 G G^T & 0 \\ 0 & \sigma_v^2 \end{bmatrix}, G = \begin{bmatrix} \frac{t^2}{2} & 0 \\ t & 0 \\ 0 & \frac{t^2}{2} \\ 0 & t \end{bmatrix}. \tag{3.41}$$

The sample period is set at $t = 0.15\,(h)$ and the standard deviations of speed noise and course noise are $\sigma_v = 2\,(kn)$ and $\sigma_\alpha = \pi/180(rad/h)$, respectively. The survival probability is $p_S = 0.95$, and the prediction for the augmented part of the state is set according to coefficient $k_\beta = 1.1$.

The measurement system uses the Doppler effect to measure the speed of a target at a distance by computing the altered frequency of the returned signals that originate from the emitting pulses of radio signals and are reflected to a radar after reaching the target [134]. Specifically in this work, each observed measurement is a $2D$ vector $z = \left[z^{(1)}, z^{(2)}\right]$, where $z^{(s)}$ is the Doppler measurement observed from the s^{th} receiver which is computed as:

$$z^{(s)} = -v^T \left(\frac{p - p_r^{(s)}}{\left\| p - p_r^{(s)} \right\|} + \frac{p - p_t}{\|p - p_t\|} \right) \frac{f_t}{c} C + w, \tag{3.42}$$

in which $p = [\mu, \lambda]^T$ and $v = \left[\dot{\mu}, \dot{\lambda}\right]^T$ are the position and velocity of a target; $p_t = [\mu_t, \lambda_t]^T$ and $p_r^{(s)} = [\mu_r^{(s)}, \lambda_r^{(s)}]^T$ are the positions of the transmitter and the s^{th} receiver,

[1] Equation Eq. (3.41) is resulted from the assumption that the surveillance area is far from the two poles.

respectively. Specifically:

$$p_t = \begin{bmatrix} 16°58'16''N & 107.02'48''E \end{bmatrix}^T,$$
$$p_r^{(1)} = \begin{bmatrix} 12°22'43''N & 116°28'25''E \end{bmatrix}^T,$$
$$p_r^{(2)} = \begin{bmatrix} 25°22'47''N & 115°07'19''E \end{bmatrix}^T.$$

where w be zero-mean Gaussian noise; $w \sim \mathcal{N}(\cdot; 0, R)$, with covariance $R = \text{diag}\left(\begin{bmatrix} 1Hz^2 & 1Hz^2 \end{bmatrix}^T\right)$, $f_t = 300MHz$ be the frequency of the signal emitted from the transmitter; $c = 3 \times 10^8\,(m/s)$ be the light speed; and $C \approx 1.94$ be the unit conversion constant.

Note that in this experiment, each target is dynamic in its direction which is different from the other targets. Hence, the value of measurement $z^{(s)}$ in Eq. (3.42) could either negative or positive in the known interval $[-f_0, +f_0]$ of the Doppler sensor. Two receivers share the same measurement space of $[-200Hz, 200Hz]$. Both the state equation and the measurement equation are highly nonlinear.

The newborn targets are assumed to be distributed with LMB RFS distributions of parameters $f_B(x) = \left\{r_B^{(i)}, p_B^{(i)}\right\}_{i=1}^4$ where the common existence probabilities are $r_B^{(1)} = r_B^{(2)} = 0.04$,$r_B^{(3)} = r_B^{(4)} = 0.02$, and $p_B^{(i)}(x) = \mathcal{N}\left(x, \hat{x}_B^{(i)}, P_B\right)$ with

$$\hat{x}_B^{(1)} = [15.6°N, 0, 113°E, 0, 0]^T;$$
$$\hat{x}_B^{(2)} = [13.2°N, 0, 107.5°E, 0, 0]^T$$
$$\hat{x}_B^{(3)} = [18.2°N, 0, 110.7°E, 0, 0]^T;$$
$$\hat{x}_B^{(4)} = [22.3°N, 0, 118.8°E, 0, 0]^T;$$
$$P_B = diag\left(\left[2'N, 30\,(kn), 2'E, 30\,(kn), 6\pi/180\left(radh^{-1}\right)\right]\right).$$

The surveillance area is $S_r = [10°N - 30°N, 100°E - 125°E]$. The probability that the sensor can detect a target and generate a measurement is set to $\tilde{p}_D^{(1)} = 0.98$, and clutter returns are generated according to a binomial cardinality distribution with parameters $N^{(0)} = 70$ and $p_D^{(0)} = 0.4$. Therefore, the mean clutter rate is 28 points per scan. Table 3.1 tabulates the initial states of 10 vessels with a random time of birth and death. The average turn rate is set to $\bar{\alpha} = \pi/90(rad/h)$.

Target	μ	λ	$\dot{\mu}$	$\dot{\lambda}$	$\alpha(rad/h)$	Time of birth(h)	Time of Death (h)
1	$18°12'15''$	$110°42'06''$	32	-5	$-5\bar{\alpha}/8$	1	100
2	$15°37'52''$	$113°57'14''$	13	-9	$-\bar{\alpha}/2$	5	80
3	$18°11'40''$	$110°41'43''$	-18	0	$2\bar{\alpha}$	10	90
4	$13°13'52''$	$107°29'31''$	2	32	$-\bar{\alpha}/4$	20	100
5	$22°17'11''$	$118°49'24''$	6	-20	$-5\bar{\alpha}/6$	20	100
6	$22°17'58''$	$118°48'05''$	-22	6	$3\bar{\alpha}/4$	30	70
7	$18°12'15''$	$110°42'06''$	15	-30	$\bar{\alpha}/8$	30	70
8	$15°35'57''$	$113°01'06''$	-30	32	$3\bar{\alpha}/5$	45	85
9	$13°11'44''$	$107°30'19''$	28	-30	$5\bar{\alpha}/3$	55	100
10	$15°36'04''$	$112°53'30''$	30	5	$7\bar{\alpha}/4$	55	100

Table 3.1: Target initial states

The implementation of the Bootstrapped-GLMB filter is compared with the three filters (the ideal-GLMB filter [24], the λ–CPHD filter [16] and the Robust-GLMB filter [131]). In this experiment, the ideal-GLMB filter uses the fixed and known parameters $p_D = 0.98$ and $\lambda_c = 30$ points per scan. However, the mean clutter rate λ_c is unknown to the other three filters. All filters are initiated with zero intensity of actual targets and no number of actual targets with the average birth $N_B^{(0)} = 30$. The initial clutter rate is calculated based on the total measurements received at the first time step and the corresponding values for average birth and detection rate of actual targets for the linear scenario given in Section 3.3.1.

The comparison results using the OSPA metric are illustrated in Figure 3.7. All filters accurately estimate target cardinality. In terms of the errors on OSPA miss distance and localisation, the results of the Bootstrapped-GLMB are almost identical to those of the ideal-GLMB. The ideal-GLMB filter has the best performance on the OSPA metric of all filters. This best performance is due to the correct parameters supplied to the ideal-GLMB filter. While the performances of the λ–CPHD and the Robust-GLMB are nearly coincident, they are significantly worse than those of the ideal-GLMB filter. The Robust-GLMB filter shows a higher number of OSPA errors than the Bootstrapped-GLMB filter. This result might be the consequence of the additional data association performed in the GLMB recursion due to the measurements of clutter targets. More importantly, the λ–CPHD inherites the CPHD filter downside of the spooky effect, which causes this filter to temporarily drop tracks due to missed detections and to declare multiple estimates for existing tracks in place of dropped tracks.

The results of OSPA$^{(2)}$ evaluation with window length $l_w = 10$ among three GLMB-based filters are given in Figure 3.8. The ideal-GLMB filter has the smallest OSPA$^{(2)}$ errors as it is assumed using the correct value of clutter rate. The Bootstrapped-GLMB filter performes target tracking better than the Robust-GLMB in the presence of an unknown clutter rate. By comparison, the Bootstrapped-GLMB filter performes better on the OSPA$^{(2)}$ miss distance and cardinality components than the Robust-GLMB filter. This might arise as while the Robust-GLMB filter uses the same number of hypotheses as the other two GLMB filters, it needs a higher number of hypotheses to handle measurement clutter targets. The cardinality statistics for three filters over 100 MC trials are shown in Figure 3.9. This result could be foreseen from OSPA cardinality and OSPA$^{(2)}$

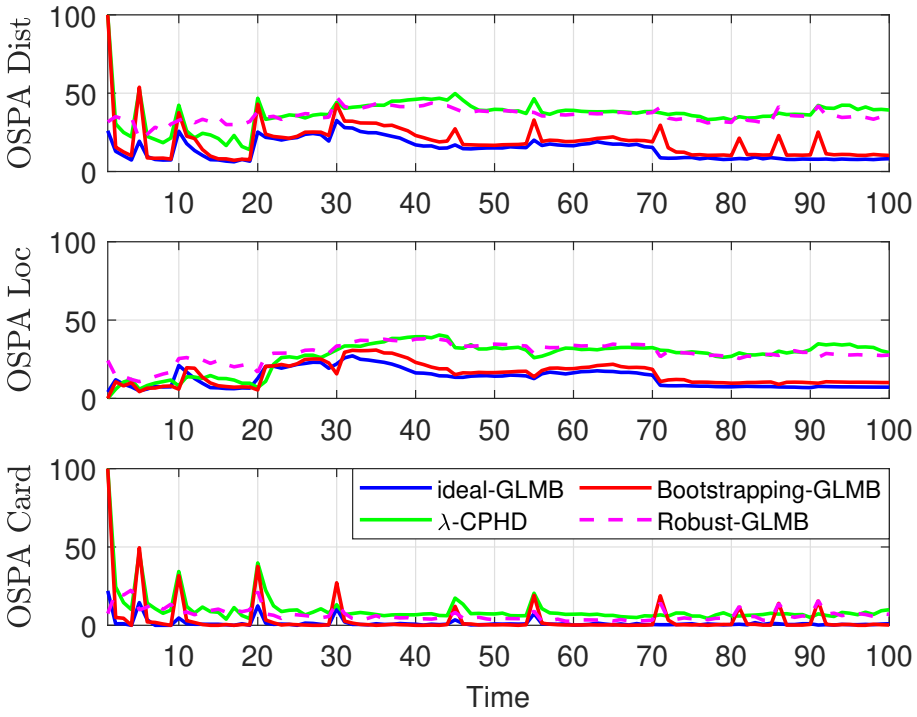

Figure 3.7: Comparison of cardinality, location and distance errors for the four filters using the OSPA metric.

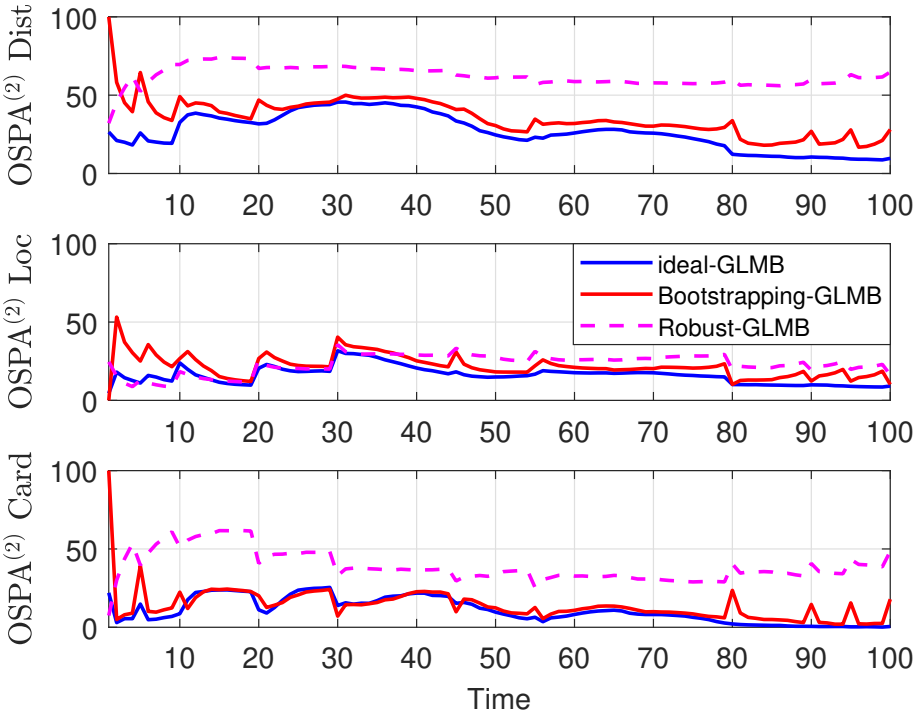

Figure 3.8: Comparison of cardinality, location and distance errors for the three GLMB - based filters using the OSPA$^{(2)}$ metric.

cardinality. In this tracking scenario, the Bootstrapped-GLMB and ideal-GLMB outperform the Robust-GLMB and the λ–CPHD filters on the mean estimated cardinality versus time.

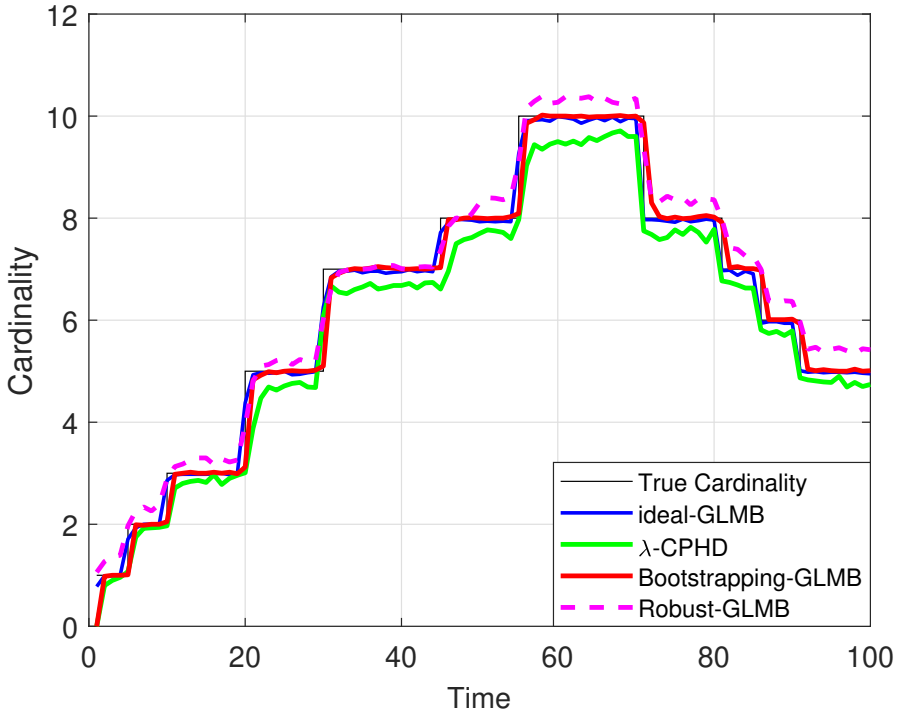

Figure 3.9: Cardinality estimations for the four filters.

3.4 Conclusion

This chapter presents the tracking algorithm using the bootstrapping method, which combines the advantages of the existing filters to handle the unknown information on clutter rate. Using the GLMB filter with an unknown clutter rate requires performing data association for both actual targets and measurement clutter targets which increases computational expense. The λ–CPHD filter, therefore, is applied to run independently with the conventional GLMB filter to accomodate the random variation of the clutter rate only. Then, the conventional GLMB filter uses this estimated clutter rate as a known parameter for tracking targets with their identities. Using this simple combination of the λ–CPHD and the GLMB filters, the computational expense from the tracking implementation of the GLMB filter with an unknown clutter rate is significantly reduced compared to that of the Robust-GLMB filter. The effectiveness and accuracy of this combination are validated in Section 3.3 for the linear and non-linear

tracking scenarios. While the former simulates the theoretical linear tracking problem, the latter tracks multiple marine ships using Doppler measurements. These experiments show that the Bootstrapped-GLMB filter can accurately estimate targets in an unknown clutter rate environment.

CHAPTER 4

ADAPTIVE TRACKING USING THE BOOTSTRAPPING METHOD

This chapter extends the work described in Chapter 3 to provide an online adaptive multi-target tracker, developed from the Gibbs sampler - based efficient GLMB filter, that:

- does not need prior information of detection probability
- does not need prior information of joint detection probability and clutter rate
- can initiate new tracks without prior information of birth locations.

Specifically, the unknown detection probability is first considered in the bootstrapping method by using the p_D–CPHD filter technique given in [96]. Second, this unknown parameter and the unknown clutter rate are jointly estimated by an independent, robust CPHD filter [96]. The resulting values are then bootstrapped to a standard GLMB filter [40] for filtering process. Conversely, the method of using the measurement-driven birth model proposed in [101] is adopted to initiate new tracks at each time step. The information on measurement-to-track association is obtained from the GLMB filter. In addition to not requiring prior knowledge of detection probability, clutter rate and parameters of newborn targets' model, the proposed algorithm in this work inherits all advantages of a labelled RFS filter. The results of this chapter have been published in the author's journal articles [70, 71] and [72].

Section 4.1 briefly introduces some existing methods for tracking with unknown detection probability, jointly unknown detection profile and clutter rate, and unknown birth model. In Section 4.2, the techniques to accommodate the unknown detection profile solely and the unknown background (i.e., the jointly unknown detection pro-

file and clutter rate) are presented in Section 4.2.1 and Section 4.2.2, respectively. Section 4.2.3 extends the technique reported in Section 4.2.2 to solve the problem of an unknown background and an unknown birth model. Section 4.3 demonstrates the implementation and efficacy of the proposed algorithm using using numerical studies of linear and nonlinear models. Finally, Section 4.4 concludes some main points of this chapter.

4.1 Introduction

In the context of multi-target tracking, adaptive tracking refers to the task of tracking multiple targets with unknown information on the probability of target detection, clutter statistics, and locations of newborn targets. This problem is generally hard to solve, because of the increases in state-space dimension and uncertainty. For an unknown target's detection probability, current approaches accommodate the this parameter by augmenting it into the single-target state, then it is jointly estimated alongside with the single-target state in the augmented state space. Conversely, the clutter rate is estimated by considering clutter as the false targets, which is assumed to be different from and independent of the actual targets. Then, by estimating the clutter set, the clutter profile can be inferred as described in Section 3.1.Despite the difficulties, several filtering approaches used the concept of the RFSs have been proposed to tackle this adaptive tracking problem in the literature. In [135], the authors introduced a method to estimate the detection probability online based on the standard CPHD filter. This method was then further investigated in additionally estimating the clutter rate as presented in [96]. The resultant algorithm of this investigation is referred to as the robust CPHD filter. Several approaches constructed based on the other available filters have also been introduced to estimate these two unknown parameters on-the-fly such as the Kronecker delta mixture and Poisson (KDMP) filter and the MeMBer filter [129, 132, 136]. Ong et al. [45], used a new detection model for multiple cameras with varying detection probability to track people in a $3D$ setting. Recently, a variation of the standard GLMB filter has been presented in [131] to address the problem of estimating the unknown information on the background parameters (i.e., the probability of target detection and clutter rate). Nonetheless, since clutter targets are also included in the data association, this filter requires large computational memory.

In addition to the two mentioned parameters, the third parameter that significantly

affects the accuracy of the tracking algorithm is the model of newborn target locations (i.e., the model for track initiations). In most of the RFS-based filtering algorithms, the prior knowledge about the locations and number of newborn targets is assumed to be known and fixed. The other assumption on homogeneity of the newborn targets in the field of view is also given to reduce the challenge in the initiation of newborn target tracks. However, newborn targets can appear randomly in time and places with unknown number in the surveillance area. Furthermore the intensity of newborn targets is unknown in practice. Consequently, these assumptions may not hold in practice and lead to the inaccuracy and inefficiency of the tracker such as biased prediction, large computational cost, high clutter rate and deferred confirmation of newborn targets [137]. Moreover, the convergent rate and matching time of the estimates and the actual targets rely on the correctness of the track initiation. Hence, it is desired to model the newborn target tracks from the measurement data.

To resolve unknown parameters of the birth model, Maggio and Cavallaro [138] proposed using the PHD filter to spatially adapt new births and clutter intensities using the Gaussian mixture model. Based on the SMC-PHD/CPHD filter, Ristic et al. [139] proposed a method to adapt with the variation in the intensity of newborn targets at each time scan by distinguishing the newborn and persistent targets using the measurement-driven birth intensity. Beard et al. [140] proposed a method acommodating the benefit of measurement origins in the state space to initiate the tracks of newborn targets. This method is resulted in a partially uniform birth model applying for the PHD and CPHD filtering recursions. Huang et al. [137] introduced a discrete kernel estimator with an exponential weighted moving average scheme to estimate the intensity and cardinality distribution of the newborn targets. The estimated target birth intensity and cardinality are then fed back to the GM-CPHD filter for filtering at each time step. Further, in [141], and [101], Reuter et al., respectively, proposed the use of measurement-driven birth models for the cardinality balanced MeMBer filter and the LMB filter. Lin et al. [142] presented a measurement-driven birth model to reduce the dependence on a prior knowledge of the newborn target distribution for the GLMB filter by adatively generating newborn targets from the measurement data. Beard et al. [26] used the measurement-driven approach to generate birth intensities to track over a million targets in a large-scale surveillance region using the GLMB filter.

Recently, a method proposed in [143] can tractably initialise new tracks by extending the measurement-driven birth model given in [101] and [142] in the multiple sensor GLMB filtering context.

4.2 Bootstrapped GLMB filter

This section describes the detailed techniques of the Bootstrapped-GLMB filter that has the capability of tracking multiple targets with minimum prior knowledge from users. Specifically, the technique that handles the unknown detection probability and the technique that jointly estimates the unknown clutter rate and detection probability are described. Finally, the unknown prior knowledge of locations of newborn targets is managed by adopting a measurement-driven birth model. These techniques are then combined with the conventional joint prediction update GLMB filter given in Section 3.2.1 to estimate target trajectories given the labelled RFS formulation of the GLMB filter.

4.2.1 Detection probability estimation

The underlying idea of the filter to estimate the unknown information on the probability of target detection is that the this unknown parameter is augmented into the single target state. It can then be estimated using the CPHD recursion. This estimated value is then bootstrapped into the joint prediction update GLMB filter for producing target trajectories. In this method, clutter is assumed to be a known and fixed parameter to the filter. The diagram of the Boostraping GLMB filter with unknown detection probability is presented in Figure 4.1.

Since the detection probability is unknown and augmented into the single target state, the target state becomes an augmented one and belongs to the augmented state space. For consistency in notations, we use the superscript $^{(\bar{a})}$ to denote functions or variables in the augmented state space.

$$\mathbb{X}^{(\bar{a})} = \mathbb{X}^{(1)} \times \mathbb{X}^{(\Delta)} \tag{4.1}$$

where $\mathbb{X}^{(1)} = \mathbb{R}^{n_x}$ (with n_x is the dimension of the kinematic state of a target) and $\mathbb{X}^{(\Delta)} = [0, 1]$ denote the state space of target kinematics and detection probability, respectively.

Each usual kinematic state $x \in \mathbb{X}^{(1)}$ is replaced by an augmented state $x^{(\bar{a})} = (x, a) \in$

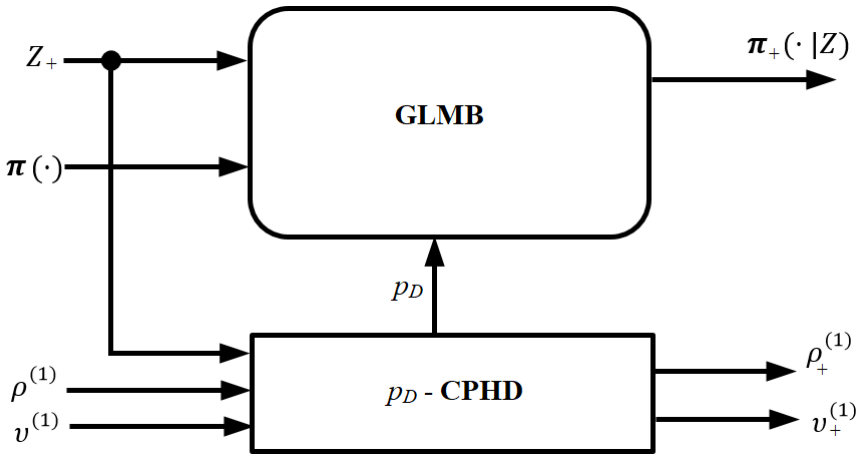

Figure 4.1: Structure of the Bootstrapped-GLMB filter with an unknown detection profile. The meaning of the input and output notations has been given in Section 2.3.2 and Section 2.5.1.

$\mathbb{X}^{(\bar{a})}$ where $a \in \mathbb{X}^{(\Delta)} = [0,1]$ is the unknown target detection probability of x. Consequently, the augmented multi-target state of n targets at the current time step is:

$$X^{(\bar{a})} = \left\{x_1^{(\bar{a})}, \ldots, x_n^{(\bar{a})}\right\} = \{(x_1, a_1), \ldots, (x_n, a_n)\}. \tag{4.2}$$

The set integral of a function $f^{(\bar{a})} : \mathbb{X}^{(\bar{a})} \to \mathbb{R}$ has the form [96]:

$$\int_{\mathbb{X}^{(\bar{a})}} f^{(\bar{a})}\left(x^{(\bar{a})}\right) dx^{(\bar{a})} = \int_{\mathbb{X}^{(\Delta)}} \int_{\mathbb{X}^{(1)}} f^{(\bar{a})}(x, a)\, dx da \tag{4.3}$$

The augmented single-target survival probability and augmented transition density at the next time step are given by:

$$p_{S,+}\left(x^{(\bar{a})}\right) = p_{S,+}^{(\bar{a})}(x, a) = p_{S,+}^{(1)}(x) \tag{4.4}$$

$$\begin{aligned} f_+^{(\bar{a})}\left(x_+^{(\bar{a})} | x^{(\bar{a})}\right) &= f_+^{(\bar{a})}(x_+, a_+ | x, a) \\ &= f_+^{(1)}(x_+|x)\, f_+^{(\Delta)}(a_+|a). \end{aligned} \tag{4.5}$$

The newborn targets are represented by an intensity $\nu_{B,+}^{(1)}(x, a)$ for augmented states and the corresponding cardinality distribution $\rho_{B,+}^{(1)}(\cdot)$. The augmented detection probability and single-target likelihood function are described in Eq. (2.33) and Eq. (2.35). Compared to the conventional CPHD filter, the likelihood function is $g\left(z|x^{(h)}\right) = g^{(1)}(z|x)$ (for $x \in \mathbb{X}^{(1)}$ is the kinematic state of the target), but the detection probability $p_D(x)$ in

Eq. (2.23) is replaced by a.

The probability of detection can be estimated using the derivation of the conventional CPHD recursion in which the augmented state is applied in single-target motion and measurement models. This resulting filter propagates the posterior cardinality distribution $\rho(\cdot)$ and posterior intensity function $\nu^{(1)}(\cdot)$ in the prediction and update recursion as given in [96, Propositions 7 and 8]. Further, clutter follows the conventional CPHD model given by Poisson false alarms with intensity function $\kappa(\cdot)$.

Prediction: Given the pair $\left(\nu^{(1)}(\cdot), \rho(\cdot)\right)$ at the current time step, the predicted cardinality distribution ρ_+ and predicted intensity $\nu_+^{(1)}$ are given by:

$$\rho_+(n) = \sum_{j=1}^{n} \rho_{B,+}^{(1)}(n-j)\, \Pi_+\left[\nu^{(1)}, \rho\right](j) \tag{4.6}$$

$$\nu_+^{(1)}(x_+, a_+) = \nu_{B,+}^{(1)}(x_+, a_+) + \iint_0^1 p_{S,+}(x)\, f_+^{(\Delta)}(a_+|a)\, f_+^{(1)}(x_+|x)\, \nu^{(1)}(a, x)\, da dx \tag{4.7}$$

where

$$\Pi_+\left[\nu^{(1)}, \rho\right](j) = \sum_{l=j}^{\infty} C_j^l \rho(l) \frac{\left\langle p_{S,+}, \nu^{(1)}\right\rangle^j \left\langle 1 - p_{S,+}, \nu^{(1)}\right\rangle^{l-j}}{\left\langle 1, \nu^{(1)}\right\rangle^l} \tag{4.8}$$

Update: Given measurement set Z_+, the predicted intensity and cardinality distribution is updated at the next time step as follows:

$$\begin{aligned}\nu_+^{(1)}(x_+, a_+|Z_+) = {} & (1-a_+) \frac{\left\langle \Upsilon_{+|Z_+}^{(1)}\left[\nu_+^{(1)}; Z_+\right], \rho_+\right\rangle}{\left\langle \Upsilon_{+|Z_+}^{(0)}\left[\nu_+^{(1)}; Z_+\right], \rho_+\right\rangle} \nu_+^{(1)}(x_+, a_+) \\ & + \sum_{z \in Z_+} \psi_{+,z}^{(\bar{a})}(x_+, a_+) \frac{\left\langle \Upsilon_{+|Z_+}^{(1)}\left[\nu_+^{(1)}; Z_+ - \{z\}\right], \rho_+\right\rangle}{\left\langle \Upsilon_{+|Z_+}^{(0)}\left[\nu_+^{(1)}; Z_+\right], \rho_+\right\rangle} \nu_+^{(1)}(x_+, a_+), \end{aligned} \tag{4.9}$$

$$\rho_+(n|Z_+) = \frac{\Upsilon_{+|Z_+}^{(0)}\left[\nu_+^{(1)}; Z_+\right](n)\, \rho_+(n)}{\left\langle \Upsilon_{+|Z_+}^{(0)}\left[\nu_+^{(1)}; Z_+\right], \rho_+\right\rangle}, \tag{4.10}$$

where

$$\Upsilon^{(u)}_{+|z_+}\left[\nu^{(1)}_+, Z_+\right](n) = \sum_{j=0}^{min(|Z_+|,n)} (|Z_+|-j)!\rho_{K,+|Z_+}(|Z_+|-j) \times P^n_{j+u}\frac{\langle 1-p^{(\bar{a})}_{D,+}, \nu^{(1)}_+\rangle^{n-(j+u)}}{\langle 1, \nu^{(1)}_+\rangle^n} e_j\left(\Xi_{+|Z_+}\left(\nu^{(1)}_+, Z_+\right)\right), \tag{4.11}$$

$$p^{(\bar{a})}_{D,+}(x_+, a_+) = a_+, \tag{4.12}$$

$$\psi^{(\bar{a})}_{+,z}(x_+, a_+) = \frac{\langle 1, \kappa_+\rangle}{\kappa_+(z)} g_+(z|x_+)\cdot a_+, \tag{4.13}$$

$$\Xi_+\left(\nu^{(1)}_+, Z_+\right) = \left\{\left\langle \nu^{(1)}_+, \psi^{(\bar{a})}_{+,z}\right\rangle : z \in Z_+\right\}, \tag{4.14}$$

$$e_j(Z_+) = \sum_{S\subseteq Z_+, |S|=j}\left(\prod_{\xi\in S}\xi\right) \text{ with } e_0(Z_+) = 1. \tag{4.15}$$

The target cardinality can be estimated from either the cardinality distribution or the intensity by using the mode $N^{(1)}_+ = \arg\max_n \rho_+(n)$ or the mean $N^{(1)}_+ = \left\langle 1, \nu^{(1)}_+\right\rangle$, respectively.

Note that, when the cardinalities are described by the Poisson distribution, the CPHD recursion reduces to the PHD recursion as follows:

$$\nu^{(1)}_+(x_+, a_+) = \nu^{(1)}_{B,+}(x_+, a_+) + \iint_0^1 p_{S,+}(x) f^{(\Delta)}_+(a_+|a) f^{(1)}_+(x_+|x)\nu^{(1)}(a, x)\, dadx \tag{4.16}$$

$$\nu^{(1)}_+(x_+, a_+|Z_+) = (1-a_+)\nu^{(1)}_+(x_+, a_+) + \sum_{z\in Z_+}\frac{a_+\cdot g_+(z|x_+)\nu^{(1)}_+(x_+, a_+)}{\kappa_+(z) + \left\langle a_+\cdot g_+(z|\cdot), \nu^{(1)}_+\right\rangle}. \tag{4.17}$$

The CPHD filter for unknown detection profiles can be implemented using the Beta - Gaussian mixture technique. Specifically, the augmented target state includes two parts: the augmented part for unknown detection probability and the kinematic part. The unknown parameter a is modelled by Beta distribution $\beta_{s,t}(\cdot)$, and the kinematic part of the state x is modelled by Gaussian distribution. The term Beta - Gaussian distribution refers to a product of a Beta distribution and a Gaussian distribution.

For the convenience of representation, let $\beta(\cdot; s, t)$ denote a Beta distribution with parameter $s > 1, t > 1$ where the mean value is $\mu_\beta = \frac{s}{s+t}$ and the variance is $\sigma^2_\beta = \frac{st}{(s+t)^2(s+t+1)}$. Since Eq. (4.9) involves both a and $1-a$, it results in products of the form

$a^s (1-a)^t$ after multiple recursions. The Gaussian density with mean m and covariance P is denoted as $\mathcal{N}(\cdot; m, P)$.

The implementation of the CPHD filter using the Beta - Gaussian mixture technique is based on the following assumptions.

• Each actual target follows a Gaussian dynamical model given in Eq. (3.12) and Eq. (3.13).

• While the target survival probability $p_{S+}(\cdot)$ is state-independent, the probability of detection is the augmented part of the state $p_{D+}^{(a)}(x_+, a_+) = a_+$.

• The intensity of the newborn target RFS is a Beta - Gaussian mixture

$$\nu_{B,+}^{(1)}(x_+, a_+) = \sum_{i=1}^{J\nu_{B,+}} \omega_{\nu_{B,+}}^{(i)} \beta\left(a_+; s_{\nu_{B,+}}^{(i)}, t_{\nu_{B,+}}^{(i)}\right) \mathcal{N}\left(x_+; m_{\nu_{B,+}}^{(i)}, P_{\nu_{B,+}}^{(i)}\right) \tag{4.18}$$

where $J_{\nu_{B,+}}, \omega_{\nu_{B,+}}^{(i)}, s_{\nu_{B,+}}^{(i)}, t_{\nu_{B,+}}^{(i)}, m_{\nu_{B,+}}^{(i)}, P_{\nu_{B,+}}^{(i)}, i = 1, \ldots, J_{\nu_{B,+}}$ are given model parameters in which $J_{\nu_{B,+}}$, $\omega_{\nu_B}^{(i)}$,$m_{\nu_{B,+}}^{(i)}$, $P_{\nu_{B,+}}^{(i)}$ have been defined below Eq. (3.14), and $s_{\nu_{B,+}}^{(i)}, t_{\nu_{B,+}}^{(i)}$ are the two parameters of a Beta distribution of the i^{th} newborn target.

• The time prediction for the augmented variable a_+ is completely governed by Beta densities:

$$\beta(a; s, t) \to (a_+; s_+, t_+)$$

• The mean $\mu_{\beta,+}$ is kept unchanged while the variance is multiplied by a prescribed factor k_β, which is typically chosen as $k_\beta > 1$ to enlarge the predicted variance (i.e., $\sigma_{\beta,+}^2 = k_\beta \sigma_\beta^2$).

Given a predicted density is a Beta - Gaussian mixture which is the product of Beta density and a Gaussian mixture, the update of each Beta-Gaussian component involving the computation of particular forms of this product is described in the following. Given two Gaussians $\mathcal{N}(x; m, P)$ and $\mathcal{N}(z; Hx, R)$ with R and P positive definite, their product is [18]:

$$\mathcal{N}(x; m, P)\mathcal{N}(z; Hx, R) = q(z)\mathcal{N}\left(x; \tilde{m}, \tilde{P}\right) \tag{4.19}$$

where

$$q(z) = \mathcal{N}\left(z, Hm, R + HPH^T\right) \tag{4.20}$$

$$\tilde{m} = m + K(z - Hm) \tag{4.21}$$

$$\tilde{P} = (I - KH)P \tag{4.22}$$

$$K = PH^T\left(HPH^T + R\right)^{-1}. \tag{4.23}$$

It means that the product of two Gaussians is replaced by appropriate Gaussians that are used to update intensity in the conventional CPHD recursion. The products of Beta density with a given weight are described by the following identities

$$(1 - a_+)\,\beta(a_+; s_+, t_+) = \frac{B(s_+, t_+ + 1)}{B(s_+, t_+)}\beta(a_+; s_+, t_+ + 1), \tag{4.24}$$

$$a_+\beta(a_+; s_+, t_+) = \frac{B(s_+ + 1, t_+)}{B(s_+, t_+)}\beta(a_+; s_+ + 1, t_+), \tag{4.25}$$

which results in weighted Beta densities in a_+. In the above identities, the Beta function evaluated at s, t is defined as $B(s,t) = \int_0^1 a^{s-1}(1-a)^{t-1}\,da$. By using the augmented state, the integration $\iint a_+\beta(a_+; s_+, t_+)\mathcal{N}(x_+; m_+, P_+)\,da_+dx_+$ in the update step reduces to $\frac{s_+}{s_+ + t_+}$ [96].

$$(1 - a_+)\,\beta(a_+; s_+, t_+) = \frac{B(s_+, t_+ + 1)}{B(s_+, t_+)}\beta(a_+; s_+, t_+ + 1), \tag{4.26}$$

$$a_+\beta(a_+; s_+, t_+) = \frac{B(s_+ + 1, t_+)}{B(s_+, t_+)}\beta(a_+; s_+ + 1, t_+), \tag{4.27}$$

which results in weighted Beta densities in a_+. Hence, using the assumption of Beta - Gaussian mixture for predicted intensity in Eq. (4.18), the CPHD filter can update the intensity with an unknown probability of detection.

As mentioned in Section 4.2.1, the number of targets can be estimated from the mean $\hat{N}_+^{(1)} = \sum_{j=1}^{J_+}\omega_+^{(j)}$ or the mode $\hat{N}_+^{(1)} = \arg\max_n \rho_+(n)$.

Since the number of mixture components grows unboundedly, pruning and merging need to be used. By using component pruning, the mixture components with weights lower than a predetermined threshold will be removed. Component merging is implemented using the Hellinger distance $0 < d_{ij} < 1$ between two Beta - Gaus-

sian components $\beta\left(a_+; s_+^{(i)}, t_+^{(i)}\right)\mathcal{N}\left(x_+; m_+^{(i)} P_+^{(i)}\right)$ and $\beta\left(a_+; s_+^{(j)}, t_+^{(j)}\right)\mathcal{N}\left(x_+; m_+^{(j)} P_+^{(j)}\right)$ as follows.

$$d_{ij} = \sqrt{1 - \frac{B\left(\frac{s_+^{(i)}+s_+^{(j)}}{2}, \frac{t_+^{(i)}+t_+^{(j)}}{2}\right)}{\sqrt{B\left(s_+^{(i)}, t_+^{(i)}\right) B\left(s_+^{(j)}, t_+^{(j)}\right)}} \frac{\sqrt{\mathcal{N}\left(0; m_+^{(i)} - m_+^{(j)}, P_+^{(i)} + P_+^{(j)}\right)}}{\det 8\pi \left(\left[P_+^{(i)}\right]^{-1} + \left[P_+^{(j)}\right]^{-1}\right)^{\frac{1}{4}}}}. \tag{4.28}$$

The number of components is limitted to a predetermined threshold, and only the highest weighted components are retained. These remaining weights are re-normalised to maintain the total mass. Further, the truncation on the distribution of the target cardinality is implemented to make it a tractable propagation.

Given the PHD of the form:

$$\nu_+^{(1)}(x_+, a_+) = \sum_{i=1}^{J\nu_{B,+}} \omega_{\nu,+}^{(i)} \beta\left(a; s_{\nu,+}^{(i)}, t_{\nu_B,+}^{(i)}\right)\mathcal{N}\left(x_+; m_{\nu,+}^{(i)}, P_{\nu,+}^{(i)}\right) \tag{4.29}$$

The average $\bar{p}_{D,+}$ is computed as:

$$\bar{p}_{D,+} = \sum_{i=1}^{J\nu,+} \omega_{\nu,+}^{(i)} \mathbb{E}\left(\beta\left(a_+; s_{\nu_B,+}^{(i)}, t_{\nu_B,+}^{(i)}\right)\right) \tag{4.30}$$

where $\mathbb{E}(\beta(\cdot;\cdot,\cdot))$ is the expected value of $\beta(\cdot;\cdot,\cdot)$.

4.2.2 Estimation of the joint clutter rate and detection probability

This section develops the methods presensted in Section 3.2.2 and Section 4.2.1 to address the estimation problem that exists when the clutter rate and probability of detection are both unknown. From the discussion in Section 2.3.3, the joint probability of survival and the joint transition density are redefined piecewise as follows [96]:

$$p_{S,+}^{(h)}\left(x^{(h)}\right) = \begin{cases} p_{S,+}^{(1)}(x) & \text{if } x^{(h)} = (x, a) \in \mathbb{X}^{(1)} \times \mathbb{X}^{(\Delta)} \\ p_{S,+}^{(0)} & \text{if } x^{(h)} = (x_c, b) \in \mathbb{X}^{(0)} \times \mathbb{X}^{(\Delta)} \end{cases}, \tag{4.31}$$

$$f_+^{(h)}\left(x_+^{(h)}|x^{(h)}\right) = \begin{cases} f_+^{(1)}(x_+|x)\, f_+^{(\Delta)}(a_+|a) & \text{if } x_+^{(h)} = (x_+, a_+), x^{(h)} = (x, a) \in \mathbb{X}^{(1)} \times \mathbb{X}^{(\Delta)} \\ f_+^{(0)}(x_{c+}|x_c) & \text{if } x_+^{(h)} = (x_{c+}, b_+), x^{(h)} = (x_c, b) \in \mathbb{X}^{(0)} \times \mathbb{X}^{(\Delta)} \\ 0 & \text{otherwise} \end{cases}. \tag{4.32}$$

For a definition of the superscripts used in this section, see Section 2.3.3. Similarly, the joint birth intensity is given by $\nu_{B,+}^{(1)}(x_+, a_+)$ for the actual target state or $\nu_{B,+}^{(0)}(x_{c+}, b_+)$ for the clutter state. The joint birth cardinality distribution is

$$\rho_{B,+}^{(h)}\left(n^{(h)}\right) = \left(\rho_{B,+}^{(1)} * \rho_{B,+}^{(0)}\right)\left(n^{(h)}\right) \tag{4.33}$$

The robust CPHD filter propagates the posterior intensity $\nu_+^{(h)}$ and the posterior cardinality distribution $\rho_+^{(h)}(\cdot)$ of the hybrid and augmented state $X_+^{(h)}$ in time. Note that , in this propagation, the intensity $\nu_+^{(h)}$ is decomposed into the intensity functions of actual targets $\nu_+^{(1)}(\cdot,\cdot)$ and clutter-generated targets $\nu_+^{(0)}(\cdot,\cdot)$. The unknown values of the clutter rate and detection probability are estimated in this recursion. Since the detections b_+ generated by clutter targets are independent of the actual value of the clutter state c_+, the posterior intensity $\nu_+^{(0)}(c_+, b_+)$ is characterised by a dependent variable $\nu_+^{(0)}(b_+)$.

Using the filtering formulation given in Section 2.3.3, the recursion of the CPHD for estimating these two unknown parameters is as follows.

Prediction: [96, Proposition 11] Given the intensities $\nu^{(1)}, \nu^{(0)}$, and the hybrid cardinality distribution $\rho^{(h)}$, their respective predictions to next time step are calculated as follows

$$\nu_+^{(1)}(x_+, a_+) = \nu_{B,+}^{(1)}(x_+, a_+) + \iint_0^1 p_{S,+}(x)\, f_+^{(\Delta)}(a_+|a)\, f_+^{(1)}(x_+|x)\, \nu^{(1)}(a, x)\, da dx, \tag{4.34}$$

$$\nu^{(0)}(b) = \nu_{B,+}^{(0)}(b) + p_{S,+}^{(0)} \nu^{(0)}(b), \tag{4.35}$$

$$\rho_+^{(h)}\left(n^{(h)}\right) = \sum_{j=0}^{n^{(h)}} \rho_{B,+}^{(h)}\left(n^{(h)} - j\right) \sum_{l=j}^{\infty} C_j^l \rho^{(h)}(l)\,(1-\phi)^{l-j}\,\phi^j. \tag{4.36}$$

where

$$\phi = \left(\frac{\left\langle \nu^{(1)}, p_{S,+}^{(1)} \right\rangle + \left\langle \nu^{(0)}, p_{S,+}^{(0)} \right\rangle}{\left\langle 1, \nu^{(1)} \right\rangle + \left\langle 1, \nu^{(0)} \right\rangle}\right) \tag{4.37}$$

It can be observed that while Eq. (4.34) is identical to Eq. (4.7), the posterior mean number of clutter targets $N^{(0)}$ in Eq. (3.17) is replaced by the posterior intensity of clutter targets $\nu^{(0)}(b)$, and the clutter state-space $^{(\bar{c})}$ in Eq. (3.18) is replaced by the

hybrid and augmented state-space $^{(h)}$ in Eq. (4.36).

Update : [96, Proposition 12] Given measurement set Z_+, the predicted intensities and cardinality distributions are updated as follows

$$\nu_+^{(1)}(x_+, a_+|Z_+) = \nu_+^{(1)}(x_+, a_+)\frac{(1-a_+)\frac{\left\langle \Upsilon_+^{(1)}\left[\nu_+^{(h)};Z_+\right],\rho_+^{(h)}\right\rangle}{\left\langle \Upsilon_+^{(0)}\left[\nu_+^{(h)};Z_+\right],\rho_+^{(h)}\right\rangle}}{\left\langle 1,\nu_+^{(1)}\right\rangle + \left\langle 1,\nu_+^{(0)}\right\rangle} + \sum_{z\in Z_+}\frac{a_+\cdot g_+^{(1)}(z|x_+)}{\left\langle \nu_+^{(0)}, p_{D,+}^{(0)}g_+^{(0)}(z)\right\rangle + \left\langle \nu_+^{(1)}, p_{D,+}^{(1)}g_+^{(1)}(z|\cdot)\right\rangle}\nu_+^{(1)}(x_+, a_+) \tag{4.38}$$

$$\nu_+^{(0)}(b_+|Z_+) = \nu_+^{(0)}(b_+)\frac{(1-b_+)\frac{\left\langle \Upsilon_+^{(1)}\left[\nu_+^{(h)};Z_+\right],\rho_+^{(h)}\right\rangle}{\left\langle \Upsilon_+^{(0)}\left[\nu_+^{(h)};Z_+\right],\rho_+^{(h)}\right\rangle}}{\left\langle 1,\nu_+^{(1)}\right\rangle + \left\langle 1,\nu_+^{(0)}\right\rangle} + \sum_{z\in Z_+}\frac{b_+\cdot g_+^{(0)}(z)}{\left\langle \nu_+^{(0)}, p_{D,+}^{(0)}g_+^{(0)}(z)\right\rangle + \left\langle \nu_+^{(1)}, p_{D,+}^{(1)}g_+^{(1)}(z|\cdot)\right\rangle}\nu_+^{(0)}(b_+) \tag{4.39}$$

$$\rho_+^{(h)}\left(n^{(h)}\right) = \begin{cases} 0 & n^{(h)} < |Z_+| \\ \frac{\rho_+^{(h)}(n^{(h)})\Upsilon_+^{(0)}[\nu_+;Z_+](n^{(h)})}{\left\langle \rho_+^{(h)},\Upsilon_+^{(0)}\right\rangle} & n^{(c)} \geq |Z_+| \end{cases} \tag{4.40}$$

where

$$\Upsilon_+^{(u)}\left[\nu_+^{(h)};Z_+\right]\left(n^{(h)}\right) = \begin{cases} 0 & n^{(h)} < Z_+ + u \\ P_{|Z_+|+u}^{(n^{(h)})}\Phi_+^{n^{(h)}-(|Z_+|+u|)} & n^{(h)} \geq |Z_+ + u \end{cases}, \tag{4.41}$$

$$\Phi = 1 - \frac{\left\langle \nu_+^{(1)}, p_{D,+}^{(1)}\right\rangle + \left\langle \nu_+^{(0)}, p_{D,+}^{(0)}\right\rangle}{\left\langle 1,\nu_+^{(1)}\right\rangle + \left\langle 1,\nu_+^{(0)}\right\rangle}, \tag{4.42}$$

$$p_{D,+}^{(1)}(x_+, a_+) = a_+, \tag{4.43}$$

$$p_{D,+}^{(0)}(b_+) = b_+. \tag{4.44}$$

where $P_j^n = \frac{n!}{(n-j)!}$ is the permutation coefficient, and $u = 0, 1$.

Remark 6. At each time step, the clutter rate can be inferred via the updated cardinality distribution (from which the average clutter intensity λ_c can be calculated). In particular, the average number of measurement clutter targets can be computed at any given

time using [96]:

$$N_{+}^{(0)} = \left\langle \nu_{+}^{(0)}, p_{D,+}^{(0)} \right\rangle. \tag{4.45}$$

Moreover, the mean value of the detection probability, $\bar{p}_{D,+}^{(1)}$, can be calculated by averaging the estimated detection probability of actual targets.

The performance of the robust CPHD recursion is based on the following assumptions:

- The intensity of the actual target birth RFS is a Beta - Gaussian mixture
- The intensity of the birth RFS for clutter targets is a Beta mixture

Remark 7. The implementation of the robust CPHD filter can be derived via Beta and Gaussian mixtures as given in Section 4.2.1 and Section 3.2.2. While assumptions on the dynamic and measurement models are the same, there is a difference in the assumptions for newborn targets. Specifically, the intensity of newborn actual target RFS is a Beta - Gaussian mixture, and that of clutter newborn target RFS is a Beta mixture as given in Eq. (4.46) and Eq. (4.47), respectively.

$$\nu_{B,+}^{(1)}(x_+, a_+) = \sum_{i=1}^{J_{\nu_{B^+}}^{(1)}} \omega_{\nu_{B,+}}^{(i,1)} \beta\left(a_+; s_{\nu_{B,+}}^{(i,1)}, t_{\nu_{B,+}}^{(i,1)}\right) \mathcal{N}\left(x_+; m_{\nu_{B,+}}^{(i,1)}, P_{\nu_{B,+}}^{(i,1)}\right), \tag{4.46}$$

$$\nu_{B,+}^{(0)}(b_+) = \sum_{i=1}^{J_{\nu_{B,+}}^{(0)}} \omega_{\nu_{B,+}}^{(i,0)} \beta\left(b_+; s_{\nu_{B,+}}^{(i,0)}, t_{\nu_{B,+}}^{(i,0)}\right). \tag{4.47}$$

Following [96, Proposition 13], given the posterior hybrid cardinality distribution $\rho^{(h)}$, and the posterior intensities $\nu^{(1)}$ and $\nu^{(0)}$ in the form of Beta - Gaussian and Beta mixtures:

$$\nu^{(1)}(x, a) = \sum_{i=1}^{J^{(1)}} \omega^{(i,1)} \beta\left(a, s^{(i,1)}, t^{(i,1)}\right) \mathcal{N}\left(x; m^{(i,1)}, P^{(i,1)}\right), \tag{4.48}$$

$$\nu^{(0)}(b) = \sum_{i=1}^{J^{(0)}} \omega^{(i,0)} \beta\left(b, s^{(i,0)}, t^{(i,0)}\right), \tag{4.49}$$

then the predicted intensities $\nu_{+}^{(1)}$ and $\nu_{+}^{(0)}$ are also Beta - Gaussian and Beta mixtures,

respectively, and:

$$\nu_+^{(1)}(x_+,a_+) = \nu_{B,+}^{(1)}(x_+,a_+) + p_{S,+}^{(1)} \sum_{j=1}^{J^{(1)}} \omega^{(j,1)} \beta\left(a; s_{S,+}^{(j,1)}, t_{S,+}^{(j,1)}\right) \mathcal{N}\left(x; m_{S,+}^{(j,1)}, P_{S,+}^{(j,1)}\right), \tag{4.50}$$

$$\nu_+^{(0)}(b_+) = p_{S,+}^{(0)} \nu^{(0)}(b) + \nu_{B,+}^{(0)}(b_+), \tag{4.51}$$

$$\rho_+^{(h)}\left(n^{(h)}\right) = \sum_{j=0}^{n^{(h)}} \rho_{B,+}^{(h)}\left(n^{(h)} - j\right) \sum_{l=j}^{\infty} C_j^l \rho^{(h)}(l) (1-\phi)^{l-j} \phi^j. \tag{4.52}$$

where $\nu_{B,+}^{(1)}(x_+,a_+)$ is given in Eq. (3.14):

$$\phi = \frac{p_{S,+}^{(1)} \sum_{i=1}^{J^{(1)}} \omega^{(i,1)} + p_{S,+}^{(0)} \sum_{i=1}^{J^{(0)}} \omega^{(i,0)}}{\sum_{i=1}^{J^{(1)}} \omega^{(i,1)} + \sum_{i=1}^{J^{(0)}} \omega^{(i,0)}}, \tag{4.53}$$

$$s_{S,+}^{(j,1)} = \left(\frac{\mu_{\beta,+}^{(j,1)}\left(1-\mu_{\beta,+}^{(j,1)}\right)}{\left[\sigma_{\beta,+}^{(j,1)}\right]^2} - 1 \right) \mu_{\beta,+}^{(j,1)}, \tag{4.54}$$

$$t_{S,+}^{(j,1)} = \left(\frac{\mu_{\beta,+}^{(j,1)}\left(1-\mu_{\beta,+}^{(j,1)}\right)}{\left[\sigma_{\beta,+}^{(j,1)}\right]^2} - 1 \right) \left(1-\mu_{\beta,+}^{(j,1)}\right), \tag{4.55}$$

$$m_{S,+}^{(j,1)} = F m^{(j,1)}, \tag{4.56}$$

$$P_{S,+}^{(j,1)} = Q + F P^{(j,1)} F^T, \tag{4.57}$$

with $\mu_{\beta,+}^{(j,1)} = \mu_{\beta}^{(j,1)} = \frac{s^{(j,1)}}{s^{(j,1)}+t^{(j,1)}}$ and $\left[\sigma_{\beta,+}^{(j,1)}\right]^2 = |k_\beta| \left[\sigma_{\beta}^{(j,1)}\right]^2 = |k_\beta| \frac{s^{(j,1)} t^{(j,1)}}{\left(s^{(j,1)}+t^{(j,1)}\right)^2 \left(s^{(j,1)}+t^{(j,1)}+1\right)}$.

Given a measurement set Z_+, the predicted hybrid cardinality $\rho_+^{(h)}$ and predicted intensities $\nu_+^{(1)}$ and $\nu_+^{(0)}$ given by the Beta - Gaussian and Gaussian mixtures

$$\nu_+^{(1)}(x_+,a_+) = \sum_{i=1}^{J_+^{(1)}} \omega_+^{(i,1)} \beta\left(a_+, s_+^{(i,1)}, t_+^{(i,1)}\right) \mathcal{N}\left(x_+; m_+^{(i,1)}, P_+^{(i,1)}\right), \tag{4.58}$$

$$\nu_+^{(0)}(b_+) = \sum_{i=1}^{J_+^{(0)}} \omega_+^{(i,0)} \beta\left(b_+, s_+^{(i,0)}, t_+^{(i,0)}\right), \tag{4.59}$$

then the updated intensities $\nu_+^{(1)}(\cdot|Z_+)$ and $\nu_+^{(0)}(\cdot|Z_+)$ are also Beta - Gaussian and Gaussian mixtures in which

$$\nu_+^{(1)}(x_+, a_+|Z_+) = \sum_{j=1}^{J_+^{(1)}} \omega_{M,+}^{(j,1)}(z)\,\beta\left(a_+, s_+^{(j,1)}, t_+^{(j,1)}+1\right)\mathcal{N}\left(x_+; m_+^{(j,1)}, P_+^{(j,1)}\right), \\ + \sum_{z\in Z_+}\sum_{j=1}^{J_+^{(1)}} \omega_{D,+}^{(j,1)}(z)\,\beta\left(a_+, s_+^{(j,1)}+1, t_+^{(j,1)}\right)\mathcal{N}\left(x_+; m_{+|Z_+}^{(j,1)}, P_{+|Z_+}^{(j,1)}\right) \tag{4.60}$$

$$\nu_+^{(0)}(b_+|Z_+) = \sum_{j=1}^{J_+^{(0)}} \omega_{M,+}^{(j,0)}(z)\,\beta\left(b_+, s_+^{(j,0)}, t_+^{(j,0)}+1\right) \\ + \sum_{z\in Z_+}\sum_{j=1}^{J_+^{(0)}} \omega_{D,+}^{(j,0)}(z)\,\beta\left(b_+, s_+^{(j,0)}+1, t_+^{(j,0)}\right), \tag{4.61}$$

$$\rho_+^{(h)}\left(n^{(h)}|Z_+\right) = \begin{cases} 0 & n^{(h)} < |Z_+| \\ \frac{\rho_+^{(h)}(n^{(h)})\Upsilon_+^{(0)}\left[\nu_+^{(h)}, Z_+\right](n^{(h)})}{\left\langle \rho_+^{(h)}, \Upsilon_+^{(0)}\right\rangle} & n^{(h)} \geq |Z_+| \end{cases}, \tag{4.62}$$

where $\Upsilon_+^{(u)}$ with $u = 0, 1$ has been given in Eq. (4.41) with

$$\Phi_+ = 1 - \frac{\sum_{i=1}^{J_+^{(1)}} \omega_+^{(i,1)} d_+^{(j,1)} + \sum_{i=1}^{J_+^{(0)}} \omega_+^{(i,0)} d_+^{(j,0)}}{\sum_{i=1}^{J_+^{(1)}} \omega_+^{(i,1)} + \sum_{i=1}^{J_+^{(0)}} \omega_+^{(i,0)}} \tag{4.63}$$

$$d_+^{(j,u)} = \frac{s_+^{(j,u)}}{s_+^{(j,u)} + t_+^{(j,u)}}, \tag{4.64}$$

$$\omega_{M,+}^{(j,u)}(z) = \omega_+^{(j,u)} \frac{\frac{B\left(s_+^{(j,u)}, t_+^{(j,u)}+1\right)}{B\left(s_+^{(j,u)}, t_+^{(j,u)}\right)} \frac{\left\langle \Upsilon_+^{(1)}\left[\nu_+^{(h)}, Z_+\right], \rho_+^{(h)}\right\rangle}{\left\langle \Upsilon_+^{(0)}\left[\nu_+^{(h)}, Z_+\right], \rho_+^{(h)}\right\rangle}}{\sum_{i=1}^{J_+^{(1)}} \omega_+^{(i,1)} + \sum_{i=1}^{J_+^{(0)}} \omega_+^{(i,0)}}, \tag{4.65}$$

$$\omega_{D,+}^{(j,0)}(z) = \frac{\omega_+^{(j,0)} \frac{B\left(s_+^{(j,0)}+1, t_+^{(j,0)}\right)}{B\left(s_+^{(j,0)}, t_+^{(j,0)}\right)} g_+^{(0)}(z)}{\sum_{i=1}^{J_+^{(0)}} d_+^{(j,0)} \omega_+^{(i,0)} g_+^{(0)}(z) + \sum_{i=1}^{J_+^{(1)}} d_+^{(j,1)} \omega_+^{(i,1)} q_+^{(j,1)}(z)}, \tag{4.66}$$

$$\omega_{D,+}^{(j,1)}(z) = \frac{\omega_+^{(j,1)} \frac{B\left(s_+^{(j,1)}+1, t_+^{(j,1)}\right)}{B\left(s_+^{(j,1)}, t_+^{(j,1)}\right)} q_+^{(1)}(z)}{\sum_{i=1}^{J_+^{(0)}} d_+^{(j,0)} \omega_+^{(i,0)} g_+^{(0)}(z) + \sum_{i=1}^{J_+^{(1)}} d_+^{(j,1)} \omega_+^{(i,1)} q_+^{(j,1)}(z)}, \tag{4.67}$$

$$q_+^{(j,1)}(z) = \mathcal{N}\left(z, H_+ m_+^{(j,1)}, H_+ P_+^{(j,1)} H_+^T + R_+\right), \tag{4.68}$$

$$m_+^{(j,1)}(z) = m_+^{(j,1)} + K_+^{(j,1)}\left(z - H_+ m_+^{(j,1)}\right), \tag{4.69}$$

$$P_{+|Z_+}^{(j,1)} = \left[I - K_+^{(j,1)} H_+\right] P_+^{(j,1)}, \tag{4.70}$$

$$K_+^{(j,1)} = P_+^{(j,1)} H_+^T \left[H_+ P_+^{(j,1)} H_+^T + R_+\right]. \tag{4.71}$$

and I denotes identity matrix. The estimated mean number of actual targets and

that of the measurement clutter targets are $\hat{N}_+^{(1)} = \sum_{j=1}^{J_+^{(0)}} \omega_+^{(i,0)}$ respectively, and the estimated mean clutter rate is $\hat{\lambda}_{c+} = \sum_{j=1}^{J_+^{(0)}} \omega_+^{(i,0)} d_+^{(j,0)}$.

Remark 8. Similar to conventional CPHD recursion, the robust CPHD uses pruning and merging of mixture components in its implementation. This This step helps retaining the highest weighted components and renormalising the remaining weights to keep the total mass unchanged. Note that a predetermined threshold $J_{\max}$ is set to limit the number of retained components. The cardinality distribution needs to be truncated to $N_{\max}$ components to make the robust CPHD filter a tractable propagation.

4.2.3 Measurement-driven birth model

The model for measurement-driven (or adaptive) births presented in [101] is adopted in this work to initialise new tracks. This model is constructed on the basis of the intuition that the lower the probability that $z \in Z$ is related to an existing target at the current time step, the higher the probability that a measurement z is generated by a newborn target at the next time step. Hence, each measurement in the current measurement set can be used to initialise a new track whose existence probability depends on the (track) association probability of the measurement.

As can be observed from Eq. (2.52), the birth targets can be modelled as an LMB distribution in the GLMB filter. This distribution can be completely characterised by a set of birth probabilities and corresponding spatial distributions, that is,

$$\left\{ r_B^{(\ell)}(z), p_B(\cdot, \cdot; z) : \ell = \ell_B(z) \right\}.$$

In other words, a newborn target initiated by a measurement z is assigned to a label $\ell_B(z)$; this target has probability of existence $r_B(z)$ and probability density $p_B(x, \ell; z)$.

The probability density of the newborn LMB RFS is given by [142]:

$$\boldsymbol{\pi}_B(\boldsymbol{X}_+) = \Delta(\boldsymbol{X}_+) \omega_B(\mathcal{L}(\boldsymbol{X}_+)) [p_B]^{\boldsymbol{X}_+} \tag{4.72}$$

where

$$\omega_B(I) = \prod_{i \in \mathbb{B}} \left(1 - r_B^{(i)}\right) \prod_{\ell \in I} \frac{1_{\mathbb{B}}(\ell) r_B^{(\ell)}}{1 - r_B^{(\ell)}}. \tag{4.73}$$

In the GLMB recursion, this weight can be used to replace ω_B in Eq. (2.58).

The measurment-driven birth model exploits this fact and generates two sets of spatial distributions of targets. The first set is with lower birth probability is around existing targets, and the second set is with higher birth weights around all other areas where measurements were received. While the measuremetn-driven birth model uses the set of current measurements Z and the set of hypotheses obtained at the current time step, it is applied at the next time step. Specifically, given a GLMB filtering density of the form Eq. (2.49), the probability that a measurement z is connected to a track $r_U(z)$ is defined as follows [101]:

$$r_U(z) = \sum_{(I,\theta)\in\mathcal{F}\left(\mathbb{L}^{(i)}\right)\times\Theta_I} 1_\theta(z)\,\omega^{(I,\theta)} \tag{4.74}$$

where the inclusion function $1_\theta(z)$ warrants that the sum of weights only considers hypotheses that assign the measurement z to one of its tracks, and $\omega^{(I,\theta)}$ is presented in Eq. (2.65). Θ_I is the subset of the current association maps with domain I. Then, the probability of a Bernoulli measurement-driven birth given the measurement z at the next time step in Eq. (4.73) depends on its newborn likelihood obtained at the current time [101]:

$$r_{B,+}(z) = \min\left(r_{B,max}, \frac{1 - r_U(z)}{\sum_{\xi\in Z}\left(1 - r_U(\xi)\right)}.\lambda_{B,+}\right) \tag{4.75}$$

where $\lambda_{B,+}$ denotes the expected number of newborn targets at the next time step and $r_{B,max} \in [0,1]$ is the maximum value of birth probability. $r_{B,max}$ is set to guarantee that the resulting $r_{B,+}(z) \leq 1$ when $\lambda_{B,+}$ is too large.

Depending on the application, the value of $r_{B,max}$ can be chosen differently. Generally, the larger the value of $r_{B,max}$, the faster the track confirmation but the higher the incidence of false tracks, and vice versa. Since the mean cardinality of a multi-Bernoulli RFS is calculated from the sum of the existence probabilities, the mean cardinality of the newborn targets is:

$$\sum_{\xi\in Z} r_{B,+}(\xi) \leq \lambda_{B,+} \tag{4.76}$$

Assuming that the new birth of a Bernoulli RFS generated near a measurement z with non-zero newborn likelihood is distributed according to a Gaussian mixture, then the

probability distribution of the measurement-driven birth model is [142]:

$$p_{B,+}\left(x_{+},\ell_{+};z\right)=\sum_{i=1}^{M_b}\frac{1}{M_b}\delta_{x_z^{(i)}}\left(x_{+}\right), \tag{4.77}$$

$$x_z^{(i)}\sim\mathcal{N}\left(x_{+};m_{B,+}\left(z\right),P_{B,+}\left(z\right)\right),i=1,\ldots,M_B \tag{4.78}$$

Where M_b denotes the number of generated states for new births, $m_{B,+}(\cdot)$ is a function mapping from a measurement z to its corresponding target state where the information can be recovered, and $P_{B,+}(\cdot)$ is the covariance matrix that specifies the distribution of newborn target states. The smaller the value of $P_{B,+}$, the better the accuracy in general.

The probability distribution given in Eq. (4.77) is then substituted into Eq. (3.6) of the joint prediction-update GLMB filter provided in Section 3.2.1.

4.2.4 Target trajectories estimation

This chapter describes the application of the conventional joint prediction update GLMB presented in Section 2.5.2 for the main filtering processes of tracking target trajectories with the aforementioned techniques. Given the GLMB filtering density, the estimated multi-target state and the trajectories can be extracted [24, 31]. The joint prediction and update approach with a Gibbs sampler was adopted to select significant components (ones with high weights) of the GLMB filtering density [40] as represented in Section 3.2.1. Since the implementation of this filter has been presented in Section 2.5.2, this subsection summarises the main points of the Bootstrapped-GLMB tracker.

This section outlines the performance of the tracker that can track multiple targets does not require the prior knowledge on background information and model for newborn targets. The technique described in Section 4.2.1 was adopted to estimate the mean value of the detection probability. This estimated value was then bootstrapped into a standard GLMB filter to generate tracking results. Similarly, the technique in Section 4.2.2 is combined with the GLMB filter to track target trajectories with unknown prior information on clutter and the detection probability. The structure of this method is demonstrated in Figure 4.2. Note that the GLMB filter formulation using these two techniques was applied for the main filtering process. The set of new births $\boldsymbol{X}_{B,+}$ is

assumed to be known by the filter.

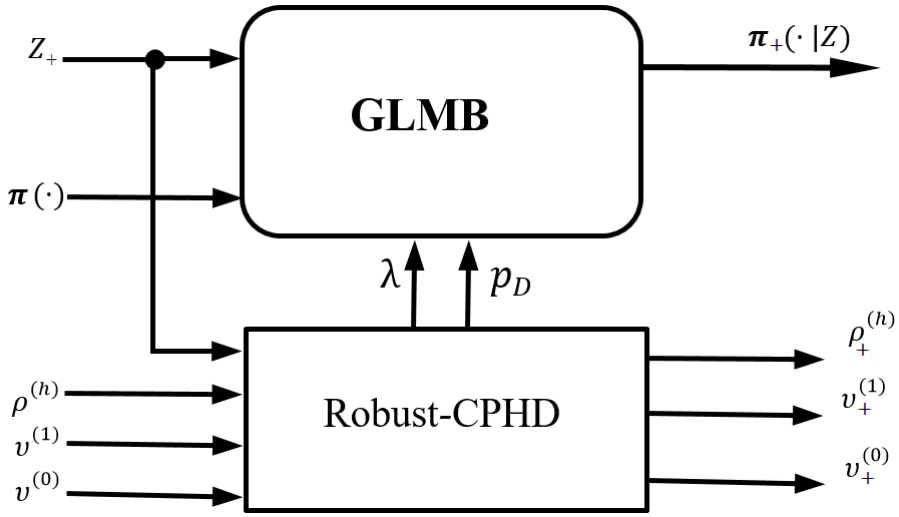

Figure 4.2: The structure of the robust Bootstrapped-GLMB filter.

As there is no prior information on the locations of newborn targets, the technique discussed in Section 4.2.3 was utilised for new track initiations. Using this technique with the GLMB filter results in an adaptive Bootstrapped-GLMB filter where the tracks of newborn targets are initiated from a measurement-driven birth model. Furthermore, in this adaptive Bootstrapped-GLMB filter, the average intensity of clutter λ_c and the detection probability p_D are unknown and are estimated using an independently run robust CPHD filter, as presented in Section 4.2.2. Therefore, this adaptive Bootstrapped-GLMB filter has the capability of tracking multiple targets with minimum prior knowledge from the users. Figure 4.3 demonstrates this proposed adaptive Bootstrapped-GLMB filter.

4.3 Numerical study

Both the linear and nonlinear dynamic models presented in Section 3.3 are re-investigated to demonstrate the effectiveness of the bootstrapped tracker. The implementation comparisons of the four filters (i.e., the ideal-GLMB [24], Robust-GLMB [131], Robust-CPHD [96], and the Bootstrapped-GLMB), are conducted in different scenarios. The OSPA [133] and OSPA$^{(2)}$ metrics [26] presented in Section 3.3 are applied over 100 MC runs to evaluate multi-target tracking performance. The norm order and cut-off parameters are respectively, set to $p = 1$ and $c_o = 100$ for both OSPA and OSPA$^{(2)}$ as in Section 3.3. The window length for OSPA$^{(2)}$ calculation is set to $l_w = 10$ time steps.

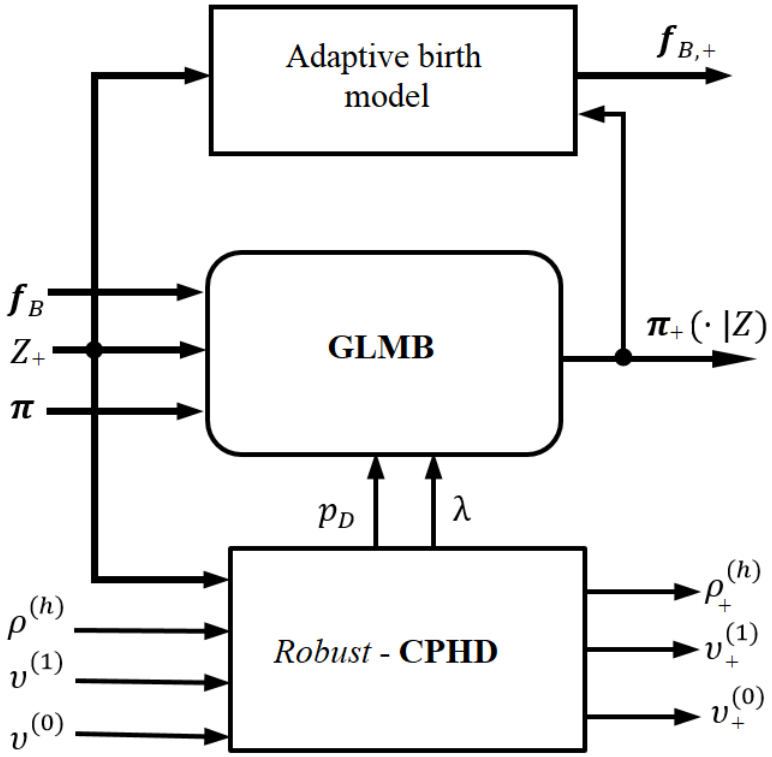

Figure 4.3: Structure of the adaptive GLMB tracker with unknown information on clutter rate, detection probability and locations of newborn targets.

4.3.1 Linear dynamic model

There are three filtering scenarios in this experiment: unknown detection probability, jointly unknown detection probability and unknown clutter rate, and unknown background combined with an unknown birth model.

Scenario 1: Linear tracking with unknown detection probability

For the filters with unknown detection probability only, the mean clutter rate is known and fixed at $\lambda_c = 30$ points per scan. Since the target state, in this case, is an augmented state, the intensity of the birth process for actual targets is rewritten with additional Beta mixture $\nu_B^{(1)}(a,x) = \sum_{i=1}^{4} r_B \beta(a;u_B,v_B)\mathcal{N}\left(x;m_B^{(i)},P_B\right)$ where $u_B = v_B = 1, r_B^{(1)} = r_B^{(2)} = 0.02; r_B^{(3)} = r_B^{(4)} = 0.04$. The detection probability $p_D^{(1)} = 0.98$ is used in the ideal-GLMB filter to generate measurements, but this value is not known to the filters and it must be implicitly estimated at the location of each track at each time step. For coherency, the p_D-CPHD filter [96] used in this scenario is called the robust CPHD filter. Filters are initiated to a zero state.

Pruning and merging of the Beta - Gaussian mixture is applied at each time step with a weight threshold of 10^{-5}, a merging threshold of 4 and a maximum of J_{max} = 1000 Beta - Gaussians. Maximum terms to calculate the cardinality distribution is capped at N_{max} = 300.

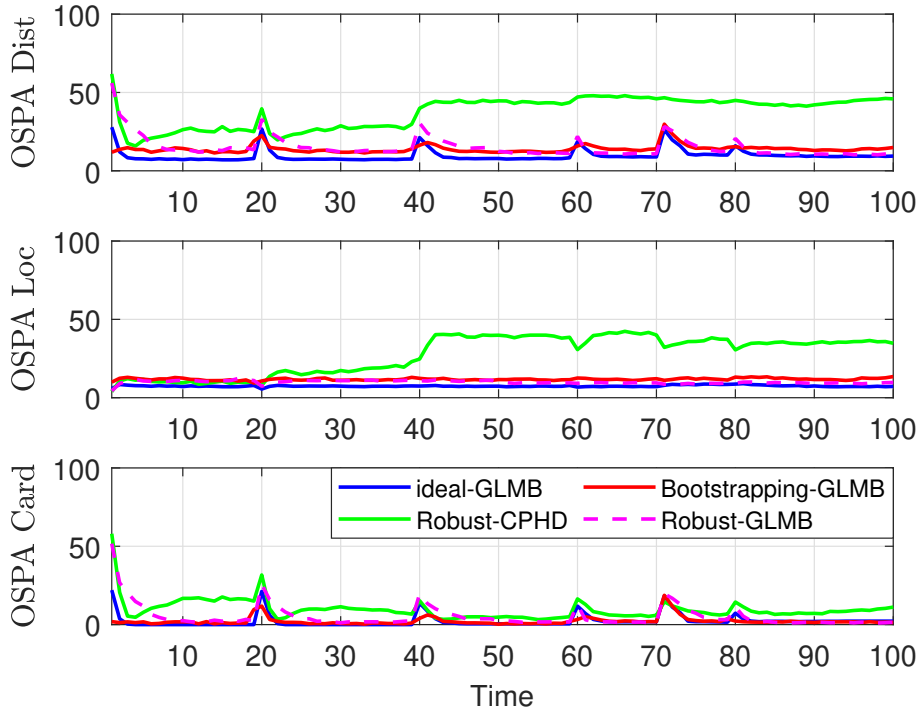

Figure 4.4: Comparisions of estimation errors for the four filters using the OSPA metric.

The OSPA metric given in Section 3.3 is applied in this experiment over 100 MC runs and its results are shown in Figure 4.4. It could be observed that three GLMB filters estimated target states much more accurately than the Robust-CPHD filter with unknown detection probability. Further consideration of the improved localisation component reveals that due to the spooky effect, the robust CPHD filter temporarily drops tracks that are subjected to miss detections and declare multi-target estimates for existing target states in place of dropped tracks. The three GLMB filters propagate filtering density more accurately due to the use of target identities; the filters generally localise targets better than the Robust-CPHD filter. The improvement in cardinality performance of the three GLMB filters over the Robust-CPHD filter is mainly the result of a lower estimated cardinality variance, which is not shown in Figure 4.4. The evaluation of the OSPA miss distance and its localisation and cardinality components for the three GLMB filters shows that while the best performance is with the ideal-GLMB fil-

ter, which runs with correct parameters of detection probability, the difference between this ideal filter and the other two GLMB filters is insignificant.

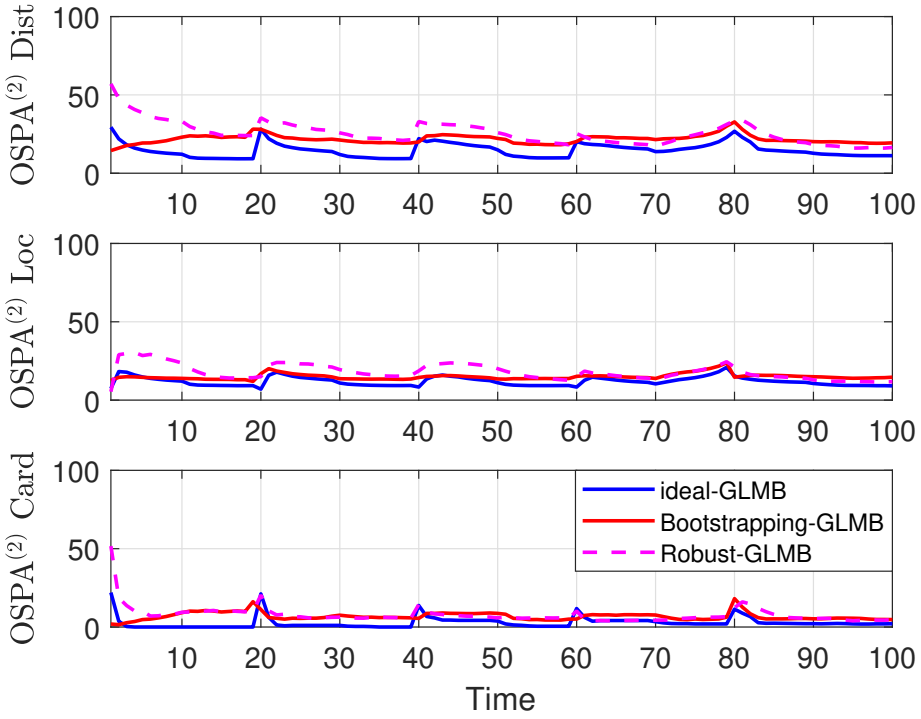

Figure 4.5: Comparisons of trajectory estimations for the three GLMB-based filters using the OSPA$^{(2)}$ metric.

Similarly, the errors for trajectory estimations using the OSPA$^{(2)}$ metric are shown in Figure 4.5. Comparisons once again show the similarity among the results for the trajectory estimations of the three GLMB-based filters. Using OSPA$^{(2)}$ miss distance, the performance of the Bootstrapped-GLMB filter is slightly better than that of the Robust-GLMB since its main filtering process uses the known average detection probability, which is estimated from an independently run CPHD filter. The OSPA$^{(2)}$ errors also exhibit that the multi-target tracking performance of the ideal-GLMB filter is the best of the GLMB filters.

The cardinality estimations from GLMB filters shown in Figure 4.6 are superior to that of the Robust-CPHD filter. Note that, the GLMB filters could propagate the filtering density more accurately than the Robust CPHD thank to the use of labelled RFSs, which results in a better cardinality estimate.

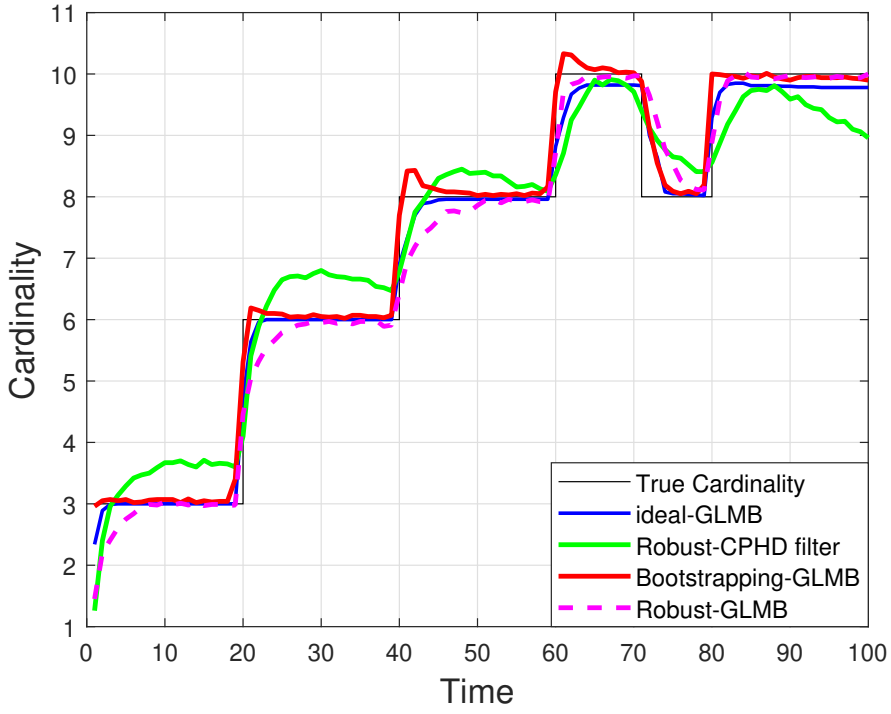

Figure 4.6: Cardinality estimations in an unknown detection probability scenario using the four different filters.

Scenario 2: Linear tracking with jointly unknown detection probability and clutter rate

This subsection illustrates and compares the performance of the four filters for jointly unknown detection profiles and clutter rate. While the ideal-GLMB filter is run with correct parameters, the other filters operate with unknown information about detection probability, as in Section 4.3.1, and unknown clutter rate, as in Section 3.3.1. The results of OSPA and OSPA$^{(2)}$ metrics in evaluating the tracking errors among the four filters are shown in Figure 4.7 and Figure 4.8, respectively. While all GLMB filters almost identically localise target states, the Robust-GLMB filter still has the highest errors in OSPA miss distance with cardinality component compared to the Bootstrapped-GLMB and ideal-GLMB filters. The evaluation of the OSPA$^{(2)}$ metric, demonstrated in Figure 4.8, indicates that the ideal-GLMB filter has the best performance for tracking target trajectories, as it is supplied the correct parameters for the clutter rate and detection probability. In addition, the Bootstrapped-GLMB performes slightly better than the Robust GLMB filter. The cardinality estimations among the four filters are compared in Figure 4.9, which once again confirms the advantage of the GLMB filters over

the CPHD filter.

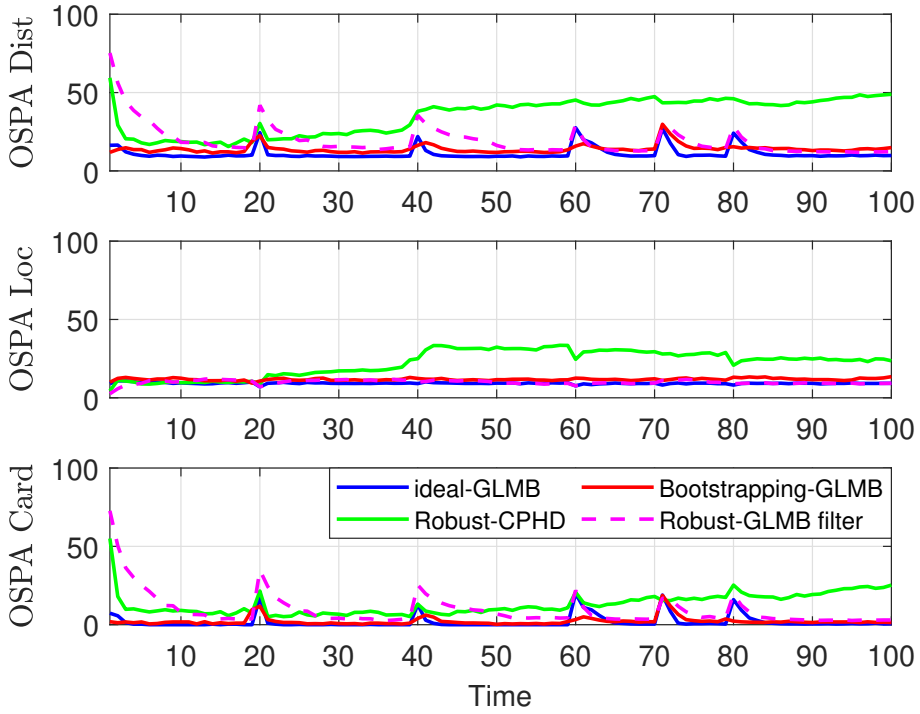

Figure 4.7: Evaluation of tracking errors for the four filters using the OSPA metric.

Scenario 3: Linear tracking with unknown background and unknown birth model

The scenario extends the experiment in Section 4.3.1 to deal with the unknown information about the birth model. The initial values of the detection probability and the surviving probability of actual targets are set to p_D=0.95, and $p_S = 0.99$, respectively. Similarly, the corresponding values of clutter-generated targets are $p_{Dc} = 0.95$ and $p_{Sc} = 0.9$. The birth probability of newborn targets is set to $r_b = 0.01$, and the birth covariance P_B is unchanged, i.e., $P_B = diag([10, 10, 10, 10])$. The correct clutter rate is set to $\lambda_c = 50$ per scan.

Since the Robust-GLMB filter [131] and the Robust-CPHD [96] consider the unknown information on clutter and detection probability only, they are not mentioned in this experiment. Rather, the performance of the Bootstrapped-GLMB filter with an unknown birth model is compared with the ideal-CPHD filter and the ideal-GLMB filter, where the word 'ideal' means that the birth model and backgrounds are prior known to the filter. There is a capped 5000 components of hypotheses for both the

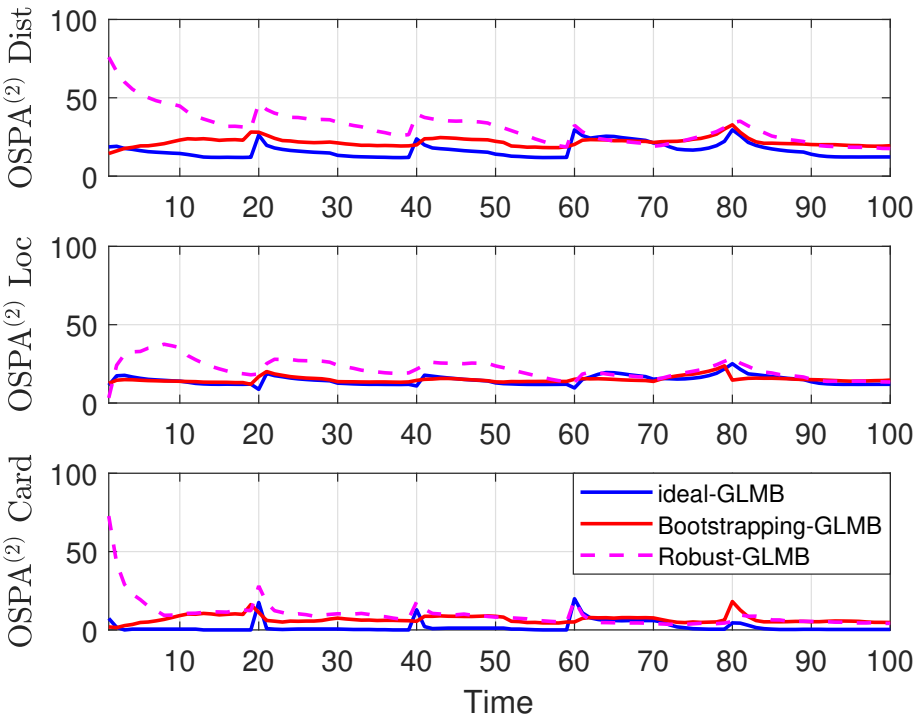

Figure 4.8: Estimation on trajectory errors among four filters using OSPA$^{(2)}$ metric

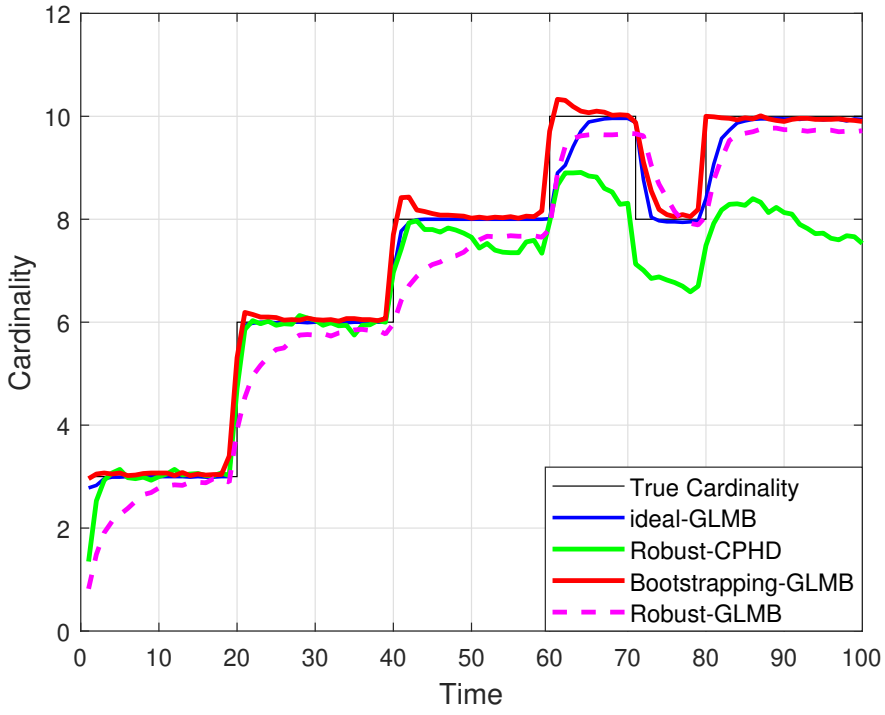

Figure 4.9: Comparison of cardinality estimation for the four filters.

Bootstrapped-GLMB and ideal-GLMB filters. Figure 4.10 and Figure 4.11 respectively demonstrate the estimated values of the detection probability and the clutter rate using the Bootstrapped-GLMB algorithm. With the adoption of the independent robust-CPHD in the Bootstrapped-GLMB tracker, the estimated clutter rate is approximately the correct value, while it takes some time to make the estimated detection probability approach to its true value.

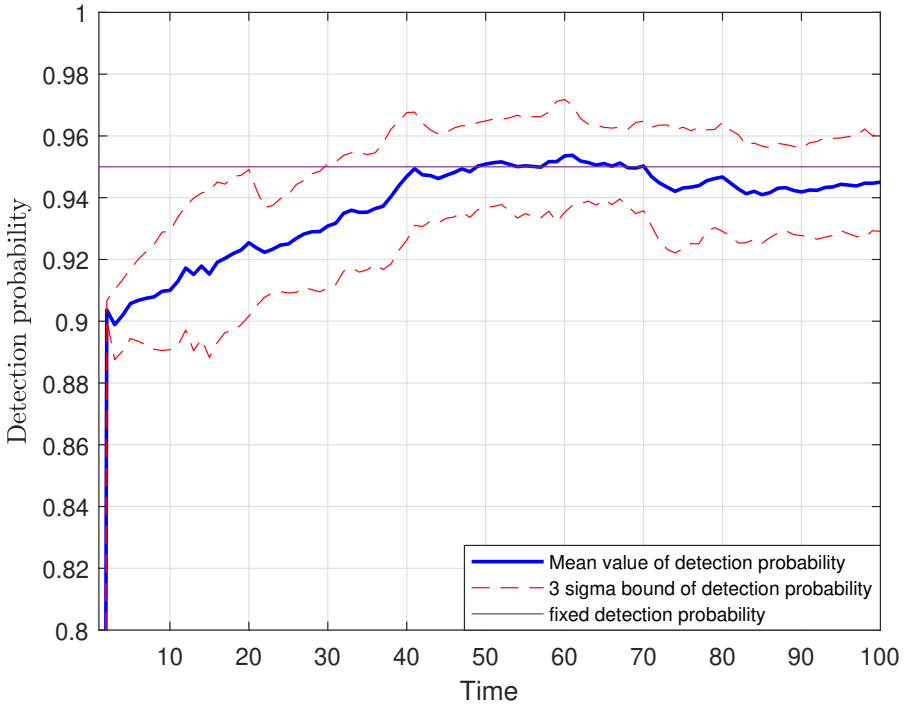

Figure 4.10: Estimated detection probability.

The comparisons of the OSPA and OSPA$^{(2)}$ errors from 100 MC runs are given in Figure 4.12 and Figure 4.13, respectively. In addition, results for the ideal-CPHD filter are excluded in OSPA$^{(2)}$ plots as this filter does not have a mechanism to provide tracks without heutistics. The OSPA errors show that while the performance of the ideal-GLMB is the best, the difference between the ideal-CPHD and the Bootstrapped-GLMB is insignificant. Furthermore, the results in the OSPA$^{(2)}$ evaluation are obvious since the ideal-GLMB filter uses the correct parameters of backgrounds and birth models.

Last but not least, Figure 4.14 compares the results of estimating target cardinality (from 100 MC runs) using three filters. These results demonstrated that the Bootstrapped-GLMB tracker adapted well with unknown information on clutter rate and detection

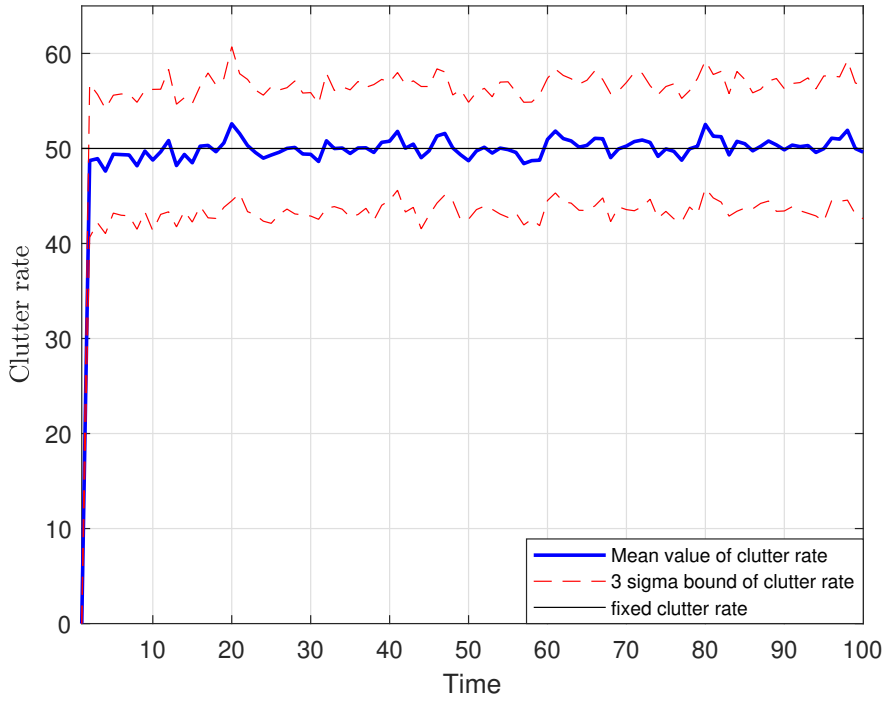

Figure 4.11: Estimated clutter rate.

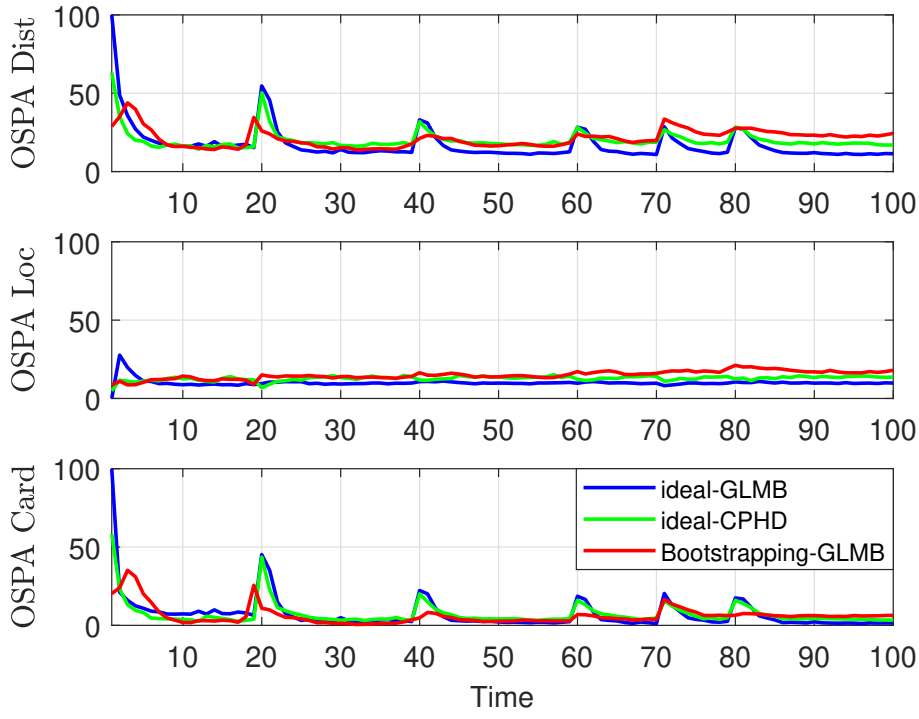

Figure 4.12: Linear tracking scenario: Mean OSPA errors for the three filters.

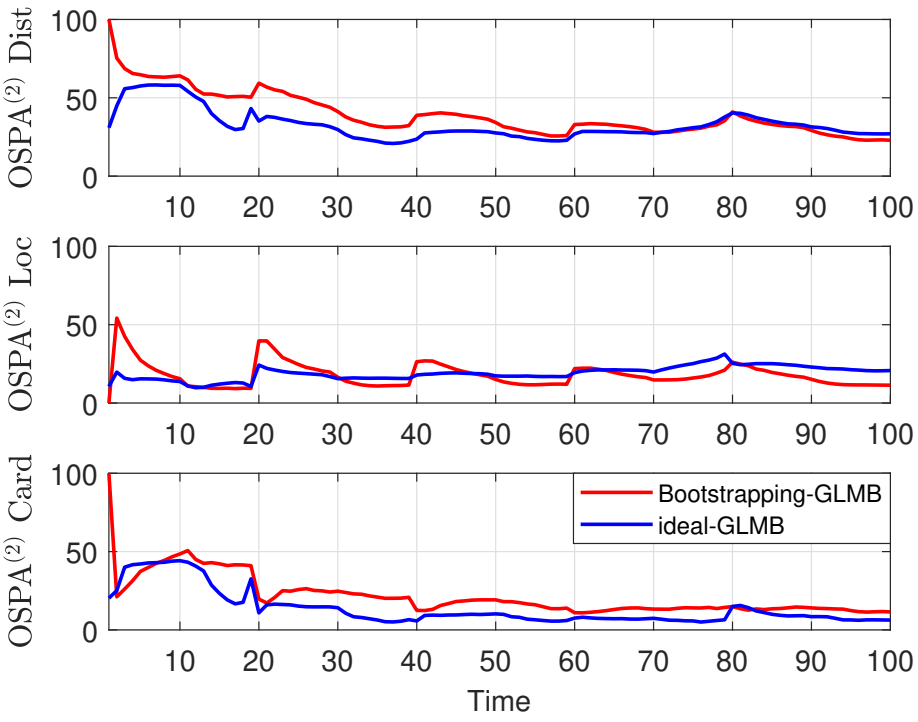

Figure 4.13: Linear tracking scenario: Mean OSPA$^{(2)}$ errors for the two GLMB filters.

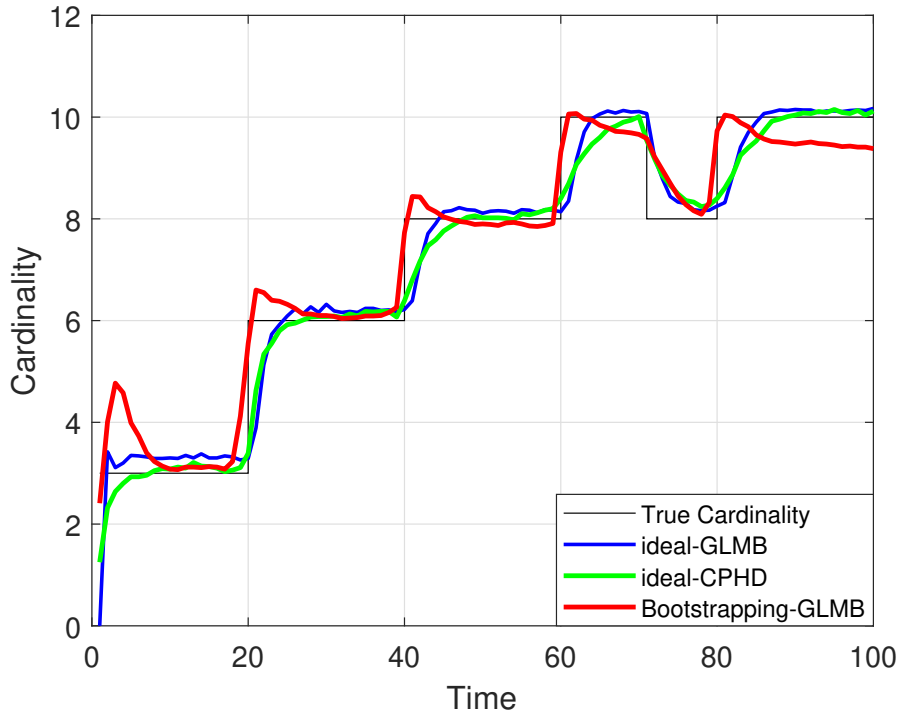

Figure 4.14: Linear tracking scenario: Cardinality estimation for the three filters.

probability as well as unknown parameters of the birth model. Its performance is comparable to the ideal-GLMB and ideal-CPHD filters in the linear tracking scenario.

4.3.2 Nonlinear dynamic model

The three filtering scenarios given in Section 4.3.1 were reapplied to implement the filters in a nonlinear dynamic model.

Scenario 1: Nonlinear tracking with unknown detection probability

This experiment is conducted to test the efficacy of the Bootstrapped-GLMB tracker in the tracking scenario with unknown detection probability. The clutter is assumed to follow a Poisson RFS with a known and fixed average rate $\lambda_c = 50$. The detection probability $p_D^{(1)}$ is unknown a priori and varies in the range $0.75,\ 0.98$.

The OSPA and OSPA$^{(2)}$ metrics, are used to evaluate the efficacy of the Bootstrapped-GLMB tracker with the other three filters the Robust-CPHD [96], Robust-GLMB [131] and ideal-GLMB [24]. The evaluations of tracking performance using the OSPA metric are demonstrated in Figure 4.15. The results illustrate the capability of the Bootstrapped-GLMB tracker, which is almost identical to the Robust-GLMB filter and outperformed the Robust-CPHD filter. Furthermore, the tracking accuracy of the Bootstrapped-GLMB filter with unknown p_D is comparable to that of the ideal-GLMB filter under the OSPA metric. These results are similar to those given in Figure 4.4.

Similarly, the results of the evaluation of tracking trajectories for the three GLMB filters using the OSPA$^{(2)}$ metric are shown in Figure 4.16. The ideal-GLMB filter has the smallest errors in OSPA$^{(2)}$ miss distance with the localisation and cardinality components. The Bootstrapped-GLMB filter slightly outperforms the Robust-GLMB filter.

Further, a comparison of estimated cardinality among these four filters is shown in Figure 4.17. All four filters accurately estimate the number of targets. However, the Robust-GLMB filter slightly underestimates the cardinality.

Scenario 2: Nonlinear tracking with jointly unknown detection probability and clutter rate

In this experiment, the problem of tracking multiple marine vessels using multiple Doppler radars presented in Section 3.3.2 with the ground truths demonstrated in Fig-

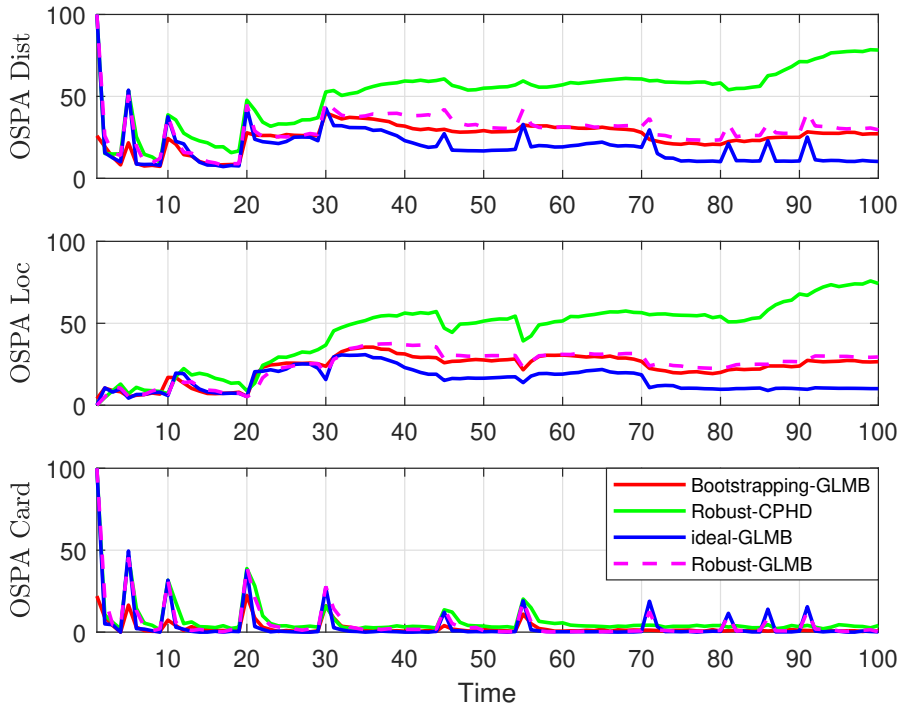

Figure 4.15: Comparison of OSPA errors for the four filters.

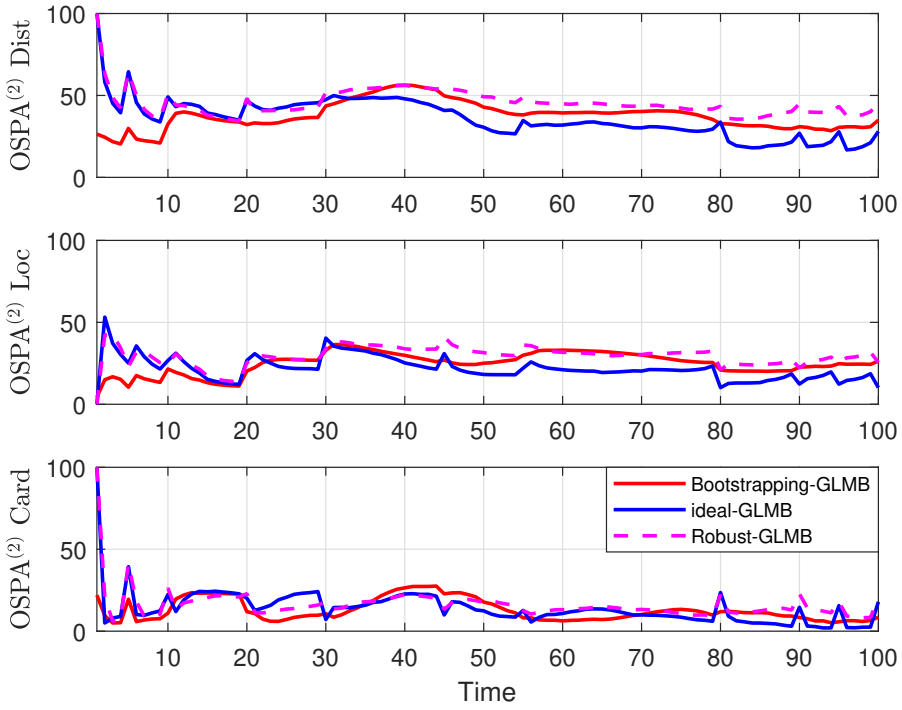

Figure 4.16: Comparison of OSPA$^{(2)}$ errors for the three GLMB filters.

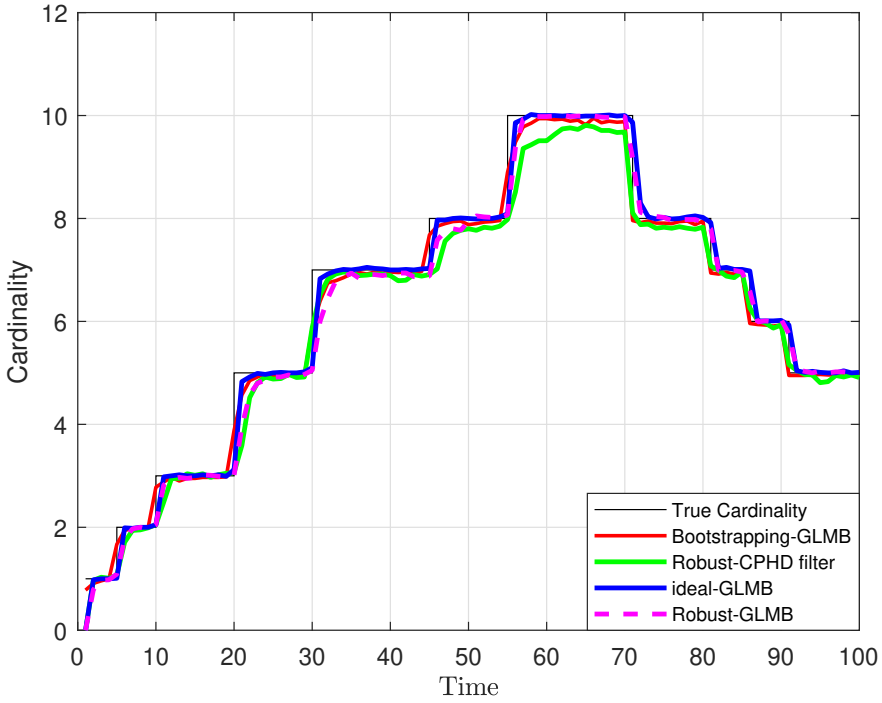

Figure 4.17: Comparison of cardinality estimation of the four filters with an unknown detection profile.

ure 3.6 is considered. The clutter rate and the detection probability are assumed to be known and fixed at $\lambda_c = 50$ and $p_D = 0.98$ to the ideal-GLMB filter. However, these parameters are unknown and fluctuated to the Boostrapping-GLMB and two robust filters. Specifically, clutter rate varies from 28 to 70 and detection probability varies 0.75 to 0.98. The OSPA$^{(2)}$ metric uses the window length $l_w = 10$ to compute the errors between the true and estimated sets of trajectories. The parameter set $c_0 = 100$ and $p = 1$ is adopted for the computation of the OSPA and OSPA$^{(2)}$ errors.

Figure 4.18 and Figure 4.19, respectively, show the estimated values of detection probability and clutter rate using the Bootstrapped-GLMB filter. While the estimated detection probability is approaching the true value, the evaluated clutter rate is around the upper bound of the clutter rate range. These results show that there is an inter-twined relationship between the detection probability and the clutter rate due to the Beta distribution of the former. Specifically, a detection event would update the Beta distribution by increasing the parameter s by 1, and a miss-detection event would increase t by 1. The details of this inter-twined relationship are analysed in Chapter 7.

One hundred MC runs is used to evaluate the effectiveness of the bootstrapping

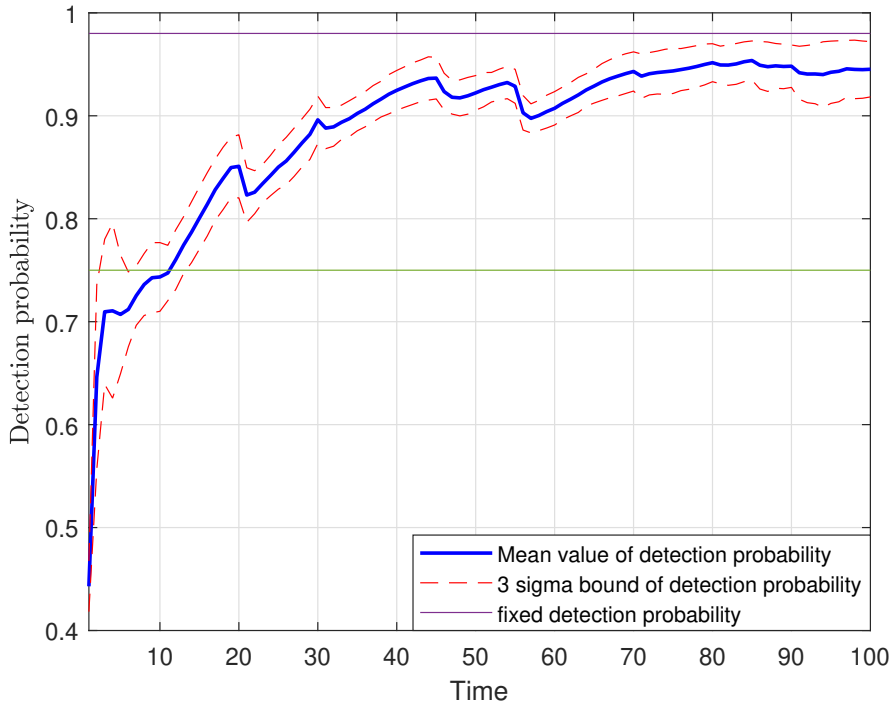

Figure 4.18: Estimations of the detection probability with respect to time using the Bootstrapped-GLMB filter.

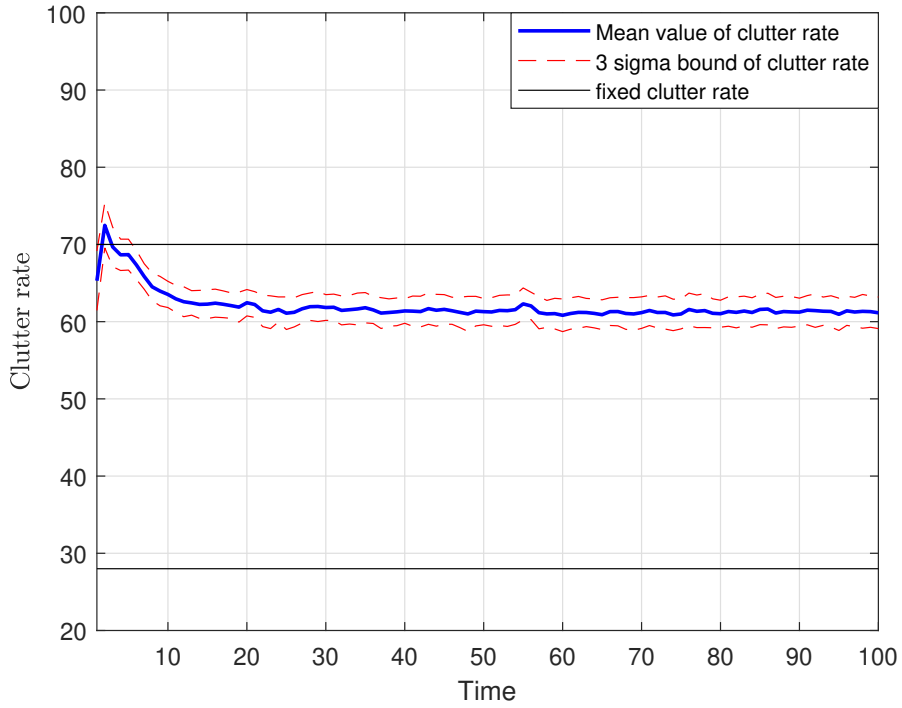

Figure 4.19: Estimations of the clutter rate with respect to time using the Bootstrapped-GLMB filter.

method compared to the ideal-GLMB, Robust-GLMB and Robust-CPHD filters. The errors on distance, location, and cardinality components between the set of true multi-target states and that of estimated target states are also computed at each time step using OSPA metric [133] (see Figure 4.20). The obvious errors in distance and location using the Bootstrapped-GLMB filter are comparable to those of the ideal-GLMB and are significantly better than those of the two robust filters (see Figure 4.20). Furthermore, while the ideal-GLMB and the Bootstrapped-GLMB are almost identical in tracking errors of cardinality statistics, these results are better than the errors measured by the Robust-CPHD and Robust-GLMB filters. One hypothesis is that in some components of the Robust-GLMB filtering density, the measurements generated by clutter statistics might be connected to truly miss-detected tracks (i.e., those components with insignificant weights).

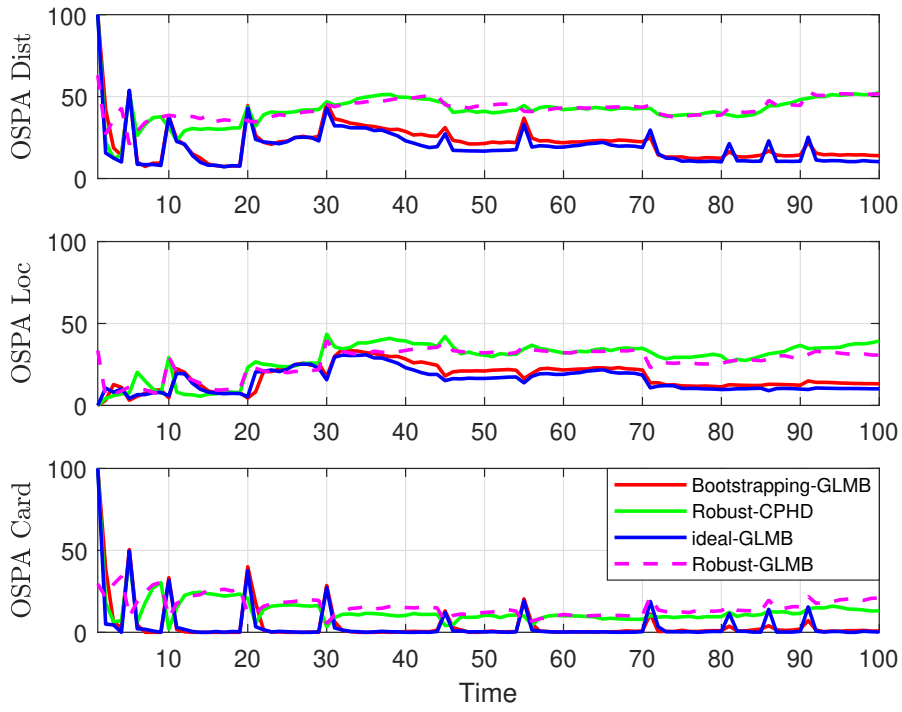

Figure 4.20: Tracking errors in distance, location and cardinality components for the four filters using the OSPA metric.

The cardinality with 100 MC runs using the Bootstrapped-GLMB filter is shown for the ideal-GLMB and the other two robust filters (see Figure 4.22). This figure again certifies the superior performance of the GLMB filters over the CPHD filter.

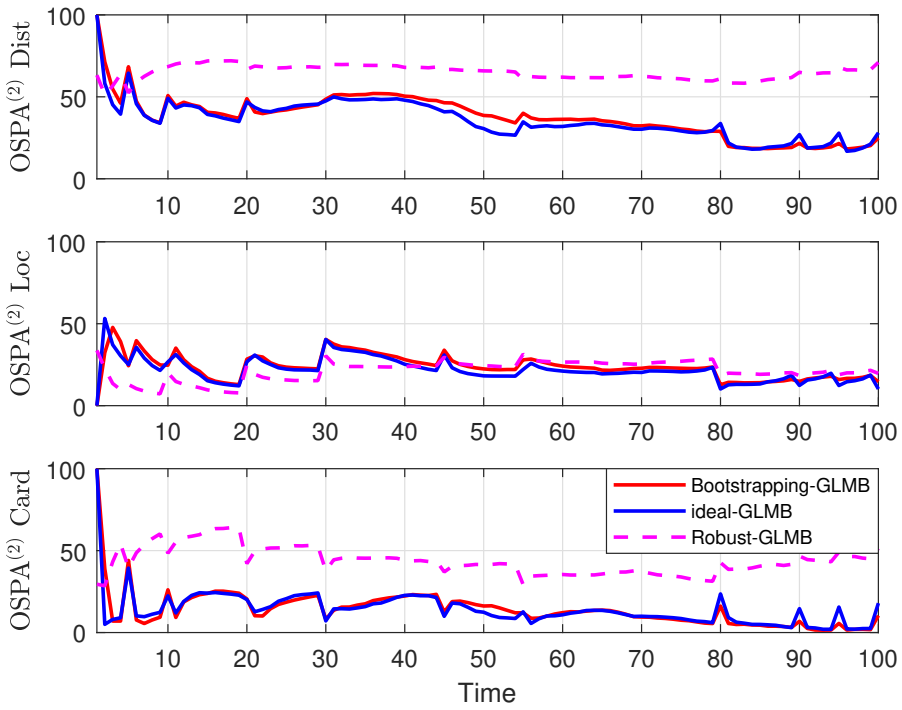

Figure 4.21: Tracking errors in distance, location and cardinality components for the three GLMB-based filters using the OSPA$^{(2)}$ metric.

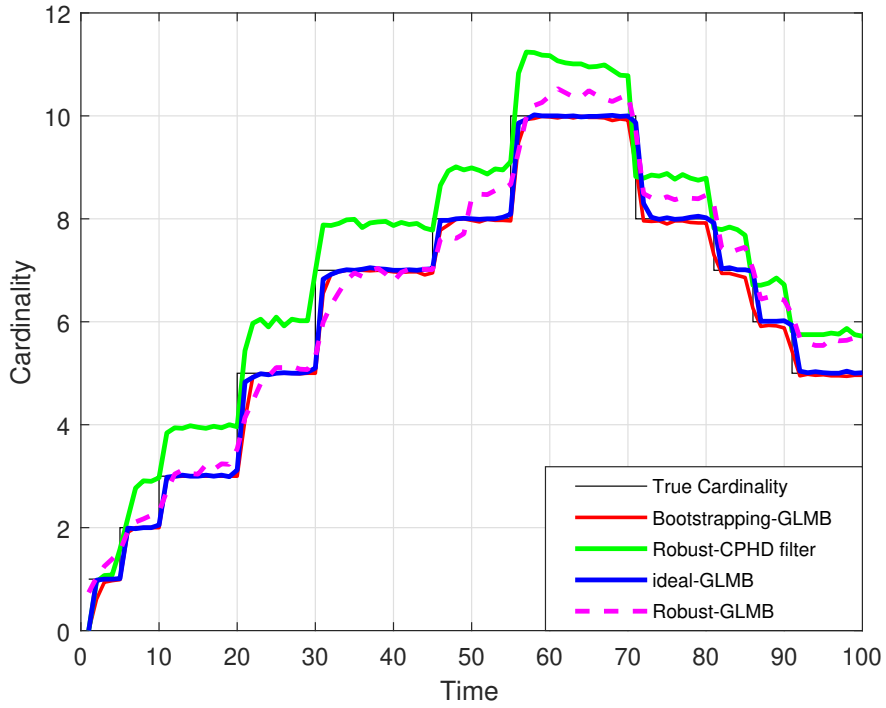

Figure 4.22: Comparison of cardinality tracking results for the four filters.

Scenario 3: Nonlinear tracking with unknown background and unknown birth model

Currently, there is no adaptive GLMB filter or adaptive CPHD filter that can manage the problem of both unknown background and unknown birth model. Therefore, the implementation of the Bootstrapped-GLMB filter is evaluated comparing to those of the ideal-GLMB and ideal-CPHD filters. Specifically, the number of hypotheses is capped at 5000 components for the Bootstrapped-GLMB and ideal-GLMB algorithms. The OSPA and OSPA$^{(2)}$ metrics are adopted to compare the tracking errors of the given filters over 100 MC runs. These comparisons are demonstrated in Figure 4.23 and Figure 4.24, respectively. The result of estimating target cardinality over time is illustrated in Figure 4.25. In addition, Figure 4.26 and Figure 4.27 present the results of estimated detection probability and estimated clutter rate with 3-sigma bounds over time using the Bootstrapped-GLMB filter, respectively,.

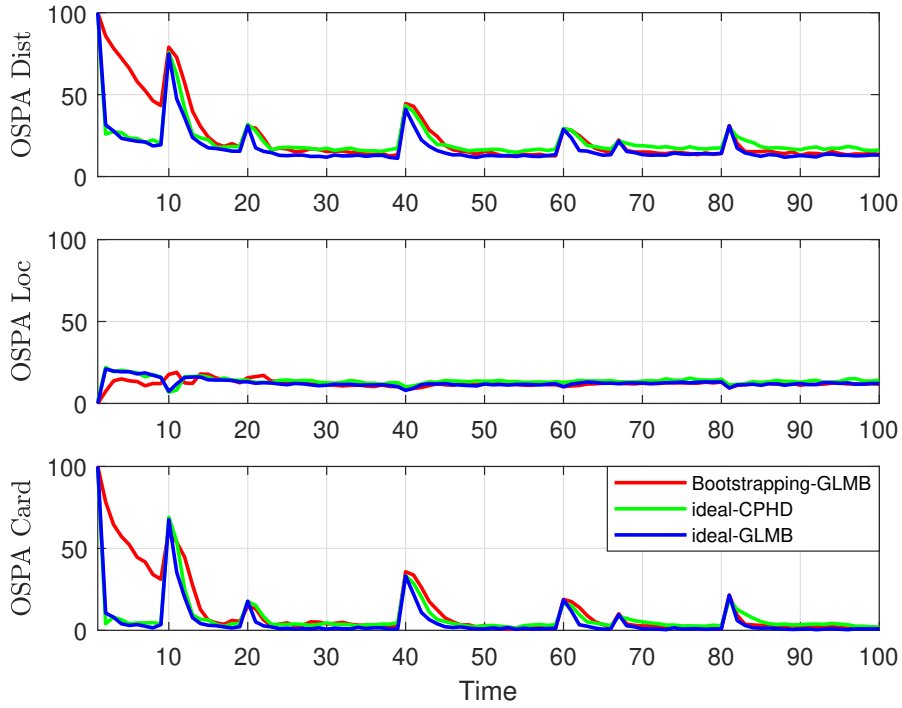

Figure 4.23: Mean OSPA errors for the three filters.

From the simulation results using the OSPA and OSPA$^{(2)}$ metrics, it could be observed that there filters were almost identical in OSPA errors. However, the ideal-GLMB filter outperforms the Bootstrapped-GLMB filter in OSPA$^{(2)}$ errors. This is reasonable since the two ideal filters are supported by correct parameters of back-

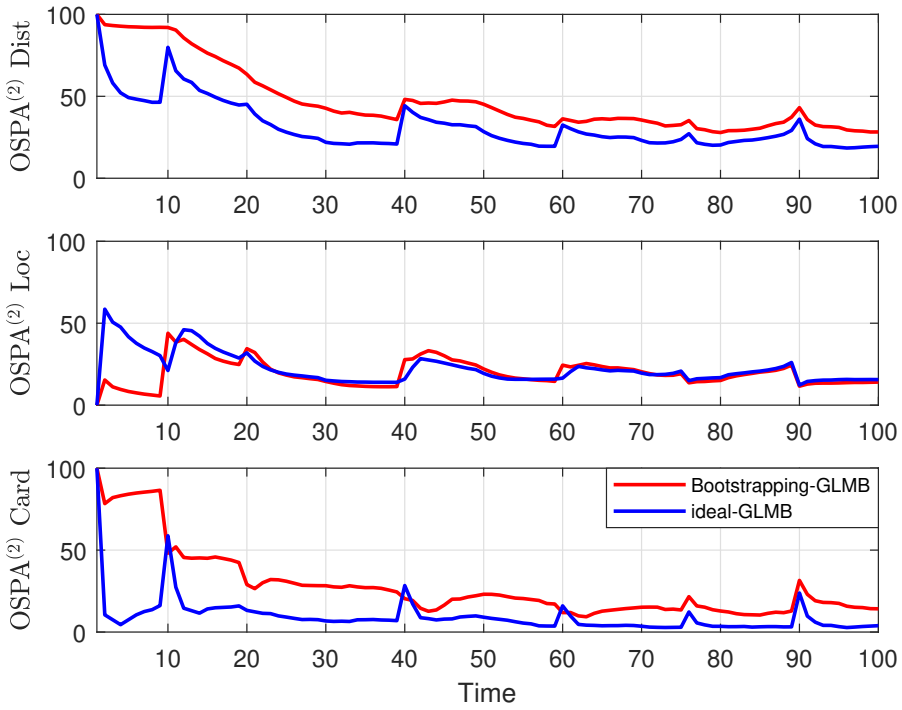

Figure 4.24: Mean OSPA$^{(2)}$ errors for the ideal-GLMB and the Bootstrapped-GLMB filters.

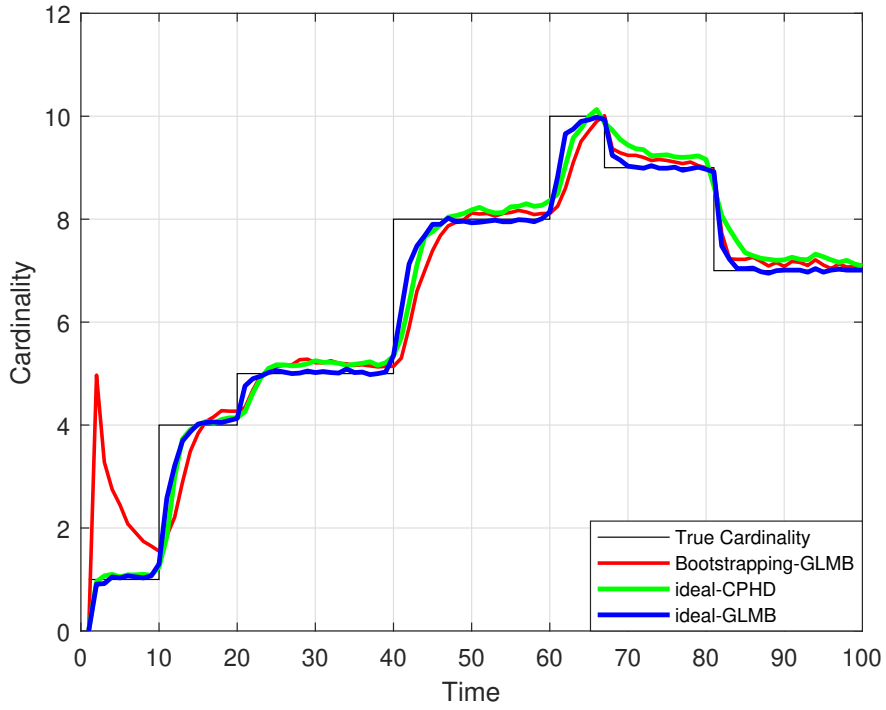

Figure 4.25: The estimated cardinalities for the two ideal filters and the Boostrapping-GLMB filter.

grounds and birth model while these parameters are unknown to the Bootstrapped-GLMB filter. Overall, the outstanding implementation of the ideal-GLMB filter further demonstrates the correct choice of using it as the backbone for the plug-and-play Bootstrapped-GLMB tracker. Most importantly even with unknown parameters such as the clutter rate, detection probability and birth model the implementation of the Bootstrapped-GLMB filter is comparable to the two ideal filters in estimating the cardinality of targets. For the estimation of unknown backgrounds, Figure 4.11 and Figure 4.26, respectively, demonstrate the convergence of the estimated values of detection probability and clutter rate to their correct value as more measurement data are updated, ceasing the initial high uncertainties.

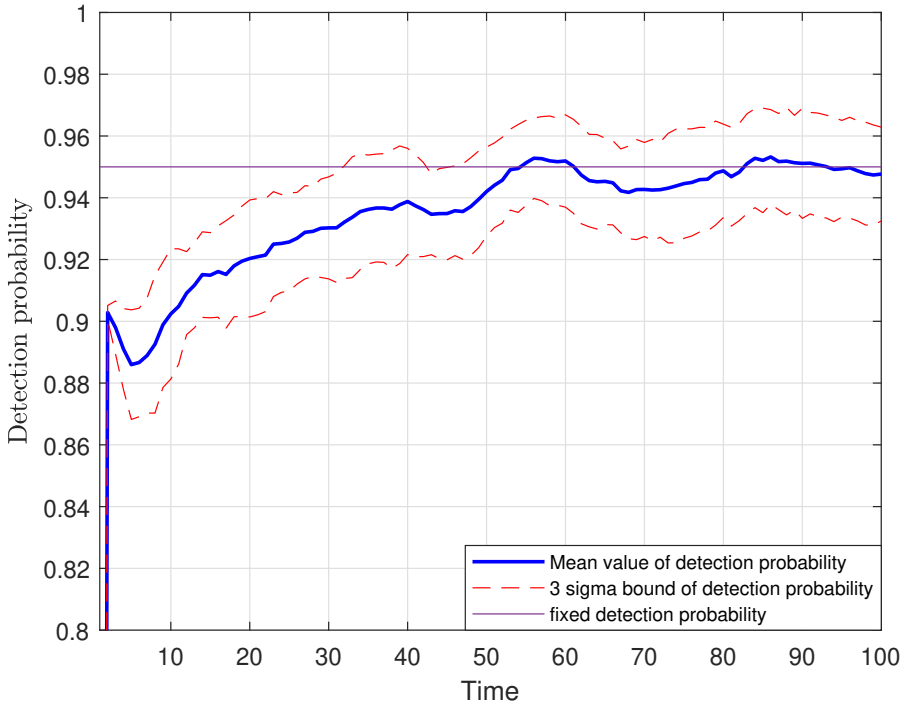

Figure 4.26: Estimated detection probability for the Bootstrapped-GLMB filter.

4.4 Conclusions

This chapter describes how the Bootstrapped-GLMB filter given in Chapter 3 has been extended to accommodate the unknown detection probability; jointly unknown clutter rate and unknown detection probability; unknown parameters of the birth model. Most importantly, using the combination of techniques given in Section 3.2.2 and Section 4.2.1, the resultant low-cost tracker mitigates the requirements for offline training

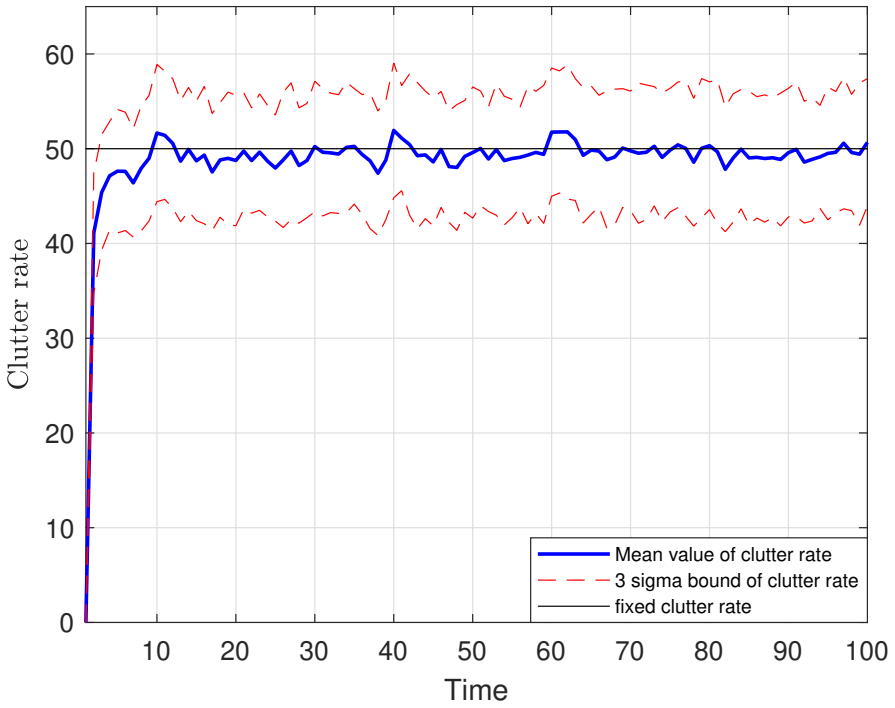

Figure 4.27: Estimations of the clutter rate using the Bootstrapped-GLMB filter.

data or tediously manually tuning. The experimental results validate the efficacy and accuracy of the proposed filter that is comparable to an ideal-GLMB filter (supplied with correct parameters) in tracking target trajectories. The resultant tracker is robust enough for many medium-clutter and low-clutter multi-target tracking applications such as air traffic control, surveillance, defence, space applications, oceanography, autonomous vehicles and robotics, remote sensing, computer vision, and biomedical research. For instance, this method has been recently applied to online cell biology tracking [35, 144]. For the future research, this bootrapping method is investigated with the use of multiple sensors, object spawning and multi-scan state estimation.

CHAPTER 5

ROBUST MULTI-SENSOR MULTI-TARGET TRACKING

This chapter presents an efficient and robust multi-sensor multi-target algorithm that leverages the advantages of existing RFS-based filters to estimate target trajectories when the probability of target detection and the clutter rate are unknown and vary over time. Specifically, this algorithm is constructed using the combination of the MS-GLMB filter and multiple robust CPHD filters. The performance of the resulting robust MS-GLMB filter has been compared to the optimal MS-GLMB filter which is supplied with correct parameters of background information. The experimental studies demonstrate the efficacy and effectiveness of the robust MS-GLMB filter with its capability of achieving the near-optimal implementation comparing to the optimal MS-GLMB filter. More impresively, this robust MS-GLMB filter outperforms other robust filters in handling the unknown background information. This is contributed to the capability of the robust bootstrapped filter to estimate the background parameters while operating.

5.1 Introduction

Multi-sensor multi-target tracking is an emerging technology that tracks multiple targets more efficiently using combined measurements from several sensors [126]. Multi-sensor settings are frequently used in multi-target tracking applications to de-escalate the uncertainty of the tracking system, thereby they enhance the ability of the tracking approaches to accomodate the ambiguity of the target states. Currently, there are three common multi-sensor architectures[1] for multi-target tracking: centralised, distributed,

[1] This categorisation is given in [126]. However, in the author's publication [73],by considering each fusion centre with its connected sensors as a node, the decentralised and distributed architectures are combined.

and decentralised [145–147], as shown in Figure 5.1.

In the centralised architecture (see Figure 5.1(a)), information collected from all sensors is delivered to a central fusion node. This central node uses this information to direct compute the multi-target density and fuses all the acquired measurements and updates the tracks. While this architecture is considered the theoretically optimal setting in terms of tracking performance as there is no information loss, it may not be feasible because of limited resources, such as communication bandwidth and computational power in a large surveillance area with many sensors [148, Chap.5].

To improve the reliability and performance of this architecture by reducing the communication among central fusions nodes, the decoupled, replicated centralised settings and distributed or hierarchical architecture without feedback were proposed [148]. The decoupled architecture partitions the centralised one into groups of sensors - fusion nodes. This architecture has the lowest computational and communication requirements as it uses multiple fusion nodes, in which each node is responsible for only the sensors in its set. However, the performance of this architecture highly depends on the partition of sensors. The replicated centralised architecture [149] uses multiple fusion nodes to process the same data from overlapping sets of all sensors. These fusion nodes do not communicate with each other. Although the decoupled architecture has high performance and reliability, it has drawbacks of heavy communication and processing.

The distributed or hierarchical architecture (see Figure 5.1(c)) is proposed to prevent the high load of communication and computational cost of the central fusion [146]. In the hierarchical architecture, the fusion nodes are hierarchised with low-level nodes and a high-level node. Data collected from each sensor group are processed by a low-level node to form local estimates. These local estimates are delivered to a high-level node for final processing to form posterior multi-target density. This hierarchical architecture reduces the communication and processing cost and increases reliability. The downside of this architecture is that it requires a strong correlation between the fused (from distributed sensor nodes) and the actual multi-sensor updated densities for a consistent capability of tracking. [22].

When the surveillance area is large and there is no communication from the central

fusion node to all local fusion nodes, then both the centralised and distributed trackings are impossible. An alternative architecture, the decentralised architecture (see Figure 5.1(b)) is applied in this case [126]. Instead of using a central fusion node, the decentralised architecture uses multiple fusion nodes to connect with one or more sensors. Each fusion node receives measurements from its connected sensor(s) then uses information in these measurements to update its tracks. As each node can communicate with its neighbours, it also updates tracks with additional information delivered from its neighbours. The limitation of this architecture is that each fusion node can only communicate with its neighbours and cannot broadcast its results.

In the RFS framework, these mentioned architectures have been adopted to solve the problem of multi-sensor multi-target tracking. The decentralised setting has been addressed with the PHD-CPHD filters [150–153], the multi-Bernoulli filter [154–157] and the LMB-GLMB filters [36, 118, 158]. The distributed architecture has been applied for the PHD and CPHD filters [85] and the LMB and marginalised GLMB filters [48, 110]. Solutions to the tracking problem using centralised architecture have been developed using PHD and CPHD filters [159, 160], the multi-Bernoulli filter [161], and the LMB filter [113, 116, 117, 162]. Notably, the recent centralised MS-GLMB filter [22] demonstrates its applicable and scalable solution in practice via efficiently implementation of the joint sensor update with low computational complexity of $\mathcal{O}\left(TP^2\prod_{s=1}^{V}m^{(s)}\right)$ as mentioned in Section 2.6.1.

The performance of multi-target trackers is highly influenced by the background information (such as the probability of target detection and clutter statistics). In practical applications, the background parameters often vary with time and and are known a priori. However, these parameters are usually assumed to be known and constant leading to the biased or degraded tracking performance of the trackers. In multi-sensor architectures, since each sensor needs the background parameters for generating accurate measurements, incorrect values of these parameters make a worsened performance of the trackers. The problem of tracking targets with unknown background information has been addressed to the single-sensor systems with the CPHD filter [96, 130] and GLMB filter [131], as well as a bootstrapped filter using a combination of the CPHD and GLMB filters [70, 71]. However, this problem has not been examined in the multi-sensor systems.

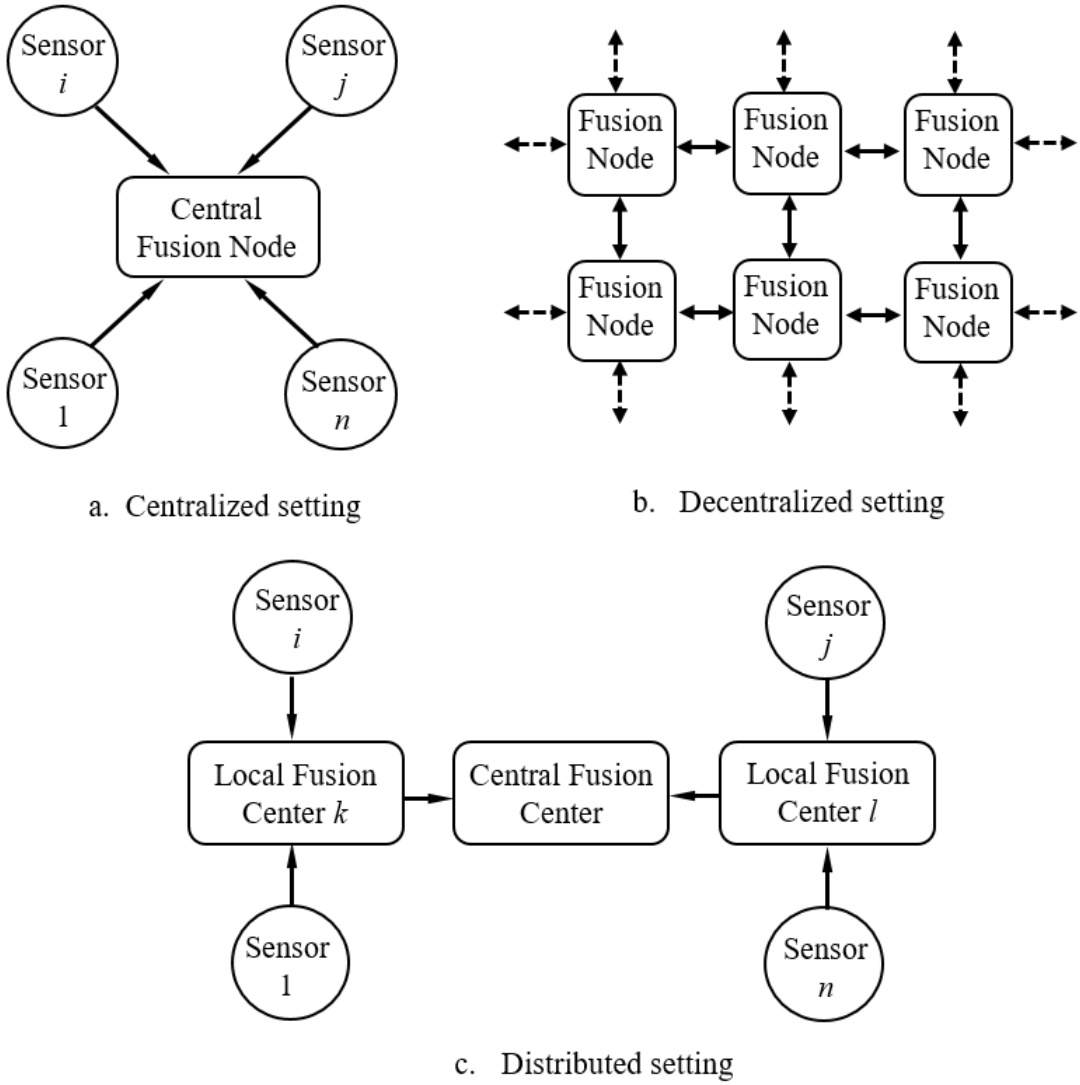

Figure 5.1: Three common multi-sensor architectures [126].

This chapter presents a robust tracker which uses the centralised multi-sensor architecture to estimate target trajectories in an unknown background information. This tracker is constructed using a systematic combination of the robust CPHD filters [96] and a MS-GLMB filter [22].

Section 5.1 delivers background information on multi-target tracking using the RFS concept. Section 5.2 outlines the formulation and implementation of the proposed robust MS-GLMB tracker. The expermental implementation of this filter in different tracking scenarios is demonstrated in Section 5.3 followed by some concluding marks on the main contribution of this chapter in Section 5.4. Although the proposed robust filter in this chapter can accommodate different types of sensors, this chapter focuses on the tracking scenario using bearing-only sensors as published in the author's journal article [73].

5.2 Robust multi-sensor multi-target tracking

This section describes the implementation of the robust MS-GLMB tracker that solves the problem of multi-target tracking without prior known information of the detection probability and clutter rate based on the advantage exploitation of the validated RFS-based filters. In particular, the MS-GLMB filter [22] is adopted for the main filtering process. In addition, a number of the robust CPHD filters [96] are used corresponding to the number of the sensors in the system in which each filter estimates the clutter rate for a sensor. These robust CPHD filters use the intensity and cardinality distribution of the targets set contained in the MS-GLMB density at the previous time step to independently estimate the clutter rates. The mean values of these estimated clutter rates is then bootstrapped into the MS-GLMB filter. The schematic of the algorithm is given in Figure 5.2.

5.2.1 Main filtering process

The MS-GLMB filter [22] is adopted for the main filtering process of the robust GLMB tracker. The MS-GLMB filter is a new version of the efficient GLMB filter [40] applied to the centralised multi-sensor architecture. Consequently, the MS-GLMB filter is formulated to propagate the labelled multi-target density, providing estimates of target tracks. The robust MS-GLMB tracker exploits this capability of tracking target trajectories of the MS-GLMB filter in its implementation. Since the unknown information

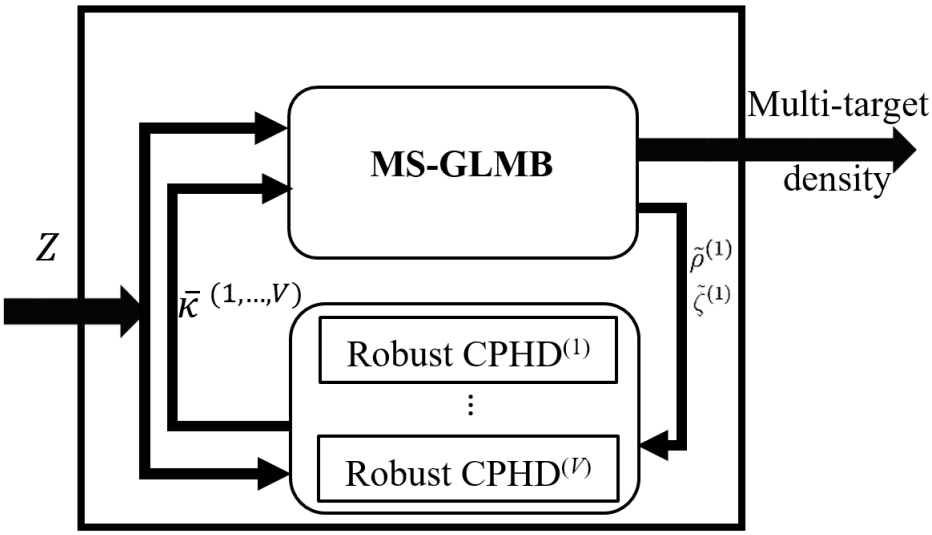

Figure 5.2: The diagram of the robust MS-GLMB tracker based on the combination of an MS-GLMB and several robust CPHD filters.

on the target detection probability is augmented into the single-target state, the MS-GLMB in this work is formulated to estimate this parameter and carries out the main process. The information on the sensors' clutter rates is bootstrapped from the robust CPHD filters.

Suppose that the probability of detecting a target on each sensor is independent of those of the other sensors. Since the detection probability α is augmented into a single target state x with label ℓ,the state distribution of this single-target state can be written as $p^{(\xi)}(x,\alpha,\ell) = p^{(\xi)}(x,\ell)\prod_{v=1}^{V} p^{(\xi)}(\alpha_v)$, where ξ is the association history. The state transition model given in Eq. (2.51) now can be described with the augmented part as follows:

$$\begin{aligned}\Phi_{S+}\left(\boldsymbol{X}_{S,+}|x,\alpha,\ell\right) = &\sum_{(x_+,\ell_+)\in\boldsymbol{X}_{S+}} \delta_{\ell}\left(\ell_+\right) p_S\left(x,\ell\right) f_{S,+}\left(x_+|x,\ell\right) \\ &\times \prod_{v=1}^{V} f_{\Delta,+}^{(v)}\left(\alpha_{i+}|\alpha_i\right) + \left[1 - 1_{\mathcal{L}(\boldsymbol{X}_{S,+})}\left(\ell\right)\right] q_S\left(x,\ell\right).\end{aligned} \tag{5.1}$$

in which $f_{\Delta,+}^{(v)}(\cdot|\cdot)$ denotes the state transition density of the probability of the sensor v^{th} in detecting a target.

The likelihood function given in Eq. (2.55) for single-sensor case is now extended to the multi-sensor case as proposed by by Vo et. al. [22]. In particularly, given the multi-target state $\boldsymbol{X}$, the sensor v^{th} can detect a target $(x,\alpha,\ell) \in \boldsymbol{X}$ or miss-detect this

target. If the target is detected then a measurement $z_j^{(v)}$ is generated with the probability of target detection α_v with likehood $g^{(v)}(z^{(v)}|x,\ell)$. If the target is miss-detected, then it becomes an empty measurement with the probability $1-\alpha_v$. In addition, the sensor v^{th} can detect clutter as actual targets and generate the corresponding measurements. Therefore, the set of all measurements produced by the sensor v^{th} is given by $Z^{(v)} = \left\{z_{1:|Z^{(v)}|}^{(v)}\right\} \in \mathbb{Z}$ which involves the measurements generated from actual targets and clutter. The set of the clutter-generated measurements is modelled by Poisson RFS with the intensity (rate) $\kappa^{(v)}$. Noting that, in the robust MS-GLMB tracker, the mean values of clutter rates estimated by the robust-CPHD filters are bootstrapped into the MS-GLMB filter. The MS-GLMB filter uses these values as its known parameters.

Using the abbreviations given in Eq. (2.70) to Eq. (2.75), and the assumption that all sensors are conditionally independent, the likelihood function for single-sensor multi-target tracking Eq. (2.55) is extended as described in Eq. (2.76).

5.2.2 Estimation of unknown background information using the robust CPHD recursion

The CPHD filter is constructed using the concept of the (unlabelled) RFSs. This filter is an extension of the PHD filter. Since the CPHD uses the cardinality distribution in addition to the intensity (PHD) of the targets to estimate the multi-target density, it is more accurate than the PHD filter. Further, as the complexity of the CPHD is $\mathcal{O}\left(|Z|^3\right)$ or even $\mathcal{O}\left(|Z|^2\log^2(|Z|)\right)$ [18], this filter is benefited from a low-cost computation. An extension of the CPHD, the robust CPHD filter, has been introduced in [96] to jointly estimate the clutter rate and detection probability while filtering. In this work, we propose using several robust CPHD filters to estimate the clutter rates of the sensors (each filter jointly estimates the two background parameters of one sensor). The mean values of the estimated clutter rates are then bootstrapped into the MS-GLMB filter. Note that, while the GLMB filter can jointly estimate these two unknown background prameters of each sensor using the data association method as presented in [131], it has a complexity of $\mathcal{O}\left(T\,|Z|^3\right)$ (where T is the number of request terms and $|Z|$ is the number of measurements) for each prior component of the GLMB density. Furthermore, this method is applied with single-sensor setting only. Due to the NP-hard dimensional assignment problem in the multi-sensor setting, the data association method is almost imposible to apply. Hence, the solution on using the GLMB filter to estimate the de-

tection profile and several robust CPHD filters to estimate the clutter rates of sensors is introduced as a trade-off between the computational cost and the accuracy of the robust MS-GLMB tracker. This chapter can be considered an extension of Chapter 3.

The robust CPHD filtering method to jointly estimate the unknown information on the clutter rate and detection profile in Section 4.2.2 is extended in this work. Note that, since the measurements from all sensors are delivered to the MS-GLMB filter, this filter have more accurate updated intensity and cardinality distribution than those using measurements from a single sensor. Therefore, in this work, the robust CPHD filter corresponding to the v^{th} sensor receives the prior intensity and cardinality distribution from the MS-GLMB density instead of using its prior information and running parallel with the GLMB filter as in Section 4.2.2. In addition to the received prior information, the robust CPHD filter uses the set of measurements from its corresponding sensor to calculate the multi-target density at each time step.

Given the GLMB prior of the form in Eq. (2.44), the intensity and cardinality distribution of an actual target state can be computed as follows:

$$\tilde{v}^{(1)}(x) = \sum_{I,\xi} \sum_{\ell \in I} \omega^{(I,\xi)} p^{(\xi)}(x,\ell) \prod_{v=1}^{V} p^{(\xi)}(\alpha_v)\, d\alpha_v, \tag{5.2}$$

$$\tilde{\rho}^{(1)}(n) = \sum_{I,\xi} \delta_n(|I|)\, \omega^{(I,\xi)}. \tag{5.3}$$

Since the targets involve actual targets and clutter-generated targets, the cardinality distribution of targets on the hybrid state space is given by the convolution $\tilde{\rho}^{(h)} = \tilde{\rho}^{(1)} * \rho^{(0)}$ ($'*'$ is the convolution operator).

Given Eq. (5.2) and Eq. (5.3) and the prior information of the current sensor clutter-generated targets, the prediction stage of the robust CPHD can be implemented as

expressed in Section 4.2.2:

$$\nu_{+}^{(v,1)}(x_{+},a_{+}) = \nu_{B+}^{(1)}(x,a) + \int\int p_{S}^{(1)}(x)\, f_{+}^{(1)}(x_{+}|x)\, f_{+}^{(\Delta)}(a_{+}|a)\, \tilde{\nu}^{(1)}(x,a)\, dadx \tag{5.4}$$

$$\nu_{+}^{(v,0)}(b) = \nu_{B,+}^{(v,0)}(b) + p_{S}^{(v,0)} \nu^{(v,0)}(b) \tag{5.5}$$

$$\rho_{+}^{(v,h)}(n) = \sum_{j=0}^{n} \rho_{B,+}^{(v,h)}(n-j) \sum_{i=j}^{\infty} C_{j}^{i} \tilde{\rho}^{(v,h)}(i)(1-\phi_{v})^{i-j} \phi_{v}^{j} \tag{5.6}$$

$$\phi_{v} = \frac{\left\langle \tilde{\nu}^{1}, p_{S}^{(1)} \right\rangle + \left\langle \nu^{(v,0)}, p_{S}^{(v,0)} \right\rangle}{\left\langle 1, \tilde{\nu}^{(1)} \right\rangle + \left\langle 1, \nu^{(v,0)} \right\rangle} \tag{5.7}$$

where $C_{j}^{i} = \frac{i!}{j!(i-j)!}$ is the binomial coefficient.

Given the set of measurements $Z_{+}^{(v)}$ of the sensor v^{th}, the updated intensity and cardinality distribution are computed as [96]:

$$\begin{aligned}\nu_{+}^{(v,1)}\left(x_{+},a_{+}|Z_{+}^{(v)}\right) = & (1-a_{+}) \times \frac{\left\langle \Gamma_{Z_{+}^{(v)}}^{(v,1)}\left[\nu_{+}^{(v,h)}, Z_{+}^{(v)}\right], \rho_{+}^{(v,h)} \right\rangle}{\left\langle \Gamma_{Z_{+}^{(v)}}^{(v,0)}\left[\nu_{+}^{(v,h)}, Z_{+}^{(v)}\right], \rho_{+}^{(v,h)} \right\rangle} \frac{\nu_{+}^{(v,1)}(x_{+},a_{+})}{\left\langle 1, \nu_{+}^{(v,1)} \right\rangle + \left\langle 1, \nu_{+}^{(v,0)} \right\rangle} \\ & + \sum_{z \in Z_{+}^{(v)}} \frac{a_{+} \times g^{(v,1)}(z|x_{+})}{\left\langle \nu_{+}^{(v,0)}, p_{D,+}^{(v,0)} \mu^{(v)} \right\rangle + \left\langle \nu_{+}^{(v,1)}, p_{D,+}^{(v,1)} g^{(v,1)}(z|\cdot) \right\rangle} \nu_{+}^{(v,1)}(x_{+},a_{+})\end{aligned} \tag{5.8}$$

$$\begin{aligned}\nu_{+}^{(v,0)}\left(b_{+}|Z_{+}^{(v)}\right) = & (1-b_{+}) \times \frac{\left\langle \Gamma_{Z_{+}^{(v)}}^{(v,1)}\left[\nu_{+}^{(v,h)}, Z_{+}^{(v)}\right], \rho_{+}^{(v,h)} \right\rangle}{\left\langle \Gamma_{+}^{(v,0)}\left[\nu_{+}^{(v,h)}, Z_{+}^{(v)}\right], \rho_{+}^{(v,h)} \right\rangle} \frac{\nu_{+}^{(v,0)}(b_{+})}{\left\langle 1, \nu_{+}^{(v,1)} \right\rangle + \left\langle 1, \nu_{+}^{(v,0)} \right\rangle} \\ & + \sum_{z \in Z_{+}^{(s)}} \frac{b_{+} \times \mu^{(v)}(z)}{\left\langle \nu_{+}^{(v,0)}, p_{D,+}^{(v,0)} \mu^{(v)} \right\rangle + \left\langle \nu_{+}^{(v,1)}, p_{D,+}^{(v,1)} g^{(v,1)}(z|\cdot) \right\rangle} \nu_{+}^{(v,0)}(b_{+})\end{aligned} \tag{5.9}$$

$$\rho_{+}^{(v,h)}(n) = \begin{cases} 0, & n < |Z_{+}^{(v)}| \\ \frac{\rho(n) \cdot \Gamma^{(v,0)}[\nu_{+} Z_{+}^{(v)}](n)}{\left\langle \rho_{+}^{(v,h)}, \Gamma_{+}^{(v,0)} \right\rangle}, & n \geq |Z_{+}^{(v)}| \end{cases} \tag{5.10}$$

where

$$\Gamma_{+}^{(v,u)}\left[\nu_{+}^{(v,h)} Z_{+}^{(v)}\right](n) = \begin{cases} 0, & n < |Z_{+}^{(v)}| + u \\ P_{|Z_{+}^{(v)}|+u}^{(n)} \Phi_{v,+}^{\left(n-\left(|Z_{+}^{(v)}|+u\right)\right)}, & n \geq |Z_{+}^{(v)}| + u, \end{cases} \tag{5.11}$$

$$\Phi_{v,+} = 1 - \frac{\left\langle \nu_+^{(v,1)}, p_{D,+}^{(v,1)} \right\rangle + \left\langle \nu_+^{(v,0)}, p_{D,+}^{(v,0)} \right\rangle}{\left\langle 1, \nu_+^{(v,1)} \right\rangle + \left\langle 1, \nu_+^{(v,0)} \right\rangle}, \tag{5.12}$$

$$p_{D,+}^{(v,1)}(x,a) = a, \tag{5.13}$$

$$p_{D,+}^{(v,0)}(b) = b, \tag{5.14}$$

and P_j^n is the permutation coefficient, i.e.,$P_j^n = \frac{n!}{(n-j)!}$.

This work used the assumption of Beta - Gaussian mixture on the distribution of joint kinematic and detection probability, as given in Section 4.2.2. The analytic implementation can be found in [96, Propositions 13, 14]. Given the assumptions that the set of clutter statistics is a Poisson RFS and the clutter state is uniformly distributed on the measurement space, the mean value $\bar{\kappa}^{(v)}$ of the clutter rate for the sensor v^{th} is calculated as [96]:

$$\bar{\kappa}^{(v)} = \sum_{i=1}^{J^{(v,0)}} \omega_i^{(v,0)} \frac{s_i^{(v,0)}}{s_i^{(v,0)} + t_i^{(v,0)}} \tag{5.15}$$

Practically, the step for estimating the clutter rate and detection profile can be parallelised for V sensors to reduce the computational time.

5.2.3 Main filtering process using MS-GLMB filter

The MS-GLMB filter uses the set of estimated clutter rates $\bar{\kappa}^{(1:V)}$ (see Eq. (5.15)) as known parameters to perform the main multi-target filtering. Given the initial GLMB density of the form in Eq. (2.44), with the transition models in Eq. (2.54) and Eq. (5.1), and the likelihood model in Eq. (2.76), at the next time step, the GLMB filtering density is computed as:

$$\boldsymbol{\pi}_+(\boldsymbol{X}_+|Z_+) \propto \Delta(\boldsymbol{X}_+) \sum_{I,\xi,I_+,\theta_+} \omega^{(I,\xi)} \omega_{Z_+}^{(I,\xi,I_+,\theta_+)} \delta_{I_+}[\mathcal{L}(\boldsymbol{X}_+)] \left[p_{Z_+}^{(\xi,\theta_+)}\right]^{\boldsymbol{X}_+}, \tag{5.16}$$

where $I \in \mathcal{F}(\mathbb{L})$, $\xi \in \Xi$, $I_+ \in \mathcal{F}(\mathbb{L}_+)$, $\theta_+ \in \Theta_+(I_+)$, and

$$\omega_{Z_+}^{(I,\xi,I_+,\theta_+)} = 1_{\Theta_+(I_+)}(\theta_+) \left[1 - \bar{P}_S^{(\xi)}\right]^{I-I_+} \left[\bar{P}_S^{(\xi)}\right]^{I \cap I_+} [1 - r_{B,+}]^{\mathbb{B}_+ - I_+} r_{B,+}^{\mathbb{B}_+ \cap I_+} \left[\bar{\psi}_{Z_+}^{(\xi,\theta_+)}\right]^{I_+}, \tag{5.17}$$

$$\bar{P}_S^{(\xi)}(\ell) = \left\langle p^{(\xi)}(\cdot,\ell), P_S(\cdot,\ell) \right\rangle, \tag{5.18}$$

$$\bar{\psi}_{Z_+}^{(\xi,\theta_+)}(\ell_+) = \int \bar{p}_+^{(\xi)}(x_+,\ell_+) \prod_{v=1}^{V} p^{(\xi)}(\alpha_v) \psi_{Z_+}^{(\theta_+(\ell_+))}(x_+,\alpha_+,\ell_+)\, dx_+ d\alpha_{1:V}, \tag{5.19}$$

$$p_S(x_+,\alpha_+,\ell_+) = \int P_S(x,\ell_+)\, f_{S,+}(x_+|x,\ell_+)\, p^{(\xi)}(x,\ell_+)\, dx \times \prod_{v=1}^{V} \int p^{(\xi)}(\alpha_v) f_{\Delta,+}^{(v)}(\alpha_{v,+}|\alpha_v) d\alpha_v, \tag{5.20}$$

$$\bar{p}_+^{(\xi)}(x_+,\alpha_+,\ell_+) = 1_{\mathbb{L}}(\ell_+) \frac{p_S(x_+,\alpha_+,\ell_+)}{\bar{P}_S^{(\xi)}(\ell_+)} + 1_{\mathbb{B}_+}(\ell_+)\, p_{B,+}(x_+,\ell_+), \tag{5.21}$$

$$p_{Z_+}^{(\xi,\theta_+)}(x_+,\alpha_+,\ell_+) = \frac{\bar{p}_+^{(\xi)}(x_+,\alpha_+,\ell_+)\, \psi_{Z_+}^{(\theta_+(\ell_+))}(x_+,\alpha_+\ell_+)}{\bar{\psi}_{Z_+}^{(\xi,\theta_+)}(\ell_+)}. \tag{5.22}$$

The truncation need to used to prevent the exponential growth in the number of the components in the GLMB filtering density. This work is performed to truncate the components with low weights and select the significant components with the highest weights to keep the filter tractable. One of the truncation methods is to formulate the multi-dimensional assignment on the extendend association maps. Nevertheless, given the high number of the sensors, solving the resulted multi-dimensional assigment problem is NP-hard, and intractable. Conversely, the Gibbs sampler can be used to effeciently sample significant components from a stationary distribution. Nevertheless, in multi-sensor scenarios, this approach requires a large amount of memory to reposit the high-dimensional distribution, that leads to the intractability of the filter. In [22], the authors assumed the minimally-Markovian (between sensors) on the stationary distribution to overcome the drawback of the mentioned Gibbs sampler in multi-sensor multi-target tracking. The resultant algorithm significantly reduces the time of computation and the requirement on memory usage. More importantly, this work allows tracking multiple targets online with a high number of sensors. The procedure of filtering process is presented in [22, Algorithm 2].

In the implementation of the robust MS-GLMB tracker, the kinematic of the system is modelled by the Gaussian distribution and the detection probability of the sensor is modelled by the independent Beta distribution. The prediction and update of each Beta distribution are given in [96]. The pseudo-code for this implementation is given in Algorithm 1. Specifically, the modelCPHD and modelGLMB involve the corresponding models of transition and likelihood for the robust CPHD and MS-GLMB filters as presented in Section 5.2.1 and Section 5.2.2. Given the posterior density, the multi-target

[24] or multi-trajectory [22, 31] filtering approaches can be adopted to extract target tracks. In this chapter, the sub-optimal multi-target filtering approach introduced in [24] is applied to estimate target tracks. Since the MS-GLMB filter has the complexity of $\mathcal{O}\left(TP^2\left(|\sum_{v=1}^{V} Z^{(v)}|\right)\right)$, the overall complexity in the robust MS-GLMB algorithm is $\mathcal{O}\left(TP^2\left(|\sum_{v=1}^{V} Z^{(v)}|\right)\right)$.

Input: modelGLMB, priorGLMB, modelCPHD, $[\text{priorCPHD}]^{(1:V)}$, Z_+
Output: posteriorGLMB, $[\text{posteriorCPHD}]^{(1:V)}$, EstimatedTracks

---

Compute $\tilde{\rho}^{(1)}$,$\tilde{\upsilon}^{(1)}$ via Eq. (5.2)) and Eq. (5.3) using priorGLMB .
for $v = 1 : V$ (parallelisable)
  posteriorCPHD$^{(v)}$=robust-CPHD-Recursion $\left(\tilde{\rho}^{(1)}, \tilde{\upsilon}^{(1)}, \text{modelCPHD}, \text{priorCPHD}^{(v)}, Z_+\right)$
  Compute $\bar{\kappa}^{(v)}$ via Eq. (5.15) and $p_D^{(v)}$ using posteriorCPHD$^{(v)}$
end
posteriorGLMB= MS-GLMB-Recursion($\bar{\kappa}^{(1:V)}$, $\bar{p}_D^{(1:V)}$, modelGLMB, priorGLMB, Z_+);
EstimatedTracks=MultiTargetEstimator(posteriorGLMB)

Algorithm 1: The pseudo-code for the implementation of the robust MS-GLMB tracker.

5.3 Numerical study

This section presents a number of experiments to test the accuracy and effectiveness of the robust MS-GLMB filter by comparing its performance with those of the MS-GLMB (sub-optimal implementation) and iterated corrector GLMB (IC-GLMB) estimators. Eight bearing-only sensors are used in a $2D$ surveillance area to track 10 targets with their true trajectories illustrated in Figure 5.3. Each kinematic state of a target is represented by a $4D$ vector $x = [p_x, p_y, \dot{p}_x, \dot{p}_y]^T$, where p_x, p_y are the planar positions and $\dot{p}_x, \dot{p}_y$ are the corresponding planar velocities of the state x, and T is the matrix transpose operator. The transition density for a single target is a Gaussian:

$$f_{S+}(x_+|x,\ell) = \mathcal{N}(x_+; Fx, Q), \tag{5.23}$$

where $\mathcal{N}(\cdot;\bar{x},P)$ denotes a Gaussian distribution with mean $\bar{x}$ and covariance P, $F = \begin{bmatrix} I_2 & \Delta I_2 \\ 0_2 & I_2 \end{bmatrix}$, $Q = \sigma_a^2 \begin{bmatrix} \frac{\Delta^4}{4} I_2 & \frac{\Delta^3}{2} I_2 \\ \frac{\Delta^3}{2} I_2 & \Delta^2 I_2 \end{bmatrix}$, with $\sigma_a = 0.15(m/s)$, $\Delta = 1(s)$ and I_n is a $n \times n$ identity matrix. The survival probability is set at $p_S = 0.98$. There are 6 new-born targets modelled by an LMB RFS with parameters $\{(r_{B+}, p_{B+}^{(i)})\}_{i=1}^{6}$ where $r_{B,+} = 0.01$

and $p_{B,+}^{(i)} = \mathcal{N}(x; m_{B,+}^{(i)}, Q_{B,+})$ with $Q_{B,+} = \text{diag}([10, 5, 10, 5])$ and:

$$m_{B,+}^{(1)} = (100, 100, 0, 0), \quad m_{B,+}^{(2)} = (100, 500, 0, 0), \quad m_{B,+}^{(3)} = (100, 900, 0, 0),$$
$$m_{B,+}^{(4)} = (900, 100, 0, 0), \quad m_{B,+}^{(5)} = (900, 500, 0, 0), \quad m_{B,+}^{(6)} = (900, 900, 0, 0).$$

Each bearing-only sensor v^{th} is located at a fixed position $s^{(v)} = \left(s_x^{(v)}, s_y^{(v)}\right), v = 1, 2, ..., 8$, as illustrated in Figure 5.3. For sensor v^{th}, the likelihood that a measurement $z^{(v)}$ is generated from a target (x, ℓ) is described as follows:

$$g^{(v)}\left(z^{(v)}|x, \ell, s^{(v)}\right) = \mathcal{N}\left(z^{(v)}; h_{\theta^{(v)}}(x, s^{(v)}), \sigma_\theta^2\right), \tag{5.24}$$

where

$$h_\theta(x, s) = \arctan\left(\frac{p_x - s_x}{p_y - s_y}\right), \tag{5.25}$$

and $\sigma_\theta = \pi/180(rad)$. Note that the single-target kinematic transition Eq. (5.23) and the likelihood Eq. (5.24) models are applied to both the MS-GLMB and robust CPHD filters.

In this experiment, there are 3000 sampled components in the update stage and a maximum 1000 components in the posterior density. These values are set identically in all three filter for a fair performance comparison. The efficacy and accuracy of these trackers are compared using the OSPA [133] and OSPA$^{(2)}$ [26] metrics with 100 MC runs. Similar to the experiment in Section 4.3.2, the cut-off parameter is set to $c_0 = 100(m)$ and the norm order of the metrics is set to $p = 1$. The OSPA$^{(2)}$ metric is performed with window length $l_w = 10$ (s). The experiment is investigated in three different scenarios with different settings of the detection probability and clutter rate. The details of these three scenarios are given in Table 5.1. These settings are the same for all eight sensors. In all scenarios, MS-GLMB and IC-GLMB are supplied with correct p_D and κ for each sensor while our robust MS-GLMB estimates these parameters on the fly.

To validate the robustness of the proposed tracker, the parameters are kept unchanged for our tracker across all scenarios. In addition, we only demonstrate the results from one sensor (for each scenario) since the estimated values of the detection probability $\bar{p}_D$ and the clutter rate $\bar{\kappa}$ for all eight sensors are similar in each tracking

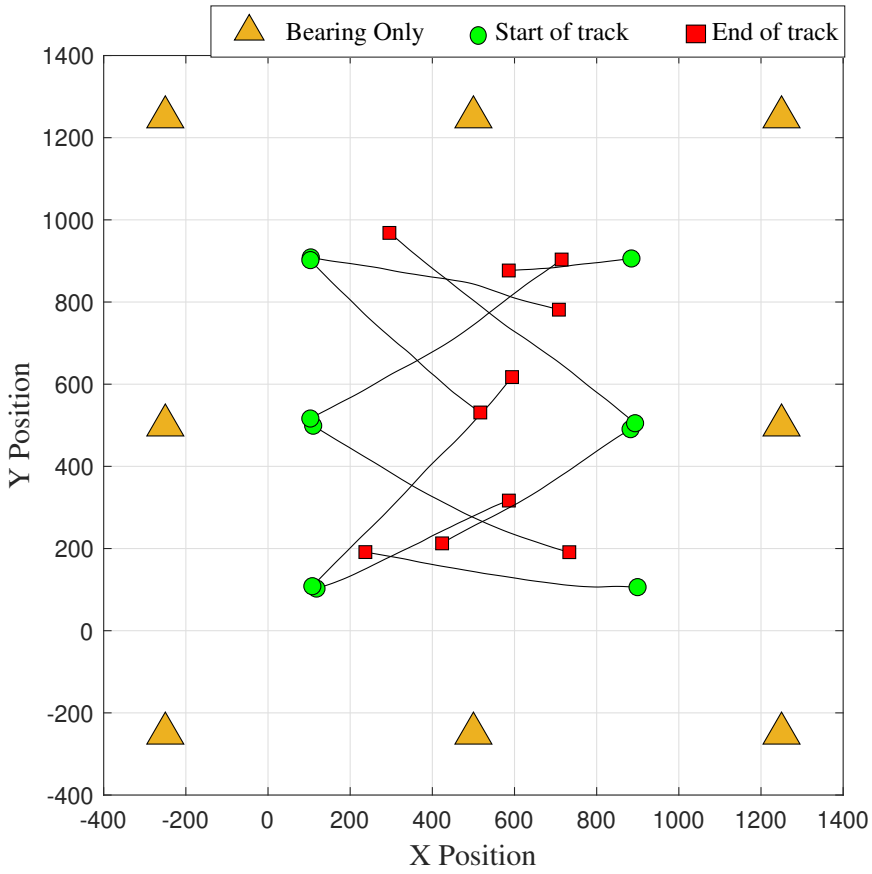

Figure 5.3: Layout of the tracking scenario with 10 targets and 8 sensors.

scenario.

	Detection probability p_D	Clutter rate $\bar{\kappa}^{(1,\ldots,V)}$
1	0.9	30
2	0.5	5
3	varying in the range [0.5 - 0.9]	varying in the range [5 - 30]

Table 5.1: Three different tracking scenarios with different settings of unknown background parameters.

5.3.1 Scenario 1

In the first tracking scenario, the implementation of the three filters are conducted with high values of the detection probability and clutter rate. Specifically, the detection probability is set at $\bar{p}_D = 0.9$ and the clutter rate is set at $\kappa = \bar{}30$. These parameters are known to the IC-GLMB and MS-GLMB filters, but unknown to the robust MS-GLMB filter.

Figure 5.4 and Figure 5.5 demonstrate the comparisons of the correct parameters of the detection probability and clutter rate with their corresponding estimated values from the robust MS-GLMB filter, respectively. From Figure 5.4, the estimated detection probability starts around 0.7 (the initial setting value of the robust MS-GLMB tracker) then approaches to the correct value at 0.9 after some fluctuations. In Figure 5.5, it could be observed that the estimated clutter rate quicky approaches to the lower vincinity of the correct value of 30.

Regarding filtering performance, Figure 5.6 and Figure 5.7 show that there are few tracking errors in the localisation and cardinality estimation of the robust MS-GLMB filter. Conversely, while the IC-GLMB filter gives reasonably few errors in localisation, this filter drastically decays in the quality of estimating the cardinality estimation, hence the high overall number of errors. Moreover, its $0.4 - \sigma$ bounds over 100 MC runs demonstrate that the tracking performance of the IC-GLMB filter is unstable at each time step. In comparison between the robust MS-GLMB and the MS-GLMB, it is shown that the tracking errors using OSPA and OSPA$^{(2)}$ metrics are similar, as given in Figure 5.6 and Figure 5.7. These results demonstrate that the robust MS-GLMB is competitive to the MS-GLMB filter. Note that, the correct parameters of the background information is supplied to the MS-GLMB filter, while there is no prior information on these parameters supplied to the robust MS-GLMB filter.

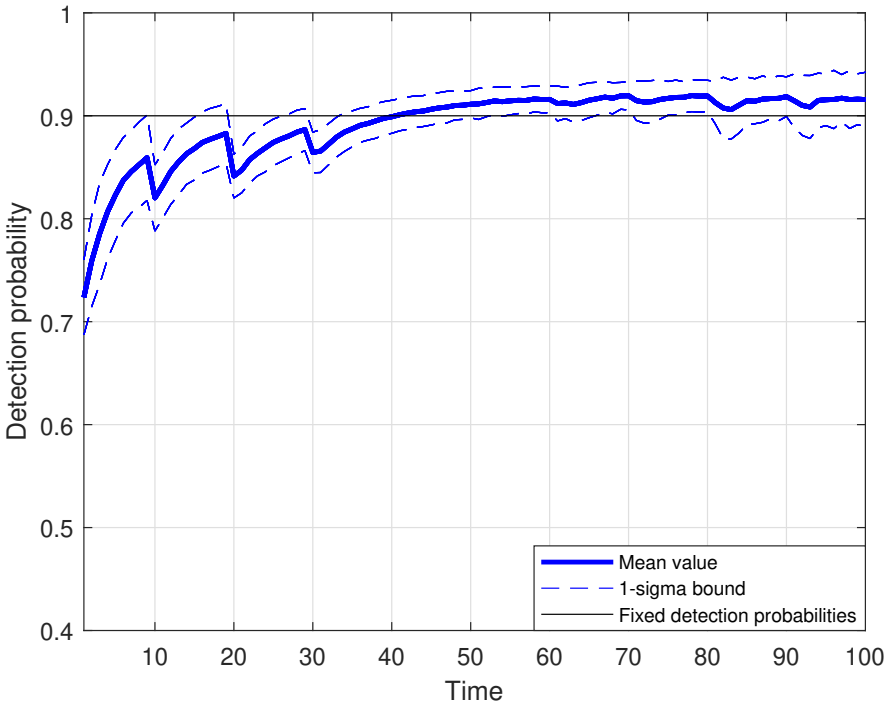

Figure 5.4: Scenario 1: Mean estimated detection probability (with $0.4-\sigma$ bound) using the robust MS-GLMB filter.

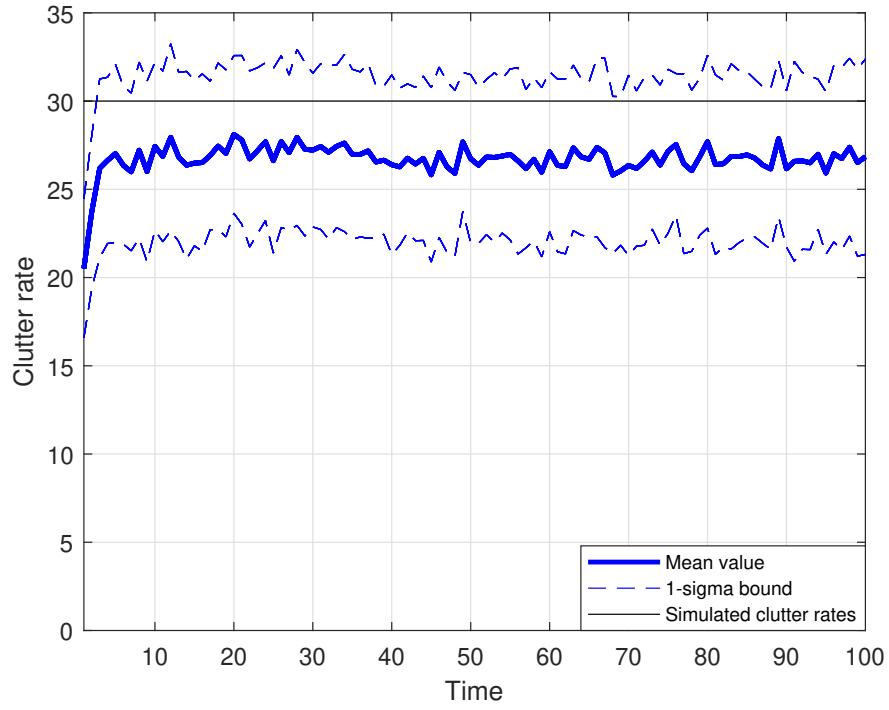

Figure 5.5: Scenario 1: Mean estimated clutter rate (with $0.4-\sigma$ bound) using the robust MS-GLMB filter.

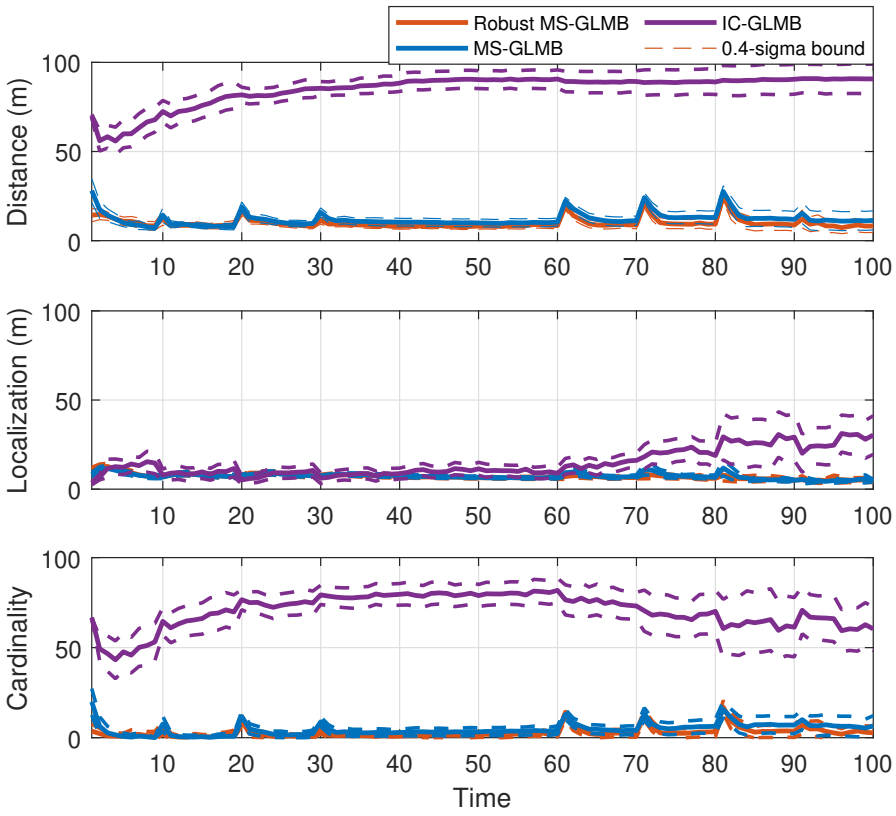

Figure 5.6: Scenario 1: Mean OSPA errors for the three filters (with $0.4 - \sigma$ bound).

Figure 5.8 shows that with the tracking scenario using multiple sensor, the IC-GLMB fails to estimate the correct number of targets. However, the robust MS-GLMB filter estimates target cardinality slightly better than the MS-GLMB filter.

5.3.2 Scenario 2

Unlike in Section 5.3.1, in this scenario, the detection probability and the clutter rate are set to low values to test the tracking capability of the IC-GLMB, MS-GLMB and the robust MS-GLMB filters. Specifically, the detection probability is set at $\bar{p}_D = 0.5$, and the clutter rate is set at $\bar{\kappa} = 5$. While these two values are known to the IC-GLMB and MS-GLMB filters, they are unknown and being estimated online in the robust MS-GLMB filter.

Figure 5.9 shows that the robust MS-GLMB filter slightly overestimates the target detection probability. Particularly, the mean value of this estimated parameter initiates from around 0.65 (closed to the initial setting value), then it decreases to 0.55 after some fluctuations. Note that the true value of detection probability in this scenario is

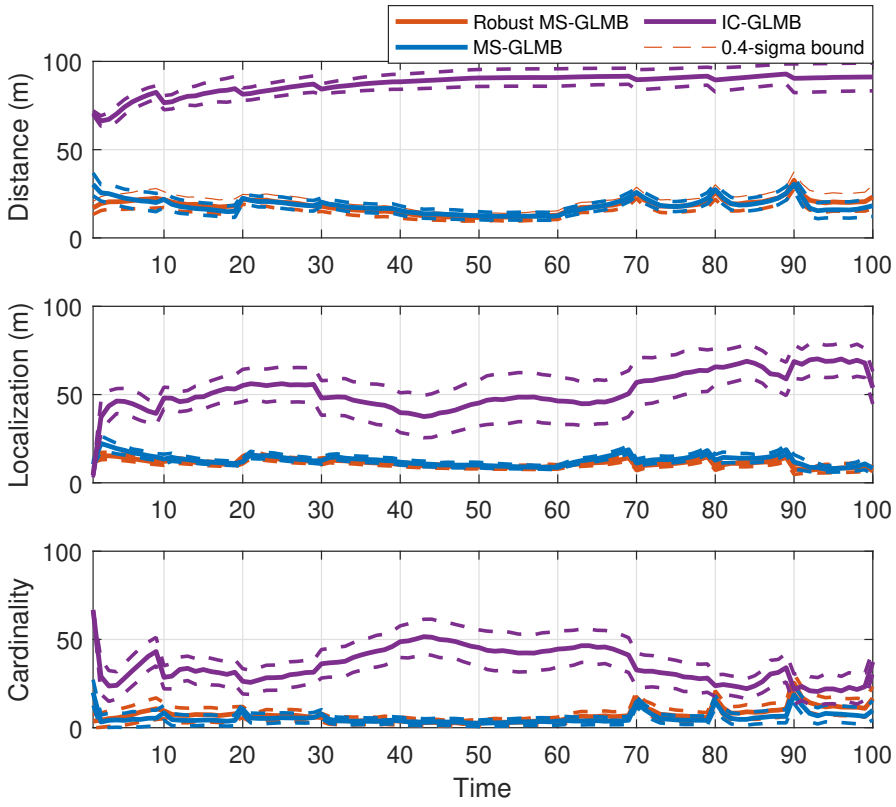

Figure 5.7: Scenario 1: Mean OSPA$^{(2)}$ errors for the three filters (with $0.4-\sigma$ bound).

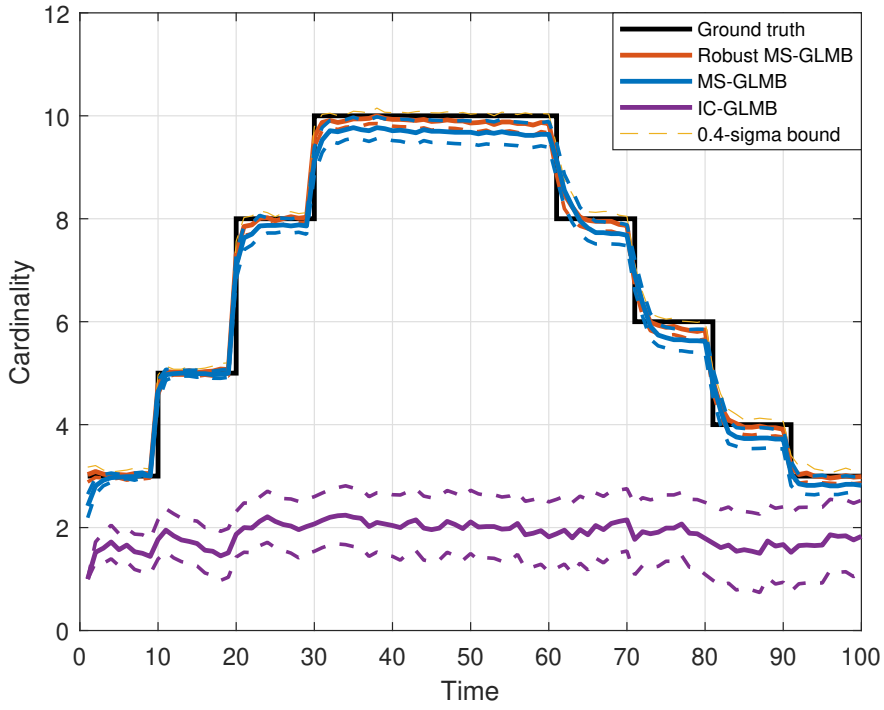

Figure 5.8: Scenario 1: Mean estimated cardinality (with $0.4-\sigma$ bound) for the three filters.

0.5. Figure 5.10 indicates that the clutter rate of sensors is correctly estimated using the robust MS-GLMB filter.

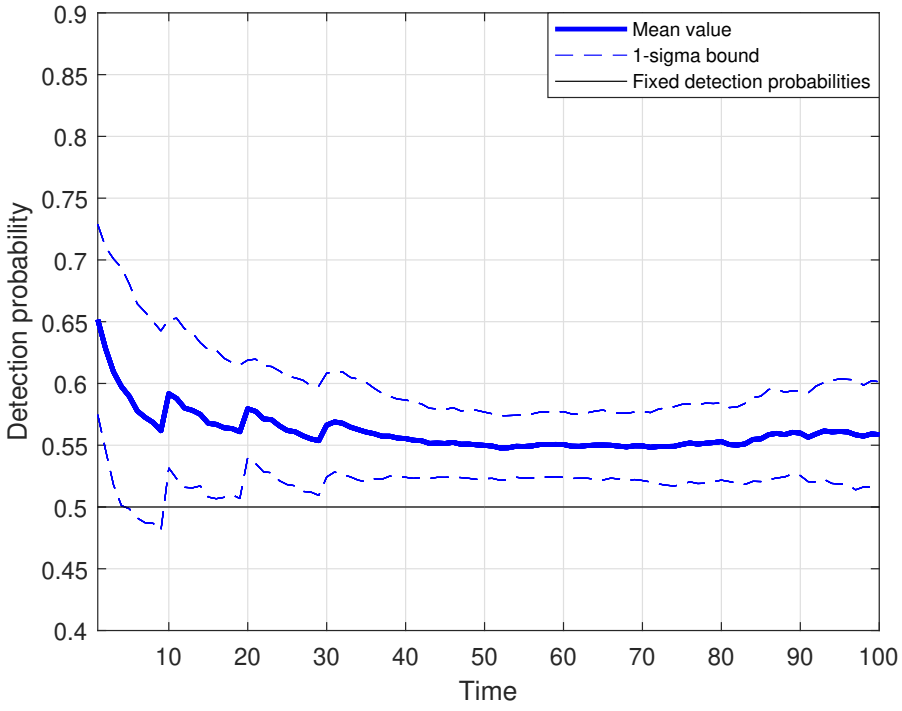

Figure 5.9: Scenario 2: Mean estimated detection probability (with $0.4 - \sigma$ bound) for the robust MS-GLMB filter.

In terms of filtering performance, Figure 5.11 and Figure 5.12 show while the MS-GLMB and the robust MS-GLMB filters provide reliable estimates with the use of multiple sensors, the IC-GLMB does not. Conversely, in comparison of the tracking errors using the OSPA and OSPA$^{(2)}$ metrics, the results of the robust MS-GLMB filter and the MS-GLMB filter are almost coincident, as demonstrated in Figure 5.11 and Figure 5.12. Engagingly, despite of using the assumption on no prior background information for the robust MS-GLMB filter, this filter has slighly lower OSPA$^{(2)}$ errors than the MS-GLMB filter.

It could be observed from Figure 5.13 that the estimated cardinality using the MS-GLMB filter and the robust MS-GLMB filter are almost identical in the first 30 time steps. From time steps 30 to 60 the MS-GLMB filter has better results of estimating target cardinality than the robust MS-GLMB filter. However, the situation is changed from time step 60 onward. In particular, the MS-GLMB filter tends to overestimate the target cardinality, while the robust MS-GLMB slightly underestimates this parameter.

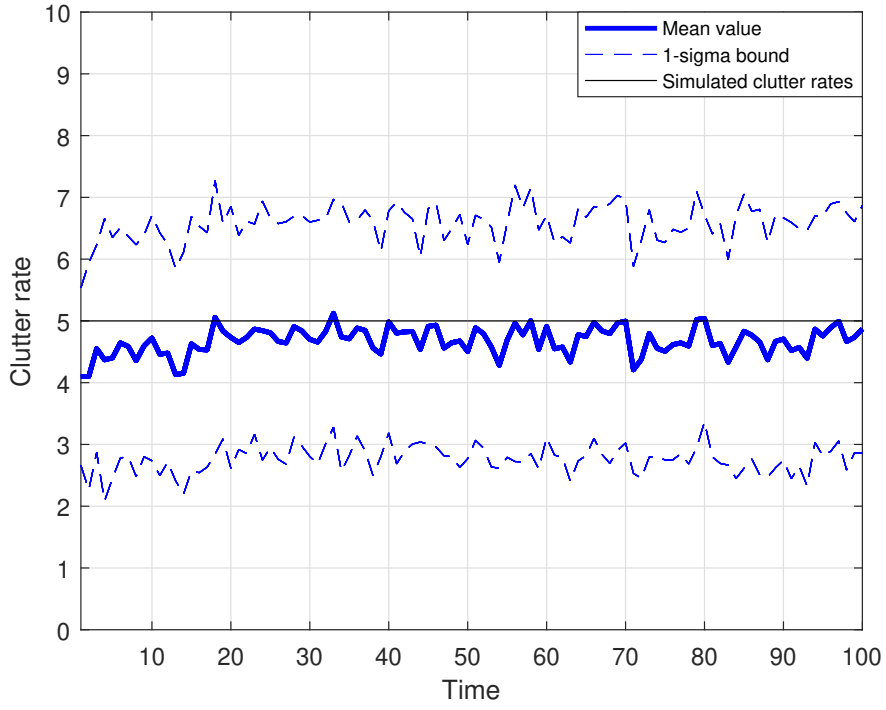

Figure 5.10: Scenario 2: Mean estimated clutter rate (with 0.4 – σ bound) using the robust MS-GLMB filter.

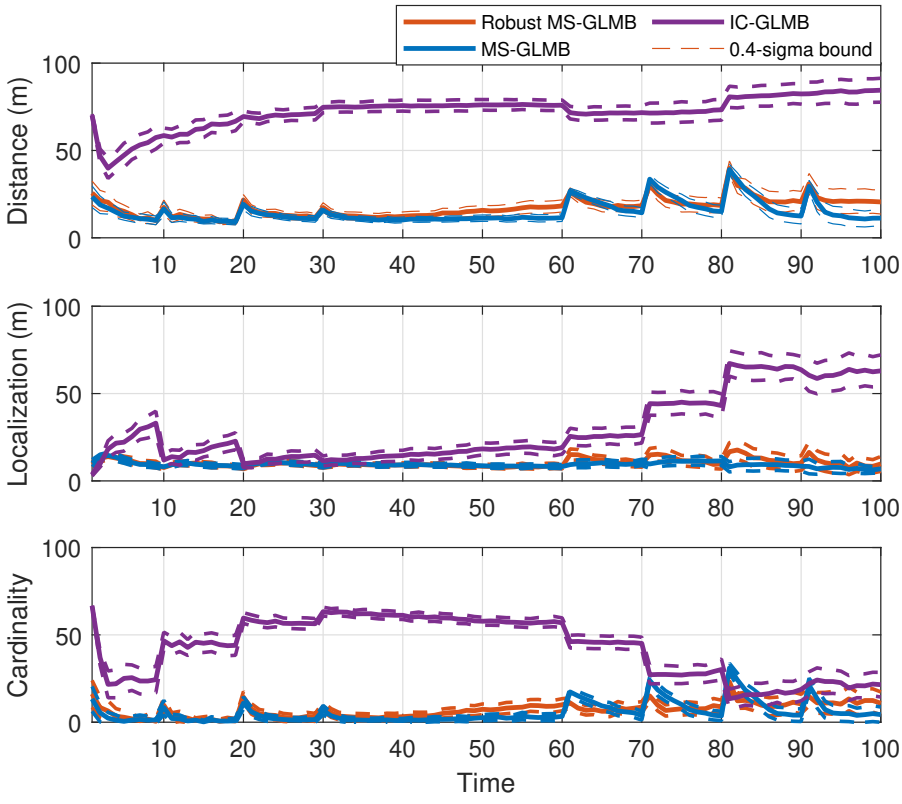

Figure 5.11: Scenario 2: Mean OSPA errors (with 0.4 – σ bound) using the three filters.

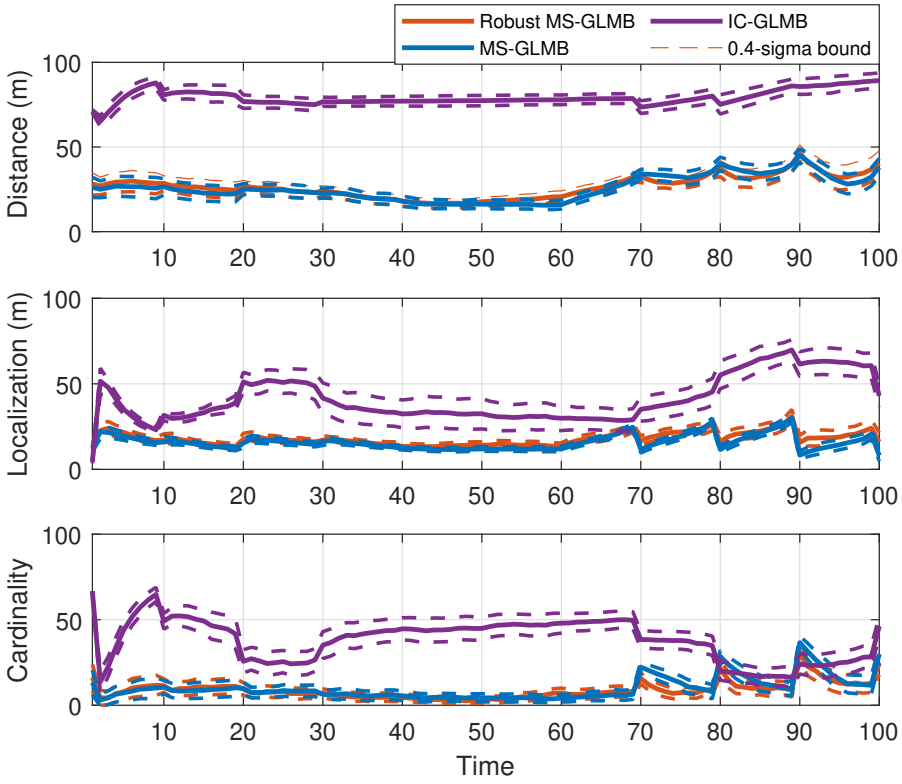

Figure 5.12: Scenario 2: Mean OSPA$^{(2)}$ errors (with $0.4-\sigma$ bound) for the three filters.

In addition, Figure 5.13 also shows that the IC-GLMB does not produce reliable target cardinality.

5.3.3 Scenario 3

This scenario tests the capability of the three filters in tracking targets with the variations of the detection probability p_D and clutter rate $\bar{\kappa}^{(1,\ldots,V)}$. Specifically, these values vary from low to high with time during the tracking period. The condition for the experiment is set for tracking period of 100 MC runs. For the first 50 time steps, the detection probability and clutter rate are set at low values (for parameters, see Section 5.3.2). For the last 50 time steps, these parameters are set at high values (for parameters, see Section 5.3.1). The IC-GLMB and MS-GLMB are performed with the average values of detection probability and clutter rate. These values are set to $p_D = 0.7$ and $\bar{\kappa} = 17.5$ (i.e., the mean of the their variation ranges).

Figure 5.14 and Figure 5.15, respectively, present the estimated detection probability and clutter rate from the robust MS-GLMB filter. This filter correctly captures the variations in the parameters of the background information. Furthermore, the robust

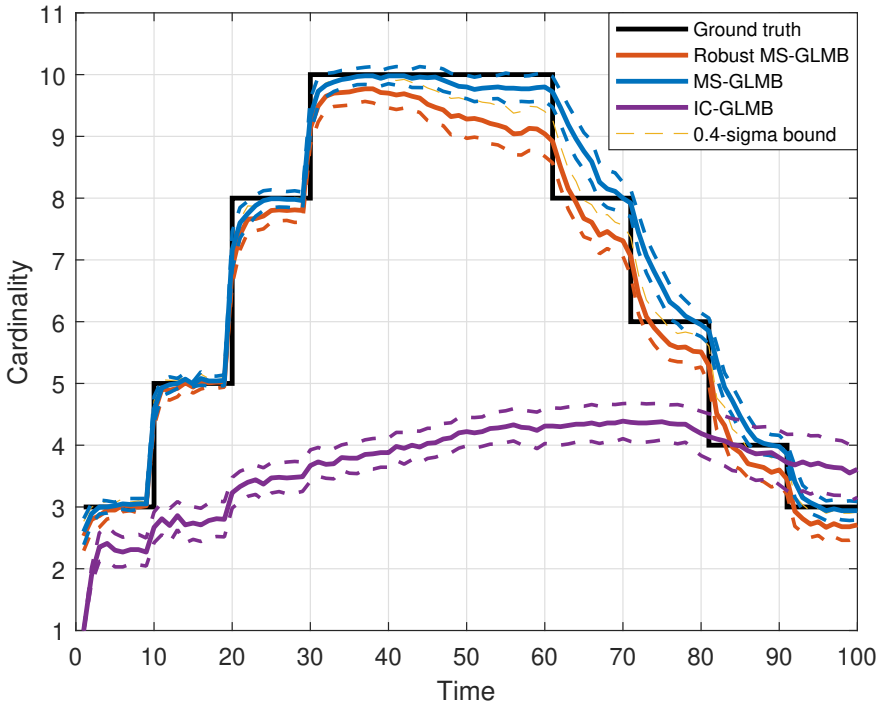

Figure 5.13: Scenario 2: Mean estimated cardinality (with $0.4-\sigma$ bound) for the three filters.

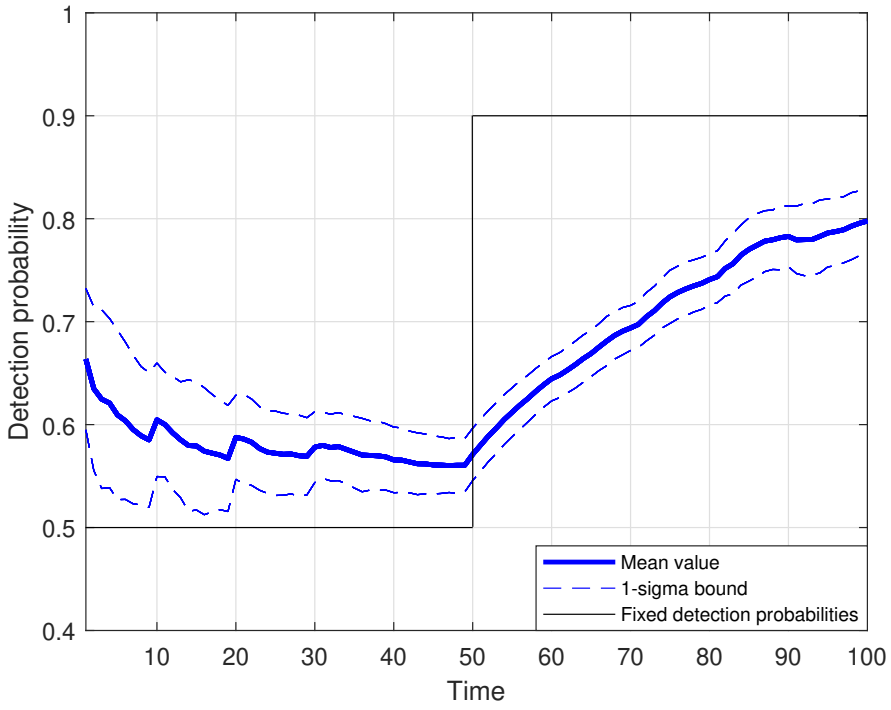

Figure 5.14: Scenario 3: Mean estimated detection probability (with $0.4-\sigma$ bound) using the robust MS-GLMB filter.

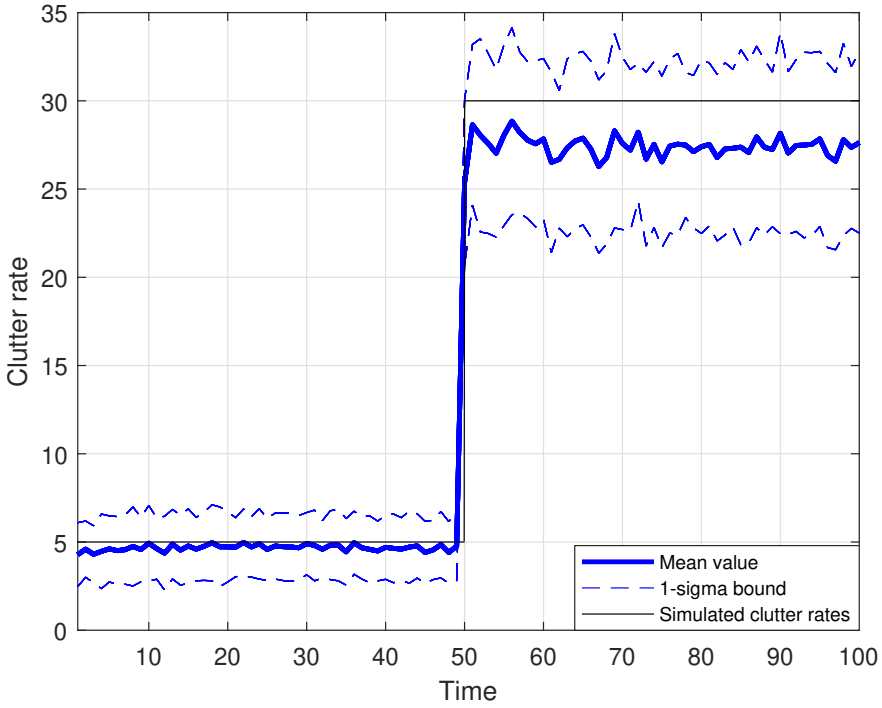

Figure 5.15: Scenario 3: Mean estimated clutter rate (with $0.4 - \sigma$ bound) using the robust MS-GLMB filter.

MS-GLMB filter is more sensitive to the variation in the clutter rate than to that in the detection probability.

The accuracy of the tracking performance is evaluated using the OSPA and OSPA$^{(2)}$ metrics. The results in Figure 5.16 demonstrate that the robust MS-GLMB filter has a high accuracy of tracking targets given its capability of adapting to the variations in the background information. More importantly, while the MS-GLMB filter has lower errors (i.e., better performance) than the IC-GLMB filter, these two filters fail to track targets. It could be observed from Figure 5.17 that, the filters with known and fixed background parameters incorrectly estimate the target cardinality in this scenario. Conversely, although the robust MS-GLMB filter tends to slightly underestimate the target cardinality from time step 30 onward, it demonstrates reliable estimation results. For the overal comparison on tracking performance of all three filters, the mean OSPA$^{(2)}$ errors is evaluated (over 100 MC runs) throughout the entire tracking period and presented in Table 5.2. The results show that the IC-GLMB filter has the worst performance in all three scenarios. While in the scenario 1, the robust MS-GLMB filter has worse performance than the MS-GLMB filter, it is competitive with the MS-GLMB fil-

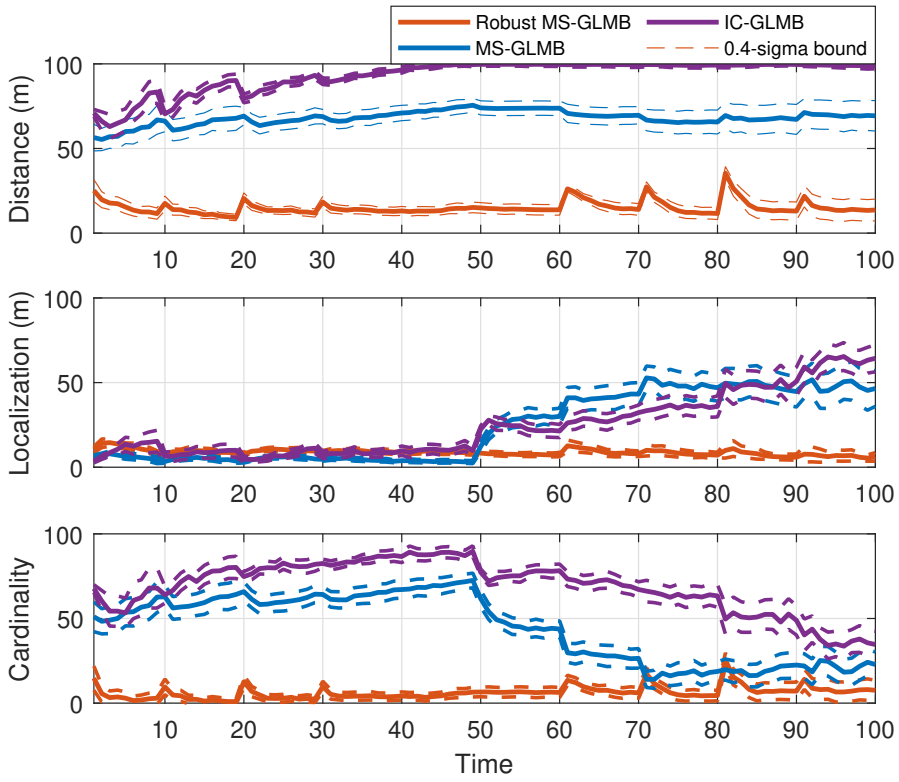

Figure 5.16: Scenario 3: Mean OSPA errors (with $0.4-\sigma$ bound) for the three filters.

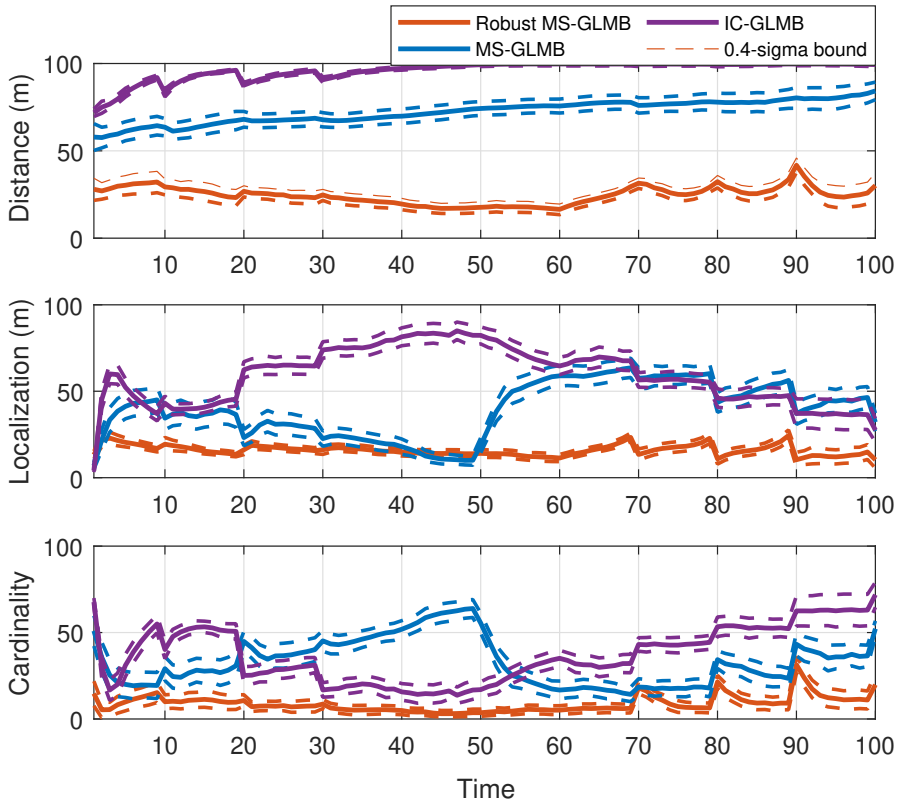

Figure 5.17: Scenario 3: Mean OSPA$^{(2)}$ errors (with $0.4-\sigma$ bound) for the three filters.

ter in the scenario 2. (Note that the MS-GLMB is supplied with the correct background parameters in all tracking scenarios). In the scenario 3, the robust MS-GLMB filter has the best performance given its capability to adapt to the notable changes in the tracking environment. Despite of accuracy in tracking target cardinality, there are some differ-

Scenario	IC-GLMB	MS-GLMB	Robust MS-GLMB
1	$94.44(\pm 7.74)$	$\mathbf{28.81}(\pm 10.45)$	$40.51(\pm 10.55)$
2	$93.24(\pm 3.61)$	$47.63(\pm 9.83)$	$\mathbf{46.59}(\pm 12.36)$
3	$99.38(\pm 1.22)$	$84.31(\pm 3.91)$	$\mathbf{30.16}(\pm 10.62)$

Table 5.2: The estimated OSPA$^{(2)}$ errors (with $\pm\sigma$ bound) (m) over 100 MC runs with window length be the entire tracking period ($l_w = 100(s)$) for the three filters in three different scenarios.

ences in the estimation of the mean detection probability and clutter rate. While the former is overestimated, the latter is underestimated. This might be associated with the hypothesis on the association of the clutter measurements and the true miss-detected tracks in some GLMB components (those with small weights). In Section 5.3.1, there is a greater underestimation of the clutter rate as the number of clutter measurements is high. Conversely, due to the characteristics of the beta distribution[2] and the high value of the detection probability in this tracking scenario, the underestimation of detection probability is unremarkable. Similarly, the under estimation of the clutter rate in Section 5.3.2 is unnoticeable since this parameter is small. However, the detection probability in Section 5.3.2 is overestimated remarkbly. This overestimation is due to the low detection probability of the tracking scenario.

5.4 Conclusions

This chapter presents a robust multi-sensor multi-target tracking algorithm for multi-target tracking. This algorithm is constructed based on the the MS-GLMB filter and the robust CPHD filters. The combination of these two types of RFS-based filters is benefited from the capability of the MS-GLMB filter in estimating multi-target trajectories using multiple sensors and the low computational cost of the CPHD filters in estimating the clutter rate. Consequently, the resultant robust tracker estimates not only the target trajectories using multiple sensors but also the background information online effeciently. The investigations in experiments with different tracking scenarios using

[2] In scenarios with low detection probability, the mean value of this parameter would be increased more significantly than in scenarios with high detection probability.

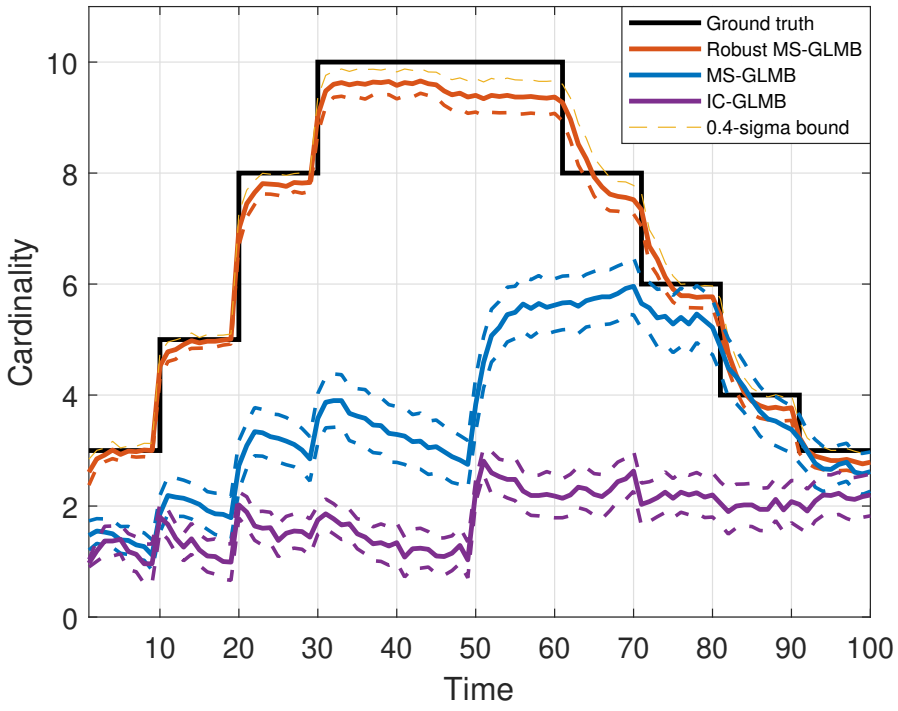

Figure 5.18: Scenario 3: Mean estimated cardinality (with $0.4-\sigma$ bound) for three filters.

bearing-only sensors demonstrate the efficacy and accuaracy in the performance of the proposed robust MS-GLMB filter compared to the IC-GLMB and MS-GLMB filters. Notably, on the one hand, these experimental results show that the IC-GLMB filter fails to track targets given a high number of the bearing-only sensors. On the other hand, while the robust MS-GLMB filter has to estimated the unknown background parameters online, its performance is almost identical to that of the MS-GLMB filter which is supplied with the correct and fixed background information. Most importantly, the robust MS-GLMB filter outperforms the MS-GLMB filter in the scenario with varying backgrounds. This outperformance is due to the capability of the robust MS-GLMB filter in learning and adapting to the changes in background parameters.

In the performance of the robust MS-GLMB filter currently proposed in this chapter, the distribution of newborn targets is assumed to be known in priori to the filter. However, this assumption does not hold in many practical applications as the appearance of newborn targets is random in time and places in the surveillance area. Recently, the measurement adaptive birth model given in [101, 142] for single-sensor multi-target tracking has been extended to the MS-GLMB filter. This method is intro-

duced in [143] to accommodate the unknown information on the model parameters of newborn targets. However, since this method associates measurements from different sensors to form the birth density, it is computationally expensive. Future avenues will invenstigate in an efficient method to handle the randomness of the newborn targets. A further expectation will be a more adaptive multi-sensor multi-target tracking algorithm that is an extension of the work in Chapter 4 to the multi-sensor version.

CHAPTER 6

CONCLUSIONS AND FUTURE RESEARCH DIRECTIONS

This chapter discusses and concludes the contents of the dissertation and presents directions for future researches.

6.1 Conclusions

This dissertation proposes two simple and effective multi-target trackers for tracking a random and time-varying number of targets without prior knowledge in model parameters based on the existing RFS-based filters. These trackers are called Bootstrapped-GLMB filters as they associate the CPHD filter with the GLMB filter in estimating unknown parameters while performing target trajectories tracking. The first Bootstrapped-GLMB tracker adaptively accommodates the unknown information on the clutter statistics, the probability of target detection, and the model of newborn targets which are usually presumed to be known a priori in conventional filters using a sensor. The second presents a robust technique for tracking multiple targets using multiple sensors that can estimate the target trajectories while estimating clutter and detection profile on-the-fly. Those trackers are meaningful in practical applications as they solve the uncertainty in multi-target tracking problems and accelerate the processing by parallelising the implementation of real-world systems.

Chapter 3 extends the existing RFS-based algorithms to tackle the tracking applications with unknown clutter rates. Specifically, the GLMB filter was combined with a generation of the CPHD filter, the λ-CPHD, to track multi-target trajectories without prior knowledge of the clutter rate. The λ–CPHD filter is applied to get the estimated value of the clutter rate before bootstrapping this parameter into the GLMB filter. To demonstrate the correctness of the proposed estimator, the implementation

of the bootstrapping algorithm was compared to those of the four other RFS-based filters in numerical studies with both linear and non-linear tracking scenarios. The Bootstrapped-GLMB filter has shown competitive performance with state-of-the-art multi-target tracking solutions in the literature.

Chapter 4 extends the work described in Chapter 3 by considering the jointly unknown clutter rate and detection profile as well as the birth model. Particularly, an adaptive multi-target tracker has been constructed based on the recent effective GLMB filtering algorithm to handle the random variations in probability of detection, clutter statistics, and model of newborn targets. This tracker used the robust CPHD filter running parallel to the GLMB filter to evaluate the unknown probability of detection, and estimated the jointly unknown clutter rate and detection probability online in two different experiment scenarios. The resultant time-varying parameters were then bootstrapped into the GLMB filter. The use of the robust CPHD filter in this tracker is benefited in low computational cost. Furthermore, the GLMB filter adopted the measurement-based adaptive birth model to handle the newborn targets. These combinations resulted in an efficient plug-and-play multi-target tracker robust enough for several medium-clutter and low-clutter multi-target tracking applications. This tracker overcomes the challenges for users in finding the parameters for initiating trajectories, clutter, and detection probability. The accuracy of the proposed method was compared to other well-known RFS-based filters and was demonstrated by numerical studies.

The second Bootstrapped-GLMB filter which handles the multi-sensor multi-target tracking problem was presented in Chapter 5. This filter is an extension of the filter presented in Chapter 4. While in Chapter 4, the robust CPHD filter ran independent of the GLMB filter, in Chapter 5, the parallel robust CPHD filters received their prior information from the output of the GLMB filter in a multi-sensor counterpart. Further, while the technique in Chapter 5 can be applied to several types of sensors, the scenario using bearing-only sensors was used for demonstration purposes.

The work in this dissertation has illustrated that by using the benefits of the existing RFS-based filters, the resultant algorithm can handle practical applications where the model parameters are usually unknown a priori in a simple but effective way.

6.2 Future research directions

The work presented in this dissertation could be further extended in terms of theoretical developments and applications in multiple ways.

• Multi-sensor multi-target tracking using the GLMB model with an unknown clutter rate and unknown detection profile has been presented in this dissertation. While the multi-sensor adaptive birth strategy for the GLMB filter was introduced recently in [143], it is based on the assumption of prior knowledge of detection probfile and clutter statistics. The work described in Chapter 5 that handles the unknown information in the birth model could be extended to develop an adaptive multi-target tracking tracker using multiple sensors.

• While this dissertation considered both single-sensor and multi-sensor multi-target tracking with unknown background information, it only considered the filtering problem (i.e., estimating target states and trajectories using filtering density). The smoothing method mentioned in Section 2.7 yields significantly better estimates than filtering since it envolves entire historcal information of the target states up to the current time in the posterior density [41]. The future work could investigate the implementation of the Bootstrapped-GLMB smoother based on the combination of multi-scan GLMB [41] with the Bootstrapped-GLMB filter given in this dissertation.

• Currently, there are two state-of-the-art techniques for tracking target trajectories: the multi-scan GLMB filter [41], the MS-GLMB filter [22] and the multi-scan MS-GLMB filter [42]. Future work could investigate on the combination of these two techniques in real-world applications to handle the unknown model parameters and produce the best estimates on target states and target trajectories.

• The new filter can be used to accommodate multi-scan filtering [41] to improve tracking performance. In applications with a large number of targets, a parallel process could be applied as in [26] to reduce the computational effort and effectively utilise the hardware. Furthermore, RFS-based multi-object Bayesian filters for merged or extended objects [27, 30] can be used to track multiple targets with an unknown background, unknown birth model and spawning targets. Conversely, the application of the proposed filter can be extended to other applications, such as spatial object surveil-

lance to track objects with collision, or after launching events.

APPENDIX 7

Relationship between the detection probability and the clutter rate

There is an inter-twined relationship between the detection probability and the clutter rate. In general, when the detection probability is overestimated, the clutter rate is underestimated since there are more hypotheses with clutter measurements being associated with tracks. In contrast, when the detection probability is underestimated, the clutter rate is overestimated since there are more hypotheses with tracks are considered as miss-detected and more true measurements not being associated with tracks.

On the other hand, the detection probability is affected by the parameters of Beta distribution. Note that from the identity presented in Mahler2011CPHD, a detection event will update the beta distribution by increasing the parameter s by 1 and a miss-detection event will increase t by 1. The relationship between s, t, and the mean detection probability is given in the following Figure 7.1.

It can be observed that, at low detection probability scenarios (usually associated with high t), if a track is associated with a measurement, the mean detection probability will increase more significantly than in the scenarios with high detection probability.

The discussed behavior is, respectively, reflected in Figure 5.4 and Figure 5.5 where the detection probability is slightly overestimated and clutter rate is underestimated. Since there are many clutter measurements, it is more likely that a truly miss-detected track being associated with clutter measurement in some hypotheses. However, due to the high detection probability, the overestimation of detection probability is not noticeable (due to the characteristic of the beta distribution).

This behavior is also observed in Figure 5.9 and Figure 5.10. However, since the number of clutter measurements is low in Section 5.3.2, the underestimation of clutter

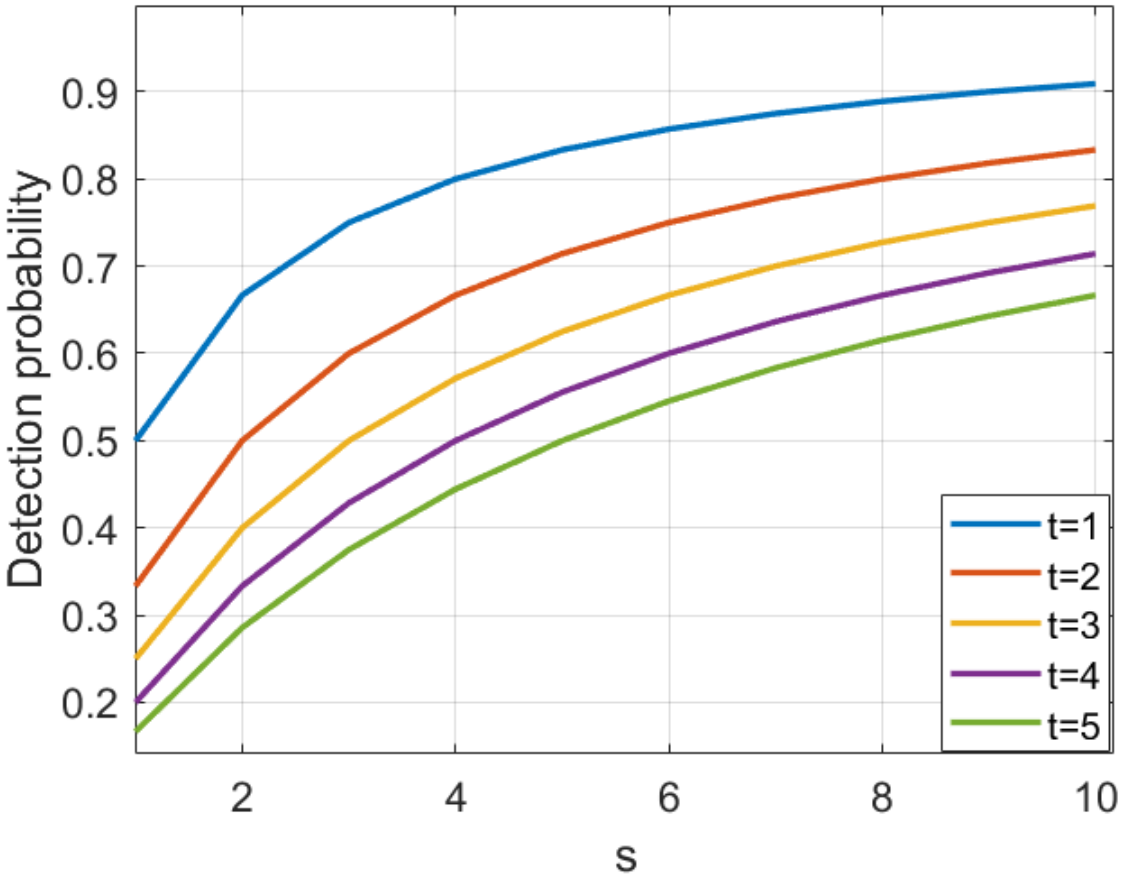

Figure 7.1: Mean detection probability versus different Beta parameters. The initial values of s and t in our experiments are 2 and 1, respectively.

rate is not remarkable. Nevertheless, given the low value of the detection probability in this scenario, the overestimation of the detection probability is more noticeable.

Although it is desirable to correctly estimate the detection probability and clutter rate, the ultimate goal of the filter is to accurately estimate the target states, which has been achieved as shown by our experimental results.

Bibliography

[1] C. Gauss, "Theory of motion of the celestial bodies moving in conic sections around the Sun," *Monatliche Correspondenz*, vol. 20, pp. 147–192, 1809. (Cited on page 1)

[2] H. W. Sorenson, "Least-squares estimation: from Gauss to Kalman," *IEEE spectrum*, vol. 7, no. 7, pp. 63–68, 1970. (Cited on page 1)

[3] R. A. Fisher, "On the mathematical foundations of theoretical statistics," *Philosophical Transactions of the Royal Society of London. Series A, Containing Papers of a Mathematical or Physical Character*, vol. 222, no. 594-604, pp. 309–368, 1922. (Cited on page 1)

[4] A. N. Kolmogorov, "Interpolation and extrapolation of stationary random sequences." *Izv. Akad. Nauk SSSR Ser. Mat*, vol. 5, no. 1, pp. 3–14, 1941, translated by Doyle, WL and Selin, Ivan, Rept. RM-3090-PR, RAND Corp, Santa Monica, California, 1962. (Cited on page 1)

[5] N. Weiner and I. Extrapolation, "Smoothing of stationary time series: With engineering applications," 1949. (Cited on page 1)

[6] R. E. Kalman, "A new approach to linear filtering and prediction problems," *Transactions of the ASME - Journal of Basic Engineering*, vol. 82 (Series D), pp. 35–45, 1960. (Cited on page 1)

[7] S. J. Julier and J. K. Uhlmann, "New extension of the Kalman filter to nonlinear systems," in *Signal processing, sensor fusion, and target recognition VI*, vol. 3068. International Society for Optics and Photonics, 1997, pp. 182–193. (Cited on page 1)

[8] A. Jazwinski, "Stochastic processes and filtering theory," *Academic Press, New York*, 1970. (Cited on page 1)

[9] S. J. Julier and J. K. Uhlmann, "Unscented filtering and nonlinear estimation," *Proceedings of the IEEE*, vol. 92, no. 3, pp. 401–422, 2004. (Cited on page 1)

[10] N. J. Gordon, D. J. Salmond, and A. F. Smith, "Novel approach to nonlinear/non-Gaussian Bayesian state estimation," in *IEE proceedings F (radar and signal processing)*, vol. 140, no. 2. IET, 1993, pp. 107–113. (Cited on page 2)

[11] A. Doucet, N. De Freitas, N. J. Gordon *et al.*, *Sequential Monte Carlo methods in practice*. Springer, 2001, vol. 1, no. 2. (Cited on page 2)

[12] Y. Bar-Shalom and T. E. Fortmann, *Tracking and Data Association and others*. Academic press San Diego, CA, USA, 1988. (Cited on page 2)

[13] S. Blackman and R. Popoli, *Design and analysis of modern tracking systems*. Artech House, Norwood, MA, 1999. (Cited on page 2)

[14] R. P. Mahler, *Statistical multisource-multitarget information fusion*. Artech House Norwood, MA, 2007, vol. 685. (Cited on pages 2, 10, 11, 13, 15, 16, 17, 21, and 31)

[15] B.-N. Vo, M. Mallick, Y. Bar-shalom, S. Coraluppi, R. Osborne III, R. P. Mahler, and B.-T. Vo, "Multitarget tracking," *Wiley Encyclopedia of Electrical and Electronics Engineering*, pp. 1–15, 1999. (Cited on pages 2 and 4)

[16] R. P. Mahler, *Advances in statistical multisource-multitarget information fusion*. Artech House Boston, MA,, 2014. (Cited on pages 2, 12, 22, 27, 31, and 56)

[17] ——, "Multitarget Bayes filtering via first-order multitarget moments," *IEEE Transactions on Aerospace and Electronic systems*, vol. 39, no. 4, pp. 1152–1178, 2003. (Cited on pages 2, 12, and 15)

[18] B.-T. Vo, B.-N. Vo, and A. Cantoni, "Analytic implementations of the cardinalized probability hypothesis density filter," *IEEE Transactions on Signal Processing*, vol. 55, no. 7, pp. 3553–3567, 2007. (Cited on pages 2, 17, 18, 38, 46, 68, and 105)

[19] R. P. Mahler, "PHD filters of higher order in target number," *IEEE Transactions on Aerospace and Electronic systems*, vol. 43, no. 4, pp. 1523–1543, 2007. (Cited on pages 2 and 17)

[20] B.-N. Vo, B.-T. Vo, N.-T. Pham, and D. Suter, "Joint detection and estimation of multiple objects from image observations," *IEEE Transactions on Signal Processing*, vol. 58, no. 10, pp. 5129–5141, 2010. (Cited on page 2)

[21] B.-T. Vo, B.-N. Vo, and A. Cantoni, "The cardinality balanced multitarget multi-Bernoulli filter and its implementations," *IEEE Trans. Signal Process.*, vol. 57, no. 2, pp. 409–423, 2009. (Cited on page 2)

[22] B.-N. Vo, B.-T. Vo, and M. Beard, "Multi-sensor multi-object tracking with the generalized labeled multi-Bernoulli filter," *IEEE Transactions on Signal Processing*, pp. 1–1, 2019. (Cited on pages 2, 3, 5, 28, 31, 32, 33, 34, 100, 101, 103, 104, 109, 110, and 129)

[23] R. P. Mahler, "Statistics 103 for multitarget tracking," *Sensors*, vol. 19, no. 1, p. 202, 2019. (Cited on pages 2, 4, 15, and 28)

[24] B.-T. Vo and B.-N. Vo, "Labeled random finite sets and multi-object conjugate priors," *IEEE Transactions on Signal Processing*, vol. 61, no. 13, pp. 3460–3475, 2013. (Cited on pages 2, 11, 14, 15, 21, 22, 23, 24, 25, 26, 27, 28, 29, 30, 31, 32, 37, 38, 40, 41, 46, 56, 78, 79, 89, and 110)

[25] R. P. Mahler, "Exact closed-form multitarget Bayes filters," *Sensors*, vol. 19, no. 12, p. 2818, 2019. (Cited on pages 2, 22, 27, 28, and 34)

[26] M. Beard, B. T. Vo, and B.-N. Vo, "A solution for large-scale multi-object tracking," *IEEE Transactions on Signal Processing*, vol. 68, 2020. (Cited on pages 2, 28, 46, 47, 63, 79, 111, and 129)

[27] M. Beard, B.-T. Vo, and B.-N. Vo, "Bayesian multi-target tracking with merged measurements using labelled random finite sets," *IEEE Transactions on Signal Processing*, vol. 63, no. 6, pp. 1433–1447, 2015. (Cited on pages 3, 28, and 129)

[28] F. Papi and D. Y. Kim, "A particle multi-target tracker for superpositional measurements using labeled random finite sets," *IEEE Transactions on Signal Processing*, vol. 63, no. 16, pp. 4348–4358, 2015. (Cited on pages 3, 28, and 38)

[29] F. Papi, B.-N. Vo, B.-T. Vo, C. Fantacci, and M. Beard, "Generalized labeled multi-Bernoulli approximation of multi-object densities," *IEEE Transactions on Signal Processing*, vol. 63, no. 20, pp. 5487–5497, 2015. (Cited on pages 3, 28, and 38)

[30] M. Beard, S. Reuter, K. Granström, B.-T. Vo, B.-N. Vo, and A. Scheel, "Multiple extended target tracking with labeled random finite sets," *IEEE Transactions on Signal Processing*, vol. 64, no. 7, pp. 1638–1653, 2015. (Cited on pages 3, 18, 28, and 129)

[31] T. T. D. Nguyen and D. Y. Kim, "GLMB Tracker with partial smoothing," *Sensors*, vol. 19, no. 20, p. 4419, 2019. (Cited on pages 3, 28, 40, 78, and 110)

[32] T. T. D. Nguyen, C. Shim, and W. Kim, "Biological cell tracking and lineage inference via random finite sets," in *2021 IEEE 18th International Symposium on Biomedical Imaging (ISBI)*. IEEE, 2021, pp. 339–343. (Cited on pages 3 and 28)

[33] M. Beard, B.-T. Vo, B.-N. Vo, and S. Arulampalam, "Void probabilities and Cauchy–Schwarz divergence for generalized labeled multi-Bernoulli models," *IEEE Transactions on Signal Processing*, vol. 65, no. 19, pp. 5047–5061, 2017. (Cited on page 3)

[34] D. S. Bryant, B.-T. Vo, B.-N. Vo, and B. A. Jones, "A generalized labeled multi-Bernoulli filter with object spawning," *IEEE Transactions on Signal Processing*, vol. 66, no. 23, pp. 6177–6189, 2018. (Cited on pages xv, 3, 22, 23, and 28)

[35] T. T. D. Nguyen, B.-N. Vo, B.-T. Vo, D. Y. Kim, and Y. S. Choi, "Tracking cells and their lineages via labeled random finite sets," *IEEE Transactions on Signal Processing*, vol. 69, pp. 5611–5626, 2021. (Cited on pages 3, 28, and 98)

[36] C. Fantacci, B.-N. Vo, B.-T. Vo, G. Battistelli, and L. Chisci, "Robust fusion for multisensor multiobject tracking," *IEEE Signal Processing Letters*, vol. 25, no. 5, pp. 640–644, 2018. (Cited on pages 3, 28, and 101)

[37] H. Deusch, S. Reuter, and K. Dietmayer, "The labeled multi-Bernoulli SLAM filter," *IEEE Signal Processing Letters*, vol. 22, no. 10, pp. 1561–1565, 2015. (Cited on pages 3 and 28)

[38] D. Moratuwage, M. Adams, and F. Inostroza, "δ-generalized labeled multi-Bernoulli simultaneous localization and mapping with an optimal kernel-based particle filtering approach," *Sensors*, vol. 19, no. 10, p. 2290, 2019. (Cited on pages 3 and 28)

[39] D. Y. Kim, B.-N. Vo, B.-T. Vo, and M. Jeon, "A labeled random finite set online multi-object tracker for video data," *Pattern Recognition*, vol. 90, pp. 377–389, 2019. (Cited on pages 3 and 28)

[40] B.-N. Vo, B.-T. Vo, and G. H. Hoang, "An efficient implementation of the generalized labeled multi-Bernoulli filter," *IEEE Trans. Signal Process.*, vol. 65, no. 8, pp. 1975–1987, 2017. (Cited on pages 3, 28, 31, 33, 40, 61, 78, and 103)

[41] B.-N. Vo and B.-T. Vo, "A multi-scan labeled random finite set model for multi-object state estimation," *IEEE Transactions on Signal Processing*, vol. 67, no. 19, pp. 4948–4963, 2019. (Cited on pages 3, 22, 28, 34, and 129)

[42] D. Moratuwage, B.-N. Vo, B.-T. Vo, and C. Shim, "Multi-scan multi-sensor multi-object state estimation," *arXiv Preprint*, 2022. (Cited on pages 3 and 129)

[43] B. Wei and B. D. Nener, "Multi-sensor space debris tracking for space situational awareness with labeled random finite sets," *IEEE Access*, vol. 7, pp. 36 991–37 003, 2019. (Cited on page 3)

[44] B. A. Jones, D. S. Bryant, B.-T. Vo, and B.-N. Vo, "Challenges of multi-target tracking for space situational awareness," in *2015 18th International Conference on Information Fusion (Fusion)*, 2015, pp. 1278–1285. (Cited on page 3)

[45] J. Ong, B.-T. Vo, B.-N. Vo, D. Y. Kim, and S. E. Nordholm, "A Bayesian filter for multi-view 3D multi-object tracking with occlusion handling," *IEEE Transactions on Pattern Analysis and Machine Intelligence*, pp. 1–1, 2020. (Cited on pages 3 and 62)

[46] H. V. Nguyen, H. Rezatofighi, B.-N. Vo, and D. C. Ranasinghe, "Online UAV path planning for joint detection and tracking of multiple radio-tagged objects," *IEEE Transactions on Signal Processing*, vol. 67, no. 20, pp. 5365–5379, 2019. (Cited on pages 3 and 28)

[47] J. Mullane, B.-N. Vo, M. D. Adams, and B.-T. Vo, "A Random-Finite-Set approach to Bayesian SLAM," *IEEE Transactions on Robotics*, vol. 27, no. 2, pp. 268–282, 2011. (Cited on page 3)

[48] H. V. Nguyen, B.-N. Vo, B.-T. Vo, H. Rezatofighi, and D. C. Ranasinghe, "Multi-objective multi-agent planning for discovering and tracking unknown and varying number of mobile objects," *arXiv preprint arXiv:2203.04551*, 2022. (Cited on pages 3 and 101)

[49] W. J. Hadden, J. L. Young, A. W. Holle, M. L. McFetridge, D. Y. Kim, P. Wijesinghe, H. Taylor-Weiner, J. H. Wen, A. R. Lee, K. Bieback *et al.*, "Stem cell migration and mechanotransduction on linear stiffness gradient hydrogels," *Proceedings of the National Academy of Sciences*, vol. 114, no. 22, pp. 5647–5652, 2017. (Cited on pages 3 and 28)

[50] C. F. Le, *Principles of radar and sonar signal processing*. Artech House, 2002. (Cited on page 3)

[51] IEEE, "IEEE Standard for Radar definitions," *IEEE P686/D2, 2017 (Revision of IEEE Std 686-2008)*, pp. 1–62, Jan 2017. (Cited on page 3)

[52] H. D. Griffiths and C. J. Baker, *An Introduction to Passive Radar*. London, UK: Artech House, 2017. (Cited on page 3)

[53] V. S. Chernyak, *Fundamentals of Multisite Radar Systems: Multistatic Radars and Multiradar Systems*, 1st ed. Routledge, 2018. (Cited on page 4)

[54] ——, "Multisite radar systems composed of MIMO radars," *IEEE Aerospace and Electronic Systems Magazine*, vol. 29, no. 12, pp. 28–37, 2014. (Cited on page 4)

[55] N. A. Goodman and D. Bruyere, "Optimum and decentralized detection for multistatic airborne radar," *IEEE Transactions on Aerospace and Electronic Systems*, vol. 43, no. 2, pp. 806–813, 2007. (Cited on page 4)

[56] G. Smith, K. Woodbridge, C. Baker, and H. Griffiths, "Multistatic micro-Doppler radar signatures of personnel targets," *IET signal processing*, vol. 4, no. 3, pp. 224–233, 2010. (Cited on page 4)

[57] S. J. Wong and B. T. Vo, "Square root Gaussian mixture PHD filter for multi-target bearings only tracking," in *2011 Seventh International Conference on Intelligent Sensors, Sensor Networks and Information Processing*. IEEE, 2011, pp. 520–525. (Cited on page 5)

[58] D. Hull, J. Speyer, and D. Burris, "Linear-quadratic guidance law for dual control of homing missiles," *Journal of Guidance, Control, and Dynamics*, vol. 13, no. 1, pp. 137–144, 1990. (Cited on page 5)

[59] J. C. Hassab, *Underwater signal and data processing*. CRC Press, 2018. (Cited on page 5)

[60] G. Fang, G. Dissanayake, N. M. Kwok, and S. Huang, "Near minimum time path planning for bearing-only localisation and mapping," in *2005 IEEE/RSJ International Conference on Intelligent Robots and Systems*. IEEE, 2005, pp. 850–855. (Cited on page 5)

[61] S. C. Nardone and V. J. Aidala, "Observability criteria for bearings-only target motion analysis," *IEEE Transactions on Aerospace and Electronic systems*, vol. AES-17, no. 2, pp. 162–166, 1981. (Cited on page 5)

[62] S. Nardone, A. Lindgren, and K. Gong, "Fundamental properties and performance of conventional bearings-only target motion analysis," *IEEE Transactions on automatic control*, vol. 29, no. 9, pp. 775–787, 1984. (Cited on page 5)

[63] T. L. Song, "Observability of target tracking with bearings-only measurements," *IEEE Transactions on Aerospace and Electronic Systems*, vol. 32, no. 4, pp. 1468–1472, 1996. (Cited on page 5)

[64] M. S. Arulampalam, B. Ristic, N. Gordon, and T. Mansell, "Bearings-only tracking of manoeuvring targets using particle filters," *EURASIP Journal on Advances in Signal Processing*, vol. 2004, no. 15, pp. 1–15, 2004. (Cited on page 5)

[65] E. Fogel and M. Gavish, "Nth–order dynamics target observability from angle measurements," *IEEE Transactions on Aerospace and Electronic Systems*, vol. 24, no. 3, pp. 305–308, 1988. (Cited on page 5)

[66] F. Dufour and M. Mariton, "Tracking a 3D maneuvering target with passive sensors," *IEEE Transactions on aerospace and electronic systems*, vol. 27, no. 4, pp. 725–739, 1991. (Cited on page 5)

[67] T.-G. Lee, "Centralized Kalman filter with adaptive measurement fusion: its application to a GPS/SDINS integration system with an additional sensor," *International Journal of Control, Automation, and Systems*, vol. 1, no. 4, pp. 444–452, 2003. (Cited on page 5)

[68] C.-T. Do and H. V. Nguyen, "Multistatic Doppler-based marine ships tracking," in *2018 International Conference on Control, Automation and Information Sciences (ICCAIS)*, 2018, pp. 151–156. (Cited on pages 6 and 28)

[69] C.-T. Do and T. T. D. Nguyen, "Multiple marine ships tracking from multistatic Doppler data with unknown clutter rate," in *2019 International Conference on Control, Automation and Information Sciences (ICCAIS)*, 2019, pp. 1–6. (Cited on pages 6 and 37)

[70] C.-T. Do and H. V. Nguyen, "Tracking multiple targets from multistatic Doppler radar with unknown probability of detection," *Sensors*, vol. 19, no. 7, p. 1672, 2019. (Cited on pages 6, 61, and 101)

[71] C.-T. Do, T. T. D. Nguyen, and W. Liu, "Tracking multiple marine ships via multiple sensors with unknown backgrounds," *Sensors*, vol. 19, no. 22, p. 5025, 2019. (Cited on pages 6, 61, and 101)

[72] C.-T. Do, T. T. D. Nguyen, D. Moratuwage, C. Shim, and Y. D. Chung, "Multi-object tracking with an adaptive generalized labeled multi-Bernoulli Filter," *Signal Processing*, vol. 196, p. 108532, 2022. (Cited on pages 6 and 61)

[73] C.-T. Do, T. T. D. Nguyen, and H. V. Nguyen, "Robust multi-sensor generalized labeled

multi-Bernoulli filter," *Signal Processing*, vol. 192, p. 108368, 2022. (Cited on pages 7, 99, and 103)

[74] B.-N. Vo, S. Singh, and A. Doucet, "Sequential Monte Carlo methods for multitarget filtering with random finite sets," *IEEE Transactions on Aerospace and electronic systems*, vol. 41, no. 4, pp. 1224–1245, 2005. (Cited on pages 11 and 16)

[75] M. Mallick, V. Krishnamurthy, and B.-N. Vo, *Integrated tracking, classification, and sensor management*. Wiley Online Library, 2012. (Cited on pages xv, 12, 13, 14, and 15)

[76] T. Zajic and R. P. Mahler, "A particle-systems implementation of the PHD multi-target tracking filter," in *SPIE 5096, Signal Processing, Sensor Fusion & Target Recognition XII,*, Florida, USA, 2003, pp. 291–299. (Cited on page 16)

[77] H. Sidenbladh, "Multi-target particle filtering for the probability hypothesis density," in *Proceedings of the Sixth International Conference of Information Fusion*, vol. 2, Jul. 2003, pp. 800–806. (Cited on page 16)

[78] B.-N. Vo and W.-K. Ma, "The Gaussian mixture probability hypothesis density filter," *IEEE Transactions on signal processing*, vol. 54, no. 11, pp. 4091–4104, 2006. (Cited on pages 16 and 46)

[79] A. M. Johansen, S. S. Singh, A. Doucet, and B.-N. Vo, "Convergence of the SMC Implementation of the PHD Filter," *Methodology and Computing in Applied Probability*, vol. 8, no. 2, pp. 265–291, 2006. (Cited on page 16)

[80] D. E. Clark and J. Bell, "Convergence results for the particle PHD filter," *IEEE Transactions on Signal Processing*, vol. 54, no. 7, pp. 2652–2661, 2006. (Cited on page 16)

[81] D. E. Clark and B.-N. Vo, "Convergence Analysis of the Gaussian Mixture PHD Filter," *IEEE Transactions on Signal Processing*, vol. 55, no. 4, pp. 1204–1212, 2007. (Cited on page 16)

[82] S. A. Pasha, B.-N. Vo, H. D. Tuan, and W.-K. Ma, "A Gaussian mixture PHD filter for jump Markov system models," *IEEE Transactions on Aerospace and Electronic systems*, vol. 45, no. 3, pp. 919–936, 2009. (Cited on page 16)

[83] L. Gao, G. Battistelli, L. Chisci, and A. Farina, "Fusion-based multi-detection multi-target tracking with random finite sets," *IEEE Transactions on Aerospace and Electronic Systems*, 2021. (Cited on page 16)

[84] Y. Sung and P. Tokekar, "GM-PHD filter for searching and tracking an unknown number of targets with a mobile sensor with limited FoV," *IEEE Transactions on Automation Science and Engineering*, pp. 1–13, 2021. (Cited on page 16)

[85] W. Yi, G. Li, and G. Battistelli, "Distributed multi-sensor fusion of PHD filters dith different sensor fields of view," *IEEE Transactions on Signal Processing*, vol. 68, pp. 5204–5218, 2020. (Cited on pages 16 and 101)

[86] P. M. Dames, "Distributed multi-target search and tracking using the PHD filter," *Autonomous robots*, vol. 44, no. 3, pp. 673–689, 2020. (Cited on page 16)

[87] B.-N. Vo, B.-T. Vo, and R. P. Mahler, "Closed-form solutions to forward–backward smoothing," *IEEE Transactions on Signal Processing*, vol. 60, no. 1, pp. 2–17, 2011. (Cited on page 16)

[88] R. P. Mahler, B.-N. Vo, and B.-T. Vo, "Multi-target forward-backward smoothing with the probability hypothesis density," *IEEE Transactions on Aerospace & Electronic Systems*, vol. 48, no. 1, pp. 707–728, 2012. (Cited on page 16)

[89] P. Borwein and T. Erdélyi, *Polynomials and polynomial inequalities*. Springer Science & Business Media, 1995, vol. 161. (Cited on page 18)

[90] B.-T. Vo, "Random finite sets in multi-object filtering," phdthesis, School of Electrical, Electronic and Computer Engineering, University of Western Australia,, 2008. (Cited on page 18)

[91] M. Ulmke, O. Erdinc, and P. Willett, "Gaussian mixture cardinalized PHD filter for ground moving target tracking," in *2007 10th International Conference on Information Fusion*. IEEE, 2007, pp. 1–8. (Cited on page 18)

[92] R. P. Mahler, "On multitarget jump-Markov filters," in *2012 15th International Conference on Information Fusion*. IEEE, 2012, pp. 149–156. (Cited on page 18)

[93] D. S. Bryant, E. D. Delande, S. Gehly, J. Houssineau, D. E. Clark, and B. A. Jones, "The CPHD filter with target spawning," *IEEE Transactions on Signal Processing*, vol. 65, no. 5, pp. 13 124–13 138, 2016. (Cited on page 18)

[94] P. Jing, J. Zou, Y. Duan, S. Xu, and Z. Chen, "Generalized CPHD filter modeling spawning targets," *Signal Processing*, vol. 128, pp. 48–56, 2016. (Cited on page 18)

[95] A.-A. Saucan, T. Chonavel, C. Sintes, and J.-M. Le Caillec, "CPHD-DOA tracking of multiple extended sonar targets in impulsive environments," *IEEE Transactions on Signal Processing*, vol. 64, no. 5, pp. 1147–1160, 2016. (Cited on page 18)

[96] R. P. Mahler, B.-T. Vo, and B.-N. Vo, "CPHD filtering with unknown clutter rate and detection profile," *IEEE Transactions on Signal Processing*, vol. 59, no. 8, pp. 3497–3513, 2011. (Cited on pages 19, 20, 21, 37, 38, 42, 43, 44, 46, 61, 62, 65, 66, 69, 70, 71, 72, 73, 79, 80, 84, 89, 101, 103, 105, 107, 108, and 109)

[97] B.-N. Vo, B.-T. Vo, and D. Phung, "Labeled random finite sets and the Bayes multi-target tracking filter," *IEEE Transactions on Signal Processing*, vol. 62, no. 24, pp. 6554–6567, 2014. (Cited on pages xv, 21, 23, 26, 27, 29, 32, and 33)

[98] I. R. Goodman, R. P. Mahler, and H. T. Nguyen, *Mathematics of Data Fusion*. New York, NY, USA: Kluwer Academic Publishers, 1997. (Cited on page 21)

[99] B.-T. Vo and B.-N. Vo, "A random finite set conjugate prior and application to multi-target tracking," in *2011 Seventh International Conference on Intelligent Sensors, Sensor Networks and Information Processing*. IEEE, 2011, pp. 431–436. (Cited on page 21)

[100] ——, "The para-normal Bayes multi-target filter and the spooky effect," in *2012 15th International Conference on Information Fusion*, 2012, pp. 173–180. (Cited on page 22)

[101] S. Reuter, B.-T. Vo, B.-N. Vo, and K. Dietmayer, "The labeled multi-Bernoulli filter," *IEEE Transactions on Signal Processing*, vol. 62, no. 12, pp. 3246–3260, 2014. (Cited on pages 24, 61, 63, 64, 76, 77, and 124)

[102] T. Rathnayake, A. Khodadadian Gostar, R. Hoseinnezhad, R. Tennakoon, and A. Bab-Hadiashar, "On-line visual tracking with occlusion handling," *Sensors*, vol. 20, no. 3, p. 929, 2020. (Cited on page 28)

[103] T. T. D. Nguyen and D. Y. Kim, "On-line tracking of cells and their lineage from time lapse video data," in *2018 International Conference on Control, Automation and Information Sciences (ICCAIS)*. IEEE, 2018, pp. 291–296. (Cited on page 28)

[104] H. V. Nguyen, H. Rezatofighi, B.-N. Vo, and D. C. Ranasinghe, "Multi-objective multi-agent planning for jointly discovering and tracking mobile objects," in *Proceedings of the AAAI Conference on Artificial Intelligence*, vol. 34, no. 05, 2020, pp. 7227–7235. (Cited on page 28)

[105] Q. Li, L. Qiu, B. Qi, and G. Liang, "Adaptive weighting for estimation of the mean of the merged measurement for multi-target bearing tracking," *Electronics Letters*, vol. 57, no. 10, pp. 412–414, 2021. (Cited on page 28)

[106] A. A. Saucan and M. Z. Win, "On the labeled multi-Bernoulli filter with merged measurements," in *ICC 2020-2020 IEEE International Conference on Communications (ICC)*. IEEE, 2020, pp. 1–5. (Cited on page 28)

[107] C. Li, Z. Fan, and R. Shi, "A generalized labelled multi-Bernoulli filter for extended targets with unknown clutter rate and detection profile," *IEEE Access*, vol. 8, pp. 213 772–213 782, 2020. (Cited on page 28)

[108] A. Daniyan, S. Lambotharan, A. Deligiannis, Y. Gong, and W.-H. Chen, "Bayesian multiple extended target tracking using labeled random finite sets and splines," *IEEE Transac-*

tions on Signal Processing, vol. 66, no. 22, pp. 6076–6091, 2018. (Cited on page 28)

[109] S. Li, W. Yi, R. Hoseinnezhad, G. Battistelli, B. Wang, and L. Kong, "Robust distributed fusion with labeled random finite sets," *IEEE Transactions on Signal Processing*, vol. 66, no. 2, pp. 278–293, 2018. (Cited on page 28)

[110] H. V. Nguyen, H. Rezatofighi, B. N. Vo, and D. C. Ranasinghe, "Distributed multi-object tracking under limited field of view sensors," *IEEE Transactions on Signal Processing*, 2021. (Cited on pages 28 and 101)

[111] G. Zhang, F. Lian, C. Han, H. Chen, and N. Fu, "Two novel sensor control schemes for multi-target tracking via delta generalised labelled multi-Bernoulli filtering," *IET Signal Processing*, vol. 12, no. 9, pp. 1131–1139, 2018. (Cited on page 28)

[112] N. Ishtiaq, S. Panicker, A. K. Gostar, A. Bab-Hadiashar, and R. Hoseinnezhad, "Selective sensor control via Cauchy Schwarz divergence," in *Smart Trends in Computing and Communications: Proceedings of SmartCom 2020*. Springer, 2021, pp. 113–124. (Cited on page 28)

[113] S. Panicker, A. K. Gostar, A. Bab-Hadiashar, and R. Hoseinnezhad, "Tracking of targets of interest using labeled multi-Bernoulli filter with multi-sensor control," *Signal Processing*, vol. 171, p. 107451, 2020. (Cited on pages 28 and 101)

[114] H. Cai, S. Gehly, Y. Yang, R. Hoseinnezhad, R. Norman, and K. Zhang, "Multisensor tasking using analytical Rényi divergence in labeled multi-Bernoulli filtering," *Journal of Guidance, Control, and Dynamics*, vol. 42, no. 9, pp. 2078–2085, 2019. (Cited on page 28)

[115] A. K. Gostar, R. Hoseinnezhad, A. Bab-Hadiashar, and W. Liu, "Sensor-management for multitarget filters via minimization of posterior dispersion," *IEEE Transactions on Aerospace and Electronic Systems*, vol. 53, no. 6, pp. 2877–2884, 2017. (Cited on page 28)

[116] G. Amirali Khodadadian, R. Tharindu, T. Ruwan Bandara, B.-H. Ali, B. Giorgio, C. Luigi, and H. Reza, "Centralized cooperative sensor fusion for dynamic sensor network with limited field-of-view via labeled multi-Bernoulli filter," *IEEE Transactions on Signal Processing*, 2020. (Cited on pages 28 and 101)

[117] A. K. Gostar, T. Rathnayake, R. Tennakoon, A. Bab-Hadiashar, G. Battistelli, L. Chisci, and R. Hoseinnezhad, "Cooperative sensor fusion in centralized sensor networks using Cauchy–Schwarz divergence," *Signal Processing*, vol. 167, p. 107278, 2020. (Cited on pages 28 and 101)

[118] S. Li, G. Battistelli, L. Chisci, W. Yi, B. Wang, and L. Kong, "Computationally efficient multi-agent multi-object tracking with labeled random finite sets," *IEEE Transactions on Signal Processing*, vol. 67, no. 1, pp. 260–275, 2018. (Cited on pages 28 and 101)

[119] Y. Zhu, "Efficient sensor management for multitarget tracking in passive sensor networks via Cauchy-Schwarz divergence," *arXiv preprint arXiv:2011.08976*, 2020. (Cited on page 28)

[120] Y. Zhu, S. Liang, M. Gong, and J. Yan, "Decomposed pomdp optimization based sensor management for multi-target tracking in passive multi-sensor systems," *IEEE Sensors Journal*, 2022. (Cited on page 28)

[121] R. P. Mahler, "A GLMB filter for unified multitarget multisensor management," in *Signal Processing, Sensor/Information Fusion, and Target Recognition XXVIII*, vol. 11018. International Society for Optics and Photonics, 2019, p. 110180D. (Cited on page 28)

[122] ——, "A generalized labeled multi-Bernoulli filter for correlated multitarget systems," in *Signal Processing, Sensor/Information Fusion, and Target Recognition XXVII*, vol. 10646. International Society for Optics and Photonics, 2018, p. 106460C. (Cited on page 28)

[123] D. Eppstein, "Finding the K-shortest paths," *SIAM Journal on computing*, vol. 28, no. 2, pp. 652–673, 1998. (Cited on page 29)

[124] K. G. Murty, "Letter to the editor–an algorithm for ranking all the assignments in order of increasing cost," *Operations research*, vol. 16, no. 3, pp. 682–687, 1968. (Cited on page 30)

[125] H. W. Kuhn, "The Hungarian method for the assignment problem," *Naval research logistics quarterly*, vol. 2, no. 1-2, pp. 83–97, 1955. (Cited on page 30)

[126] X. Chen, R. Tharmarasa, and T. Kirubarajan, "Multitarget multisensor tracking," in *Academic Press Library in Signal Processing*. Elsevier, 2014, vol. 2, pp. 759–812. (Cited on pages xvi, 31, 99, 101, and 102)

[127] W. P. Pierskalla, "Letter to the editor - the multidimensional assignment problem," *Operations Research*, vol. 16, no. 2, pp. 422 – 431, 1968. (Cited on page 33)

[128] B. Wei, B. Nener, W. Liu, and L. Ma, "Centralized multi-sensor multi-target tracking with labeled random finite sets," in *2016 International Conference on Control, Automation and Information Sciences (ICCAIS)*. IEEE, 2016, pp. 82–87. (Cited on page 33)

[129] B.-T. Vo, B.-N. Vo, R. Hoseinnezhad, and R. P. Mahler, "Robust multi-Bernoulli filtering," *IEEE Journal of Selected Topics in Signal Processing*, vol. 7, no. 3, pp. 399–409, 2013. (Cited on pages 38 and 62)

[130] M. Beard, B.-T. Vo, and B.-N. Vo, "Multitarget filtering with unknown clutter density using a bootstrap GM-CPHD filter," *IEEE Signal Processing Letters*, vol. 20, no. 4, pp. 323–326, 2013. (Cited on pages 38 and 101)

[131] Y. G. Punchihewa, B.-T. Vo, B.-N. Vo, and D. Y. Kim, "Multiple object tracking in un-

known backgrounds with labeled random finite sets," *IEEE Transactions on Signal Processing*, vol. 66, no. 11, pp. 3040–3055, 2018. (Cited on pages 38, 46, 56, 62, 79, 84, 89, 101, and 105)

[132] D. Y. Kim, "Visual multiple-object tracking for unknown clutter rate," *IET Computer Vision*, vol. 12, no. 5, pp. 728–734, 2018. (Cited on pages 38 and 62)

[133] D. Schuhmacher, B.-T. Vo, and B.-N. Vo, "A consistent metric for performance evaluation of multi-object filters," *IEEE transactions on signal processing*, vol. 56, no. 8, pp. 3447–3457, 2008. (Cited on pages 46, 47, 79, 93, and 111)

[134] F. Guo, Y. Fan, Y. Zhou, C. Xhou, and Q. Li, *Space electronic reconnaissance: localization theories and methods*. John Wiley & Sons, 2014. (Cited on page 53)

[135] R. P. Mahler and A. El-Fallah, "CPHD and PHD filters for unknown backgrounds, part III: Tractable multitarget filtering in dynamic clutter," in *Signal and Data Processing of Small Targets 2010*, vol. 7698. International Society for Optics and Photonics, 2010, p. 76980F. (Cited on page 62)

[136] J. Correa and M. Adams, "Estimating detection statistics within a Bayes-closed multi-object filter," in *2016 19th International Conference on Information Fusion (FUSION)*. IEEE, 2016, pp. 811–819. (Cited on page 62)

[137] Q. Huang, L. Xie, and H. Su, "Estimations of time-varying birth cardinality distribution and birth intensity in Gaussian mixture CPHD filter for multi-target tracking," *Signal Processing*, vol. 190, p. 108321, 2022. (Cited on page 63)

[138] M. Tobias and A. Lanterman, "Techniques for birth-particle placement in the Probability Hypothesis Density particle filter applied to passive radar," *IET Radar, Sonar & Navigation*, vol. 2, no. 5, pp. 351–365, 2008. (Cited on page 63)

[139] B. Ristic, D. Clark, B.-N. Vo, and B.-T. Vo, "Adaptive target birth intensity for PHD and CPHD filters," *IEEE Transactions on Aerospace and Electronic Systems*, vol. 48, no. 2, pp. 1656–1668, 2012. (Cited on page 63)

[140] M. Beard, B. T. Vo, B.-N. Vo, and S. Arulampalam, "A partially uniform target birth model for Gaussian mixture PHD/CPHD filtering," *IEEE Transactions on Aerospace and Electronic Systems*, vol. 49, no. 4, pp. 2835–2844, 2013. (Cited on page 63)

[141] S. Reuter, D. Meissner, B. Wilking, and K. Dietmayer, "Cardinality balanced multi-target multi-Bernoulli filtering using adaptive birth distributions," in *Proceedings of the 16th International Conference on Information Fusion*. IEEE, 2013, pp. 1608–1615. (Cited on page 63)

[142] S. Lin, B. T. Vo, and S. E. Nordholm, "Measurement driven birth model for the generalized labeled multi-Bernoulli filter," in *2016 International Conference on Control, Automation*

and Information Sciences (ICCAIS). IEEE, 2016, pp. 94–99. (Cited on pages 63, 64, 76, 78, and 124)

[143] A. Trezza, D. J. Bucci Jr, and P. K. Varshney, "Multi-sensor joint adaptive birth sampler for labeled random finite set tracking," *arXiv preprint arXiv:2109.04355*, 2021. (Cited on pages 64, 125, and 129)

[144] S. H. Rezatofighi, S. Gould, B. T. Vo, B.-N. Vo, K. Mele, and R. Hartley, "Multi-target tracking with time-varying clutter rate and detection profile: Application to time-lapse cell microscopy sequences," *IEEE transactions on medical imaging*, vol. 34, no. 6, pp. 1336–1348, 2015. (Cited on page 98)

[145] Y. Bar-Shalom, P. K. Willett, and X. Tian, *Tracking and data fusion*. YBS publishing Storrs, CT, USA:, 2011. (Cited on page 100)

[146] N. Xiong and P. Svensson, "Multi-sensor management for information fusion: issues and approaches," *Information fusion*, vol. 3, no. 2, pp. 163–186, 2002. (Cited on page 100)

[147] M. E. Liggins, C.-Y. Chong, I. Kadar, M. G. Alford, V. Vannicola, and S. Thomopoulos, "Distributed fusion architectures and algorithms for target tracking," *Proceedings of the IEEE*, vol. 85, no. 1, pp. 95–107, 1997. (Cited on page 100)

[148] D. Hall, C.-Y. Chong, J. Llinas, and M. Liggins II, *Distributed data fusion for network-centric operations*. Crc Press, 2017. (Cited on page 100)

[149] C.-Y. Chong, "Distributed architectures for data fusion," in *Proceedings of the 1st International Conference on Information Fusion*, 1998. (Cited on page 100)

[150] M. Uney, D. E. Clark, and S. J. Julier, "Distributed fusion of phd filters via exponential mixture densities," *IEEE Journal of Selected Topics in Signal Processing*, vol. 7, no. 3, pp. 521–531, 2013. (Cited on page 101)

[151] G. Battistelli, L. Chisci, C. Fantacci, A. Farina, and A. Graziano, "Consensus CPHD filter for distributed multitarget tracking," *IEEE Journal of Selected Topics in Signal Processing*, vol. 7, no. 3, pp. 508–520, 2013. (Cited on page 101)

[152] G. Battistelli, L. Chisci, C. Fantacci, A. Farina, and R. P. Mahler, "Distributed fusion of multitarget densities and consensus PHD/CPHD filters," in *Signal processing, sensor/information fusion, and target recognition XXIV*, vol. 9474. International Society for Optics and Photonics, 2015, p. 94740E. (Cited on page 101)

[153] D. Clark, S. Julier, R. Mahler, and B. Ristić, "Robust multi-object sensor fusion with unknown correlations," in *Sensor Signal Processing for Defence (SSPD 2010)*. IET, 2010, pp. 1–5. (Cited on page 101)

[154] M. B. Guldogan, "Consensus Bernoulli filter for distributed detection and tracking using multi-static Doppler shifts," *IEEE Signal Processing Letters*, vol. 21, no. 6, pp. 672–676, 2014. (Cited on page 101)

[155] W. Yi, M. Jiang, R. Hoseinnezhad, and B. Wang, "Distributed multi-sensor fusion using generalised multi-bernoulli densities," *IET Radar, Sonar & Navigation*, vol. 11, no. 3, pp. 434–443, 2017. (Cited on page 101)

[156] W. Yi, S. Li, B. Wang, R. Hoseinnezhad, and L. Kong, "Computationally efficient distributed multi-sensor fusion with multi-Bernoulli filter," *IEEE Transactions on Signal Processing*, vol. 68, pp. 241–256, 2019. (Cited on page 101)

[157] T. Li, J. M. Corchado, and S. Sun, "On generalized covariance intersection for distributed PHD filtering and a simple but better alternative," in *2017 20th International Conference on Information Fusion (Fusion)*. IEEE, 2017, pp. 1–8. (Cited on page 101)

[158] S. Li, W. Yi, R. Hoseinnezhad, G. Battistelli, B. Wang, and L. Kong, "Robust distributed fusion with labeled random finite sets," *IEEE Transactions on Signal Processing*, vol. 66, no. 2, pp. 278–293, 2017. (Cited on page 101)

[159] B.-N. Vo, S. Singh, and W. K. Ma, "Tracking multiple speakers using random sets," in *2004 IEEE International Conference on Acoustics, Speech, and Signal Processing*, vol. 2. IEEE, 2004, pp. ii–357. (Cited on page 101)

[160] S. Nannuru, S. Blouin, M. Coates, and M. Rabbat, "Multisensor CPHD filter," *IEEE Transactions on Aerospace and Electronic Systems*, vol. 52, no. 4, pp. 1834–1854, 2016. (Cited on page 101)

[161] A. Saucan, M. J. Coates, and M. Rabbat, "A multisensor multi-Bernoulli filter," *IEEE Transactions on Signal Processing*, vol. 65, no. 20, pp. 5495–5509, 2017. (Cited on page 101)

[162] X. Wang, A. K. Gostar, T. Rathnayake, B. Xu, A. Bab-Hadiashar, and R. Hoseinnezhad, "Centralized multiple-view sensor fusion using labeled multi-Bernoulli filters," *Signal Processing*, vol. 150, pp. 75–84, 2018. (Cited on page 101)

Statement of Contribution by Others

To Whom It May Concern,

I, Cong-Thanh Do, contributed to the theoretical development of the algorithm, implementation (MATLAB), evaluation, drafting and finalizing the paper entitled:

C.-T. Do, and H. V. Nguyen, "Tracking multiple targets from multistatic Doppler radar with unknown probability of detection," *Sensors* **2019**, 19(7), 1672; doi: 10.3390/s19071672.

The co-author contributed by providing insight into the development of implementation, discussion, and proof-reading the paper.

Cong-Thanh Do

I, as a Co-Author, endorse that this level of contribution by the candidate indicated above is appropriate.

Hoa Van Nguyen

Statement of Contribution by Others

To Whom It May Concern,

I, Cong-Thanh Do, contributed to the theoretical development of the algorithm, implementation (MATLAB), evaluating, drafting and finalizing the paper entitled:

C.-T. Do, W. Liu, and T. T. D. Nguyen, "Tracking multiple marine ships via multiple sensors with unknown backgrounds", *Sensors*, 19(22), 5025, doi: 10.3390/ s19225025.

The co-authors contributed by providing insight into the development of implementation, discussion, and proof-reading the paper.

Cong-Thanh Do

I, as a Co-Author, endorse that this level of contribution by the candidate indicated above is appropriate.

Weifeng Liu

Tran Thien Dat Nguyen

Statement of Contribution by Others

To Whom It May Concern,

I, Cong-Thanh Do, contributed to the theoretical development of the algorithm, implementation (MATLAB), evaluating, drafting and finalizing the paper entitled:

C.-T. Do, W. Liu, and T. T. D. Nguyen, "Multi-object tracking with an adaptive generalized labeled multi-Bernoulli filter", *Signal Processing*, **2022**, 108532, doi: 10.1016/ j. sigpro. 2022.108532.

The co-authors contributed by providing insight into the development of implementation, discussion, and proof-reading the paper.

Cong-Thanh Do

I, as a Co-Author, endorse that this level of contribution by the candidate indicated above is appropriate.

Tran Thien Dat Nguyen

Diluka Moratuwage

Changbeom Shim

Yon Dohn Chung

Statement of Contribution by Others

To Whom It May Concern,

I, Cong-Thanh Do, contributed to the theoretical development of the algorithm, implementation (MATLAB), evaluating, drafting and finalizing the paper entitled:

C.-T. Do, T. T. D. Nguyen, and H. V. Nguyen, "Robust multi-sensor generalized labeled multi-Bernoulli filter", *Signal Processing*, **2022**, 192, 108368, doi:10.1016/ j.sigpro. 2021. 108368.

The co-authors contributed by providing insight into the development of implementation, discussion, and proof-reading the paper.

Cong-Thanh Do

I, as a Co-Author, endorse that this level of contribution by the candidate indicated above is appropriate.

Tran Thien Dat Nguyen

Hoa Van Nguyen

Statement of Contribution by Others

To Whom It May Concern,

I, Cong-Thanh Do, contributed to the theoretical development of the algorithm, implementation (MATLAB), evaluating, drafting and finalizing the paper entitled:

C.-T. Do, and H. V. Nguyen, "Multistatic Doppler-based marine ships tracking", *in 2018 Proc. of the Int. Conf. Control, Automation and Information Sciences,* Hangzhou, China, Oct. 2018, doi:10.1109/ICCAIS.2018.8570690.

The co-authors contributed by providing insight into the bootstrapping method, revising the development of implementation, revision, and proof-reading the paper.

Cong-Thanh Do

I, as a Co-Author, endorse that this level of contribution by the candidate indicated above is appropriate.

Hoa Van Nguyen

Statement of Contribution by Others

To Whom It May Concern,

I, Cong-Thanh Do, contributed to the theoretical development of the algorithm, implementation (MATLAB), evaluating, drafting and finalizing the paper entitled:

C.-T. Do, and T. T. D. Nguyen, "Multiple marine ships tracking from multistatic Doppler data with unknown clutter rate", *in 2019 Proc. of the Int. Conf. Control,* Automation and Information Sciences, pp. 1-6, Chengdu, China, Oct. 2019, doi:10.1109/ ICCAIS 46528. 2019. 9074604.

The co-author contributed by providing insight into development of implementation, revising , and proof-reading the paper.

Cong-Thanh Do

I, as a Co-Author, endorse that this level of contribution by the candidate indicated above is appropriate.

Tran Thien Dat Nguyen